Soil Nitrous Oxide Hot Moments: Identification, Characterization, and Prediction Across Agroecosystems

A Dissertation Presented for the

Doctor of Philosophy

Degree

The University of Tennessee, Knoxville

Ryan Ackett

August 2025

ACKNOWLEDGEMENTS

I would like to thank first of all Dr. Debasish Saha, my advisor and mentor, for the time, energy, and guidance he has invested in me over these last years. I have grown tremendously as a scientist and writer, not to mention as a person, and I have him to thank for so much of that. As well, I have benefited tremendously from the knowledge, wisdom, and effort imparted to me by my committee members: Dr. Haileab Hilafu, Dr. Sindhu Jagadamma, Dr. Emine Fidan, and Dr. Sean Schaeffer. I am deeply indebted and profoundly appreciative of the gift of your time and faith in me.

I would also like to thank my lab members Facundo Lussich, Arjun Chhetri, Jashan Dhaliwal, and Presley Nickens who have been with me over the years, and who have always been there when I needed you. I could not have asked for a kinder or more supportive lab group. Each of you has gone out of your way to help me along the way, and I could not have done this without you. I am also grateful for the many others who generously contributed their time to assist me in conducting soil analyses and guiding me throughout the lab, especially Rachel Wooliver, Binsiya Kallingal, Rounak Patra, and Duncan McNamara. And an additional thanks to Arjun, who worked tirelessly to keep the gas chromatograph running despite its many attempts to fail.

I also extend my deepest gratitude to my friends and comrades of United Campus Workers. It is no understatement to say that I would not have made it through this if it had not been for the success this union has had in making this campus a better place for all graduate workers. So many of you have truly stood up for me, and I hope I have been able to do the same for you. Solidarity forever.

Most of all I thank my family who have never stopped supporting and believing in me. To my parents, Wayne and Jennifer, I thank you for instilling in me a love of learning and science which

I have pursued all my life. And to Onyx, who has been by my side and my most loyal ally, my most patient listener, my fiercest defender. My greatest love to you all.

ABSTRACT

Nitrous oxide (N_2O) emissions from agricultural soils contribute ~4% of total anthropogenic greenhouse gases (GHG) emissions globally. Events known as 'hot moments' can occur following environmental changes that favor N_2O production, which contribute disproportionately to annual cumulative emissions. Despite their significance, hot moments have not been statistically well defined, particularly on a global scale. I collected 13,787 soil N_2O flux measurements from 42 publications and evaluated 14 methods of statistical anomaly detection for their ability to identify hot moments within datasets. Two methods achieved highest overall performance by Matthews correlation coefficient (MCC): median absolute deviation (MCC: 0.80) and minimum covariance determinant (MCC: 0.80), the latter which also performed evenly across highly dissimilar datasets and identified more difficult-to-detect contextual hot moments than other top overall performers (39%). I next evaluated a variety of machine learning classification models for their performance in predicting daily hot moments from a limited set of management, environmental, and climate data. The XGBoost model trained using data labels of N_2O flux measurements generated through a context-informed hand labeling process produced the best overall performance (Matthews Correlation Coefficient, MCC: 0.69; Accuracy: 90%), with fewer errors made when flux was <10 g N ha^{-1} d^{-1} or >50 g N ha^{-1} d^{-1}. Finally, I investigated the impact of extreme weather events on N_2O emissions across soils ranging widely in climatological histories and textures collected from the Levant region. Soil cores were subjected to varying periods of very high moisture (90% water filled pore space) ranging from a transient flooding to seven days in an incubation experiment. I found that while cumulative emissions were primarily driven by carbon availability, longer periods of flooding significantly increased cumulative N_2O emissions ($p<0.0001$) both in soils which experienced impeded gas diffusion by

high moisture and those that did not. These findings suggest the possibility of a positive feedback loop as climate change increases the frequency of extreme weather events and flooding, which in turn contribute to greater N_2O emissions.

TABLE OF CONTENTS

CHAPTER 1: INTRODUCTION AND LITERATURE REVIEW 1

Background 2

Statement of Purpose 7

Literature Review 8

Key microbiological pathways of soil N_2O production and their controls 8

Hot moments and their environmental drivers 14

Anomaly detection 16

Research gaps and implications 20

CHAPTER 2: STATISTICAL IDENTIFICATION OF NITROUS OXIDE HOT MOMENTS AND THEIR SIGNIFICANCE ACROSS GLOBAL AGROECOSYSTEMS 22

Abstract 23

Introduction 24

Materials and Methods 27

Data collection and diversity of N_2O flux distribution 27

Supervised and contextualized identification of hot moments 29

Anomaly detection methods 32

Data handling for training and testing 35

Method tuning 35

Evaluating the performance of hot moment identification methods 37

Evaluating the impact of hot moments on total N_2O emissions 38

Results 39

Performance of methods using optimized thresholds 39

Hot moments and overall N_2O emissions 42

Discussion 43

Statistical strengths and limitations of hot moment detection methods within the research context 44

The impact of hot moments 47

Potential implications, limitations, and future work 49

Conclusion 49

CHAPTER 3: MACHINE LEARNING PREDICTS NITROUS OXIDE HOT MOMENTS ACROSS GLOBAL AGROECOSYSTEMS 51

Abstract 52

Introduction 52

Methods 55

Collection and description of a diverse agroecosystem database 55

Classification of true hot moments 61

Model tuning 63

Model evaluation 64

Model interpretation 65

Results 66

Model performances 66

Key model drivers and interactions 68

Discussion 72

ML classification models accurately predict the occurrences of hot moments 72

Model behavior replicates biogeochemical processes 73

Potential applications and future directions 75
Conclusion 76
CHAPTER 4: THE EFFECT OF EXTENDED SOIL SATURATION ON NITROUS OXIDE EMISSIONS IN MEDITERRANEAN SOILS 78
Abstract 79
Introduction 80
Materials and Methods 83
Soil collection and characterization 83
Experimental design 85
Soil moisture management 86
N_2O flux measurements 87
N_2O isotopomer analysis for microbial source identification 88
Soil chemical property measurements 89
Statistical analysis 89
Results 90
Temporal N_2O fluxes in response to flooding under different soil textures 90
Changes in soil chemical properties 91
Isotopomer analysis and biological processes driving hot moments 94
Effect of flooding period and soil properties on cumulative N_2O flux 95
Discussion 101
Expansion of clay promoted gas diffusivity during flooding period 101
Texture impacted the timing of hot moments and underlying biological drivers 102
Dissolved organic carbon availability primarily drove cumulative emissions 105

Flooding duration increased cumulative emissions to a limited extent 105

Conclusion 106

CHAPTER 5: CONCLUSION 108

REFERENCES 112

VITA 143

LIST OF TABLES

Table 1.1: Major soil N_2O producing processes and their key drivers. 13

Table 2.1: Novel anomaly detection methods evaluated for hot moment identification categorized by the method used to quantify the "anomalousness" of points. 34

Table 2.2: Parameters for the implementation of anomaly detection methods optimized for performance across a diverse range of datasets. All parameters used by methods which are not shown here were set to their default values in their respective pyOD (Zhao et al., 2019) and pyOATS (Ye, 2024) implementations. 36

Table 2.3: Optimized method performance evaluated using a variety of metrics using the testing dataset. Matthews Correlation Coefficient (MCC) measures overall model performance across the confusion matrix (Equation 2). R^2 and slope of the regression between method accuracy and the prevalence of hot moments and the measurement frequency are shown. Due to the sharp angular relationship of the accuracy of the 75th Percentile method and the hot moment prevalence, two separate linear regressions were fit and the slopes and coefficients of determination are shown: first one where the hot moment prevalence was less than 25%, and another where it was greater than or equal to 25%. 40

Table 2.4: Mean daily soil N_2O flux of background emissions and hot moments emissions, as determined by context-informed labeled data, MAD, MCD, and 1.5 IQR classification methods. The mean values are associated with 95% confidence interval. 43

Table 2.5: Contribution of hot moments to cumulative N_2O flux and their relative duration as estimated by context-informed labeled data, MAD, MCD, and 1.5 IQR methods. Values are shown for the complete dataset, which overrepresents studies emphasizing spring and

summer months, and for a subset of the data from experiments with available year-round measurement. 44

Table 3.1: Environmental and management drivers of N_2O hot moments and their representation in our ML models. 60

Table 3.2: Matthews Correlation Coefficient assesses the overall predictive power of 20 hot moment prediction models which varied by ML architecture and the method of classifying N_2O fluxes as hot moments and background emissions in training data. Average MCC of models grouped by architecture and labeling method are also given... 67

Table 4.1: Soil physical and chemical properties. 84

Table 4.2: Isotopomer analysis of gases sampled during periods of elevated emissions. Site preference (SP) of ^{15}N and relative contributions of bacterial denitrification (f_D) and nitrification/fungal denitrification (f_{N+FD}) and their standard deviations across soil textures are given. Depending on texture and flooding treatment, elevated emissions coincided with isotopomer gas sampling 24 hours after first allowing flooded soils to dry (After Flooding) or at some point during the maintenance of the flooding period (During Flooding). 96

Table 4.3: Ordinary least squares multiple linear regression of cumulative N_2O flux. 99

LIST OF FIGURES

Figure 1.1: Types of outliers. A) global outliers occur where data points deviate significantly from the distribution or behavior of the data set; B) collective outliers are groups of points which when considered together are anomalous, but not individually; C) contextual outliers are anomalous due to their position in relation to the neighbors 20

Figure 2.1: Schematic diagram of data collection process from published work and preprocessing steps. 28

Figure 2.2: Distribution of experimental sites and the primary crops grown at each site across the globe. Many sites performed multiple treatments or experiments using multiple crops. The numbers of time series data for each primary crop includes: 89 Zea mays, 18 Glycine max, 14 grassland, 9 Lolium perenne, 8 Hordeum vulgare, 4 Medicago sativa, 4 Panicum virgatum, 4 fallow, and 20 other various upland crops. 30

Figure 2.3: (a) Soil texture observed across the experimental sites, with frequent representation of loam, silt loam, clay loam, and silty clay loam soils (left panel). (b) Rate and nitrogen form used in fertilization events which occurred following experiment commencement (right panel). Diversity of fertilizer types is represented, including urea, urea ammonium nitrate (UAN), environmentally enhanced nitrogen (EEN), ammonium sulfate (AS), ammonium nitrate (AN), ammonium phosphate (AP), anhydrous ammonia (AA), livestock urine, manure, and other unreported fertilizer forms. 30

Figure 2.4: Distribution of daily average N_2O flux magnitudes across the entire dataset. Bin width is 100 g N ha^{-1} d^{-1}. Flux values near zero were orders of magnitude more common than higher flux values, and flux values become rarer with increasing magnitude up to 1500 g N ha^{-1} d^{-1}. 31

Figure 2.5: An example of data visualization for the hot moment labeling process. In this graph, N_2O emissions (orange dots, top panel) remain at a consistent background level until approximately June 4. After this date, the combination of high and frequent precipitation (bottom panel) raising the soil moisture (middle panel, blue dots) and a recent fertilizer application (green line, top panel) in the early summer led to a significant rise in emissions consistent with a hot moment. Emissions fluctuate for one month until about July 4, corresponding to fluctuations in soil moisture driven primarily by three large precipitation events above 20 mm per day. After July 4, the soil moisture remained comparatively low, and emissions gradually stabilized at a consistent background level. 33

Figure 2.6: Impact of hot moment prevalence on the performance of anomaly detection methods. The accuracy of 1.5 IQR was highest when hot moments comprised 5-25% of the dataset, and underperformed other methods when hot moments were very rare or common. The accuracy of MAD and MCD were more consistent across the full range of hot moment prevalences... 41

Figure 2.7: Temporal distribution of hot moments (red bars) and background emissions (blue bars) as predicted by the top three performing methods in the testing dataset, compared to the labeled data, using a bin width of five days (a). Histogram of the proportion of hot moments in time-series data as predicted by each method. 1.5 IQR rarely predicted hot moments to comprise more than 20% of a dataset, and more often tended to identify 15-20% of data as anomalous.. 41

Figure 2.8: Example visual demonstration of anomaly detection method performance in hot moment identification using a sample time-series data. N_2O flux measurements identified

as hot moments are highlighted in red, while background emissions are presented in blue. 1.5 IQR identified only extreme anomalies as hot moments above 60 g N ha^{-1} d^{-1}, while MCD and MAD were much more sensitive, identifying smaller hot moments with flux magnitudes of 30 g N ha^{-1} d^{-1}... 42

Figure 3.1: Global distribution of study sites and associated soil textural representation within the model dataset. Seven soil textural classes were represented by color, including a variety of loams and clays. The size of circles represents the number of treatment timeseries datasets at each site. 58

Figure 3.2: The distribution of soil moisture and temperature coincident with N_2O flux measurements. Distributions are shown for each variable independently via histograms, with volumetric water content (VWC) at the top and soil temperature at the right, and their combination shown via heatmap. Color of each tile represents the number of N_2O flux measurements for each combination of VWC and soil temperature. 58

Figure 3.3: Representation of crops and management practices represented in the dataset, as well as the range of magnitudes of daily average N_2O flux measurements. 59

Figure 3.4: Prediction performance of XGBoost model trained using context-informed data labels. a) Prediction results varied with N_2O flux magnitude, with error rate peaking when flux was moderate (which often defines the top of the background level and the lowest hot moments) and decreasing as flux approached more extreme magnitudes, low and high. Probability threshold used was 0.5, and overall model accuracy was 90%. b) The receiver operator characteristic curve plots the true positive rate (TPR) and false positive rate (FPR) across different probability thresholds (p). Using the default probability threshold of 0.5 (50% probability of a hot moment), the model resulted in a

TP rate ~60% and a FP rate ~6%. c) The predicted probability of a hot moment was correlated with the magnitude of N_2O flux, with greater model certainty associated with higher fluxes... 69

Figure 3.5: Violin plot of Shapley values of model predictors sorted from greatest (top) to least (bottom) average absolute impact. Color represents the value of the predictor, while the X-axis represents the magnitude of impact that predictor had on the output. The widths of violins indicate the frequency of data with a given Shapley value. Most violins are widest near 0 on the X-axis, indicating low impact. 70

Figure 3.6: Heatmaps indicate the proportions of N_2O flux measurements predicted to be hot moments when segmented into bins based on the synergy of two key predictors: days since fertilization and volumetric water content (VWC), soil temperature and VWC, and days since fertilization and fertilizer form. Color of each tile indicates the proportion of flux measurements within tiles were predicted to be hot moments, where dark red indicates 100% of measurements predicted to be hot moments. The numbers within each tile indicate the total number data points within each tile. 71

Figure 4.1: Daily soil moisture and N_2O, CO_2, and CH_4 fluxes measured for the a) 0F, b) 3F, and c) 7F flooding duration treatments. Multiple panels of N_2O and CO_2 fluxes are shown due to significantly different ranges of fluxes across soil textures. Light blue area indicates the flooding perion during which 90% WFPS was maintained. 92

Figure 4.2: Daily soil moisture, inorganic nitrogen content, and dissolved organic mater measured for the a) 0F, b) 3F, and c) 7F flooding duration treatments. Light blue area indicates the flooding perion during which 90% WFPS was maintained. 93

Figure 4.3: Cumulative N_2O emissions of flooding treatments segmented by soil texture. Error bars represent the standard error across replications, while letters above each bar represent significant differences in cumulative fluxes by Tukey's HSD. Significance was determined for each texture individually- equivalent letters does not indicate statistical equivalence from one quadrant graph to another. 97

Figure 4.4: Predicted impact of the interaction between flooding duration (x-axis) and clay content (y-axis) on cumulative N_2O emissions (color). 100

Figure 4.5: Actual and predicted cumulative N_2O emissions by the reduced regression model. Soil texture is indicated by color, while flooding duration is indicated by shape. 100

CHAPTER 1: INTRODUCTION AND LITERATURE REVIEW

Background

Climate change is already affecting life on Earth. Since Industrialization, the mean surface temperature of Earth has risen about 1.4 degrees Celsius (2.5 degrees Fahrenheit) as a result of greenhouse gases (GHG) which continue to be released into the atmosphere at an accelerating rate (Lamb et al., 2022). The further advancement of warming threatens to intensify natural disasters, hunger, conflict, ecosystem loss, disease, mortality, and many more dire and interrelated social and ecological consequences by the end of this century (Bowles et al., 2015; Davies & Riddell, 2017; Woodward & Porter, 2016). The Intergovernmental Panel on Climate Change (IPCC) has assessed thousands of possible reduction pathways employing various strategies and levels of ambition (Achakulwisut et al., 2023), concluding that limiting total warming to 2 °C will require substantial reductions from all major sectors worldwide (IPCC, 2023). In response to the scale and scope of this challenge, a refrain has arisen from scientists and activists that "every job is a climate job" (Project Drawdown, 2021), reminding us of our collective responsibility to each other and future generations, and our individual power to make a difference no matter what our role in society may be.

Meeting these ambitions mitigation targets within our food system will be a particularly critical and challenging task. Globally, agriculture and its associated land use change contribute between 18-30% of GHG emissions, and thus encompass a substantial portion of these necessary reductions (Crippa et al., 2021; Garnett, 2011; Rosenzweig et al., 2020). Complicating matters further, these emissions reductions must coincide with increases in calorie production worldwide to combat hunger and malnutrition amid rising crop losses associated with warming temperatures and a growing population (Cassidy et al., 2013; IPCC, 2022; Rezaei et al., 2023; Smith, 2017). Historically these aims have been at odds, with large reductions in global hunger during the 20th century achieved through mechanization, land expansion, and dramatic increases in nitrogen use made possible through the Haber-Bosh process, each of which also contributed to rapidly growing emissions (Chaplin-Kramer et al., 2023; Deng et al., 2016; Erisman et al., 2008; L. B. Guo & Gifford, 2002). Achieving both goals at once will require novel solutions.

Agriculture is a major contributor of each of the three most important GHGs, carbon dioxide (CO_2), methane (CH_4), and nitrous oxide (N_2O), with different agricultural practices acting as the major driver of each. The leading contributor to agricultural CH_4 emissions is enteric fermentation which occurs within ruminant animals (EPA, 2023; IPCC, 2023; Shindell et al., 2024). CO_2 emissions are primarily caused by land expansion of agriculture's footprint, whereby primarily native ecosystems like forests, wetlands, and grasslands are converted into grazing or cropland with generally significantly lower capacities to store carbon above and below ground (Deng et al., 2016; L. B. Guo & Gifford, 2002; Powlson et al., 2022; Sanderman et al., 2017). Global increases in animal production have contributed significantly to CH_4 emissions directly and CO_2 emissions indirectly as the leading driver of land use change worldwide, and have thus generated much attention on mitigating emissions from animal production systems and transitioning toward plant-based diets (Cassidy et al., 2013; Eshel et al., 2014; Shindell et al., 2024; Verheul, 2011). Yet while many solutions to reducing agriculture's climate impact include social action and political strategies to improving resource use and diets, these do not obviate the need to reduce emissions from cropland agriculture simultaneously, as it is from these working lands that agriculture contributes most significantly to the third major greenhouse gas: N_2O.

N_2O is a potent GHG with a warming potential 273 times that of CO_2 (IPCC, 2022), making emissions of relatively smaller amounts than other GHGs globally significant. Since the preindustrial period, anthropogenic terrestrial N_2O emissions have risen to 7.3 Tg N yr^{-1}, with more than half of these attributed to agriculture (3.8 Tg N yr^{-1}) (IPCC, 2023). Increases from agriculture have been caused by human manipulations of the nitrogen cycle in the form of nitrogen fertilizer applications to soil to improve yields (Smith, 2017; Yan et al., 2014). There are many potential fates of nitrogen upon entering the soil system, from waterways to atmospheric depositions to the desired fate of plant biomass, and the significant increase in nitrogen inputs has consequently resulted in increased quantities of nitrogen meeting these fates, including N_2O (Butterbach-Bahl et al., 2013; Caranto & Lancaster, 2017; Yan et al., 2014). In fact, N_2O emissions have demonstrated a nonlinear relationship with nitrogen fertilizer inputs, exponentially increasing in N_2O emissions as fertilizer use rises (Song et al., 2018; Thompson et al., 2019; Q. Wang et al., 2020). As a result, the agricultural emissions rate has grown rapidly by nearly 50% since the 1980's, accounting for 70% of the total rise in anthropogenic N_2O emissions over this timeframe (IPCC, 2023). In the face of this growing problem, research is needed to identify strategies capable of reducing N_2O emissions and supporting their implementation widely to meet international goals of limiting warming to 1.5 or even 2 °C by the end of this century (Clark et al., 2020; Garnett, 2011; Hénault et al., 2012; Mosier et al., 1998; Thompson et al., 2019).

One promising avenue of research ideates an opportunity to this end within the temporal pattern in which N_2O is emitted from soils. These emissions do not take place at a steady and constant rate over time, but rather exhibit two distinct states. The first is a relatively steady and low-level rate typically around 2-3 g N ha^{-1} d^{-1} which predominates throughout time, known as the "background" level (Yin et al., 2022). However, when substrates are abundant and environmental conditions favorable for biogeochemical processes which produce N_2O, the rate of emissions can rise dramatically by orders of magnitude for a period until substrates are expended or conditions change, in a phenomenon that have been termed "hot moments" (McClain et al., 2003). These hot moments are discrete events which contribute disproportionately to agricultural N_2O emissions, leading to efforts to target these hot moments to maximize the potential impact of mitigation strategies (Wagner-Riddle et al., 2020). However, because of the temporal variability and complex multifactorial processes which drive these events, hot moments have thus far proven difficult to estimate both in their magnitude and timing (Groffman et al., 2009). In fact, it is largely because of hot moments that process-based models of soil N_2O emissions have been shown to poorly represent emissions at daily temporal resolution, as they poorly represent the shifts in biogeochemical dynamics which create hot moments (Gaillard et al., 2018; Groffman et al., 2009; Necpálová et al., 2015).

Moreover, the already substantial GHG contributions of hot moments have the possibility to grow as climate change advances. This is due to the interplay between certain climate and weather factors serving as both contributing causes of hot moments and outcomes of climate change, creating the possibility of positive feedback loops. For example, the rate of denitrification- a key biogeochemical process responsible for N_2O hot moments- has been shown to have a high Q10, meaning that it accelerates with higher temperatures (Butterbach-Bahl et al., 2013; Smith, 2017). Thus, as global temperatures rise, it is expected that the rate of soil N_2O emissions will rise as well (Butterbach-Bahl et al., 2013). One other potential relationship between climate change and N_2O emissions exists around extreme weather events, particularly precipitation. Climate change's effect on precipitation patterns is expected to be geographically varied, but to overall tend to increase the frequency and intensity of extreme events (Rastogi et al., 2020). During the period of completing my PhD studies, this area of Appalachia has been devastated by a series of floods and hurricanes which have devastated local communities, and which were fueled by warming ocean conditions created by climate change. Such events are also intimately tied to hot moments, as the anoxic conditions created by raising soil moisture accelerate denitrification and frequently instigate hot moments (Butterbach-Bahl et al., 2013). However, while the primary drivers of hot moments are well understood on a broad level, they are ultimately the result of complex environmental and biogeochemical interactions between a large array of factors, making the precise predictions of the magnitude and timing of hot moments extremely challenging (Groffman et al., 2009). Process-based models have been shown to poorly represent the fine-scale temporal dynamics of N_2O emissions, meaning that while they may accurately estimate emissions over long timescales, they cannot precisely predict when hot moments occur (Brilli et al., 2017; Del Grosso et al., 2008; Fuchs et al., 2020; Gaillard et al., 2018; Jarecki et al., 2008; Parton et al., 2001; Zimmermann et al., 2018). Additionally, both process-based and machine learning models of soil N_2O emissions have demonstrated a tendency to systematically underestimate the magnitude of flux during hot moments (Adler et al., 2024; Anthony & Silver, 2024; Chiaravalloti et al., 2023; Dhaliwal et al., 2025; Hamrani et al., 2020; Joshi et al., 2024; Kotlar et al., 2022). The inability to predict when hot moments are likely to occur is a major impediment to effective mitigation efforts. N_2O emissions are highly temporally variable (Hénault et al., 2012), and thus even theoretically effective strategies if implemented at the wrong time may yield little to no benefit.

Compounding these challenges of accurate predictions of hot moments is the lack of consensus in how best to identify and define hot moments quantitatively. The original definition by McClain et al. (2003) provides a qualitative framework for identifying biogeochemical hot moments broadly, yet translating this into a quantitative framework is not straightforward. Many different numerical methods have been applied to N_2O flux datasets for the identification of hot moments, often with widely disparate results in which measurements are classified as hot moments even within the same dataset (Anthony et al., 2023; Anthony & Silver, 2021; Corre et al., 1996; Mason et al., 2016; Molodovskaya et al., 2012; Palta et al., 2014; Saha et al., 2018; Stuchiner et al., 2025). This lack of consensus has led to hesitance in applying quantitative methods to the investigation of hot moments, inhibiting this concept from arriving at practical solutions (Bernhardt et al., 2017).

Statement of Purpose

It is imperative to reduce agriculture's contributions to climate change. Hot moments are responsible for a disproportionate amount of cropland agriculture's most important pool of emissions, N_2O, and are thus critical targets for mitigation. This dissertation follows this line of reasoning by investigating N_2O hot moments, addressing critical research gaps concerning the significance, characteristics, modeling strategies, and biogeochemical drivers of these events and proposing pathways toward actionable mitigation strategies. The first task must be to determine an accurate and reliable quantitative method of identifying hot moments within N_2O flux measurement datasets. As highly impactful, anomalous events triggered by shifting environmental conditions, these events must be distinguished from background emissions so that they can be isolated for further investigation. Next, models must be developed which integrate environmental and management data to predict the occurrences of hot moments at a scale relevant to intervention, such as the field-level spatial scale and daily temporal scale. Finally, such models can only be as good as the data they are built upon. Research must continue to gather data and investigate uncertainties in biogeochemical responses to environmental conditions, especially those conditions which are likely to occur under a changing climate.

My specific research objectives and the chapters in which I will address them are:

Chapter 1: evaluate the performance of statistical methods for identifying N_2O hot moments within measurement datasets, identify guidelines for their usage, and quantify the frequency and contribution to cumulative emissions of hot moments.

Chapter 2: evaluate the use of low-input machine learning classification modeling for their ability to predict the occurrence of daily N_2O hot moments from environmental and management data across a diverse global dataset.

Chapter 3: determine the effect of soil texture and flooding duration from extreme weather events on N_2O emissions.

The methodological approaches to these objectives as well as their results are presented in the subsequent chapters.

Literature Review

Key microbiological pathways of soil N_2O production and their controls

The production of N_2O in soils is predominately mediated by microbiological redox processes (E. Baggs & Philippot, 2010). Diverse microbial communities use and transform various nitrogen species as electron donors or acceptors as part of their metabolism, potentially resulting in gaseous N_2O which may diffuse out of the soil system and accumulate in the atmosphere. Two microbial processes- nitrification, denitrification- are primarily responsible for soil N_2O production, contributing an estimated 70% of global emissions N_2O (Butterbach-Bahl et al., 2013; Firestone & Davidson, 1989; Heil et al., 2015; Smith, 2017). However, within these two broad categories exists complexity, including intersecting and contrasting subprocesses, requiring deeper investigation to understand precisely how environmental conditions drive N_2O emissions through these mechanisms. Additionally, these processes are affected by substrate availability and environmental conditions which are further influenced by management practices to dictate metabolic activity of soil microbes, especially soil oxygen, temperature, carbon availability, and pH (Butterbach-Bahl et al., 2013; Norton & Ouyang, 2019; Wallenstein et al., 2006). Thus, to understand agricultural N_2O emissions and potential pathways to mitigation, it is essential to comprehend these specific biogeochemical processes and their controls.

Nitrification is an oxidation reaction performed by both heterotrophic and autotrophic microorganisms, and has traditionally been understood as the sequential oxidation of organic nitrogen (in the case of heterotrophic nitrification) into ammonia (NH_3) and ammonium (NH_4^+), hydroxylamine (NH_2OH), nitrite (NO_2^-), and finally nitrate (NO_3^-) (Butterbach-Bahl et al., 2013). However, there is some variation in literature in which specific N_2O producing pathways (biotic and abiotic) are grouped under the umbrella of nitrification. Understanding the drivers of N_2O production via nitrification therefore requires considering the controls of both its biotic and abiotic components.

Two pathways of N_2O production are linked to the product hydroxylamine. First, the oxidation of hydroxylamine by some microbes can result in the production of N_2O as a byproduct. Contrary to the accepted model of nitrification in prior years, recent evidence has shown that ammonia oxidizing bacteria (AOB) oxidize hydroxylamine to nitric oxide (NO), which in turn is abiotically oxidized to nitrite by oxygen (Caranto & Lancaster, 2017). At relatively high rates of hydroxylamine oxidation or relatively low rates of oxygen, the accumulation of NO results in biotic nitrite reduction to N_2O as a byproduct (Caranto & Lancaster, 2017; Hu et al., 2015; Schreiber et al., 2012). As this pathway is directly related to the overall rate of nitrification, then decreasing soil pH can be said to increase the rate of biotic N_2O production via nitrification (Hu et al., 2015). This pathway is also autotrophic, thus it does not directly depend on soil carbon availability, although some evidence indicates that high carbon availability preferentially favors heterotrophic activity (Wrage-Mönnig et al., 2018). Similarly, the ideal temperature for nitrification has been shown to exist near 35 °C (Grunditz & Dalhammar, 2001), meaning that N_2O production is positively associated with soil temperature throughout the realistic temperature range.

Second, before the oxidation of hydroxylamine by nitrifiers can take place, some portion of this intermediary may also chemically decompose to NO and N_2O. The abiotic production of N_2O from hydroxylamine is sometimes attributed to nitrification due to its unique role in producing hydroxylamine in soils (Butterbach-Bahl et al., 2013), while others describe this as a coupled biotic-abiotic process with distinct controls for each (Heil et al., 2015; Zhu-Barker et al., 2015). Determinations of where to draw this line may depend on the perspective of the work at hand: from a microbiological perspective it may be logical to group abiotic decomposition of hydroxylamine to nitrification, as nitrifiers are the only microorganism community necessary to produce N_2O through this pathway. On the other hand, when considering environmental controls of N_2O production it may instead be preferrable to consider the biotic and abiotic processes separately, given that the environmental conditions favorable to one may not necessarily overlap with those favorable to the other (Heil et al., 2015). This latter perspective is relevant to emissions modelers, and the one I take here. Optimal conditions of abiotic hydroxylamine oxidation are similar to biotic oxidation in that it is negatively correlated to carbon availability and positively correlated with temperature. Organic carbon competes with transition metals like manganese and iron to react with hydroxylamine (Bremner et al., 1980; Heil et al., 2015; Zhu-Barker et al., 2015), and while abiotic hydroxylamine oxidation has a much higher ideal temperature than biotic oxidation at 50+ °C (Heil et al., 2015), in realistic conditions both are expected to simply be positively correlated with temperature. However, a key difference exists in the optimal pH range between these two subprocesses. Hydroxylamine has a pKa of 5.95, meaning that in the soil system it will protonate to the more stable species NH_3OH^+ (Heil et al., 2015). Thus, chemical decomposition rates are highest at neutral or alkaline pH.

As is true of nitrification, denitrification is a broad category of biogeochemical processes, with alternate versions taking place by different organisms and under different conditions. The first is heterotrophic denitrification, which is performed by microbial communities that have been termed denitrifiers. This pathway is heterotrophic and anaerobic, and thus its production of N_2O is positively correlated with carbon availability and negatively correlated with oxygen availability (Wallenstein et al., 2006). Denitrification also has a high ideal temperature of ~55 °C (Benoit et al., 2015), and thus is effectively always positively correlated with temperature in soil. Soil pH has also been shown to positively correlate with the overall rate of denitrification (ŠImek & Cooper, 2002), yet high pH negatively impacts the final reduction of N_2O to N_2 by damaging the necessary enzyme (Y. Wang et al., 2018). As a result, emissions of N_2O via this pathway are negatively correlated with pH (Hu et al., 2015; ŠImek & Cooper, 2002).

Finally, some nitrifiers (namely AOB) contain nitrogen reducing functional genes in addition to their nitrification-related oxidizing genes, allowing them to perform a specialized process of denitrification under anaerobic conditions. This process is termed nitrifier denitrification, and differs from the heterotrophic denitrification pathway in that it does not involve nitrate, but rather begins the reduction process with nitrite produced by nitrification directly to nitric oxide (Butterbach-Bahl et al., 2013). This metabolic pathway is autotrophic, meaning that in contrast to traditional denitrification it is not limited by low carbon availability (Wrage-Mönnig et al., 2018). Nitrifier denitrification also varies in that its production of N_2O increases with pH, which may be related to increased nitrite accumulation in alkaline environments, providing an abundance of substrate for the reduction of nitrate to N_2O (Smith, 2017; Tierling & Kuhlmann, 2018). While not strictly anaerobic, as evidence has shown nitrifier denitrification to be a substantial contributor to N_2O emissions in aerobic soils (Butterbach-Bahl et al., 2013), this pathway is nonetheless greatly accelerated by low- though not zero- oxygen availability (Hu et al., 2015; Smith, 2017; Wrage-Mönnig et al., 2018).

In summary, N_2O production is largely controlled by four major factors- oxygen, nitrogen, pH, and carbon availability- through the various ways these factors impact microbial metabolic activity (**Table 1.1**). These major controlling factors can also be related to specific environmental and management events, which is critical to modeling efforts (Groffman et al., 1988; Wallenstein et al., 2006). For example, rather than attempting to consider soil oxygen content and diffusivity across several acres to understand the dynamics of aerobic and anaerobic metabolic processes, it becomes logical to step back and use broader proxies that are simpler to measure and model. Because water inhibits gas diffusion and occupies pore space that gases otherwise would, soil moisture can be considered to be strongly negatively correlated with oxygen availability and thus used as its proxy (Groffman et al., 1988).

Taking yet another step back, soil moisture is strongly controlled by precipitation and/or irrigation, and thus in the absence of measuring soil moisture directly, these factors can be used as second-order proxies. However, each step further removed results in some loss in information: precipitation may largely control soil moisture, but soil texture and cover will also play a role in infiltration and water holding capacity. Thus, there is a tradeoff between the simplicity of measuring these more distant controlling factors and the number of factors that must be

Table 1.1: Major soil N_2O producing processes and their key drivers.

Process	Nitrogen Substrate	Carbon Availability	Oxygen Availability	Temperature	pH
Nitrification (byproduct of ammonia oxidation)	NH_2OH	Low/Neutral (Wrage-Mönnig et al., 2018)	Moderate (Caranto & Lancaster, 2017)	~35 °C (Grunditz & Dalhammar, 2001)	Acidic (Hu et al., 2015)
Chemical Decomposition of Hydroxylamine	NH_2OH	Low (Heil et al., 2015)	-	50+ °C (Heil et al., 2015)	Alkaline (Heil et al., 2015)
Heterotrophic Denitrification	NO_3^-	High	Low	~55 °C (Benoit et al., 2015)	Acidic (Hu et al., 2015)
Nitrifier denitrification	NO_2^-	Neutral/Unknown (Wrage-Mönnig et al., 2018)	Low (Hu et al., 2015)		Alkaline (Hu et al., 2015; Tierling & Kuhlmann, 2018)

measured to accurately represent the dynamics of the proximal controlling factor (Groffman et al., 1988).

Hot moments and their environmental drivers

Hot moments are events during which the rate of biogeochemical reactions sharply rise above the predominant rate over longer time periods (McClain et al., 2003). These dramatic changes to reaction rates are driven by sudden changes to the environment, as microbial activity and population dynamics are controlled by environmental conditions. In the case of N_2O, hot moments describe periods of anomalously high N_2O emissions which may be produced by multiple pathways. However, empirical evidence from field trials, isotopic labeling, microbial genetic analysis, and knowledge of drivers of specific biogeochemical pathways indicates that certain environmental changes have the greatest impact on hot moments in agroecosystems. Knowledge of these environmental and biological drivers is key to improving models of N_2O hot moments, which is urgently needed to improve overall N_2O estimations and informing mitigation efforts (Groffman et al., 2009; Wagner-Riddle et al., 2020).

The most important driver of N_2O hot moments is often considered to be oxygen availability, as oxygen's role as the preferred electron acceptor causes it to play the role of a fulcrum for various microbial metabolic pathways (Butterbach-Bahl et al., 2013; Hu et al., 2015; Zumft, 1997). Three of the four most important N_2O producing pathways have the potential to increase their rates with a decrease in oxygen from aerobic conditions: heterotrophic denitrification is an obligate anaerobic process (Zumft, 1997), nitrifier denitrification proceeds most efficiently under low oxic conditions (Hu et al., 2015; Wrage-Mönnig et al., 2018), and even enzymatic N_2O production by nitrification is highest under moderate oxygen availability (Caranto & Lancaster, 2017). The most common event which decreases soil oxygen availability is soil wetting, for example through precipitation or irrigation, in which water displaces oxygen in the pore spaces. Thus, wetting events have been shown to be critical triggers of hot moments (Anthony & Silver, 2021; Barrat et al., 2021, 2022; Smith, 2017; Wagner-Riddle et al., 2020). A thawing of aboveground snow and frozen soil water can also suddenly increase soil moisture to induce hot moments (Luo et al., 2025; X. Wang et al., 2023). Finally, rapid aerobic microbial activity induced by an increase in oxygen or substrate availability, such as cover crop incorporation, tillage, or fertilization, can also lead to the consumption of soil oxygen to the point of anoxia (Lussich et al., 2024).

Hot moments also depend on sufficient substrate availability for N_2O producing reactions. Measuring this substrate availability directly, such as soil nitrate content, typically requires destructive soil sampling and lab analysis, which is time consuming and expensive particularly at scale. Thus, models often use proxies for these controlling factors. The most obvious proxy for mineral nitrogen content is fertilization, which directly adds a known quantity of nitrogen to the soil system and the losses of which over time can be estimated (Li & Culver, 2022; Saha et al., 2021a). Fertilizer-related hot moments are major drivers of total agricultural N_2O emissions (Anthony & Silver, 2021; Tierling & Kuhlmann, 2018; Wagner-Riddle et al., 2020; C. Wang et al., 2021), and fertilization is particularly important to estimating the magnitude of hot moments (Fuchs et al., 2020; Scheer et al., 2014; Smith, 2017). Freeze-thaw events also create dramatic shifts in substrate availability, as the thawing of frozen water releases trapped nitrogen and reconnects water-mobile microbes and substrates to instigate a flurry of microbial activity (Wagner-Riddle et al., 2020; X. Wang et al., 2023). Freeze-thaw induced hot moments have been shown to be significant contributors of overall N_2O emissions in temperate climates (Groffman et al., 2009; Risk et al., 2013; Smith, 2017; Wagner-Riddle et al., 2017; C. Wang et al., 2021).

Beyond freeze-thaw events, temperature also plays an important modulating influence on hot moments that can affect their magnitude or even circumvent a hot moment when conditions are otherwise conducive (Krichels & Yang, 2019). Microbial activity rates are correlated with temperature, and the reaction rates of metabolic processes (including the production of N_2O) increases up to a certain optimal temperature (Benoit et al., 2015; Parton et al., 1996; Stanford et al., 1975). Thus, while wetting events create anoxic conditions favoring key N_2O producing pathways, the temperature controls the rate at which these processes will proceed. Wetting events which occur in warm temperatures are likely to induce hot moments, while those that occur in winter may produce smaller hot moments or none at all as a result of the temperature's inhibition of microbial processes (Krichels & Yang, 2019)

To summarize, soil water, temperature, and nitrogen availability together can explain nearly all temporal variability of N_2O flux in a given field (Butterbach-Bahl et al., 2013). In turn, hot moments are driven primarily by a handful of environmental and management events, such as precipitation, irrigation, fertilization, tillage, and thawing.

Anomaly detection

Measurement data of soil N_2O emissions typically exhibits a heavy-tailed distribution which results from the pattern of relatively stable, low-level background emissions transpiring throughout the majority of time and interrupted by high magnitude, relatively infrequent hot moments (Yates et al., 2006). As discussed, hot moments are key events worthy of identification and further study due to their disproportionate contributions to overall soil GHG emissions and their origination from shifts in environmental conditions altering biogeochemical dynamics. Isolating these events of interest from the rest of the data is a necessary step in pursuit of these goals.

One method of doing so makes us of hot moments' nature as outliers, or anomalous, in comparison to background emissions. Anomaly detection (AD), also often referred to as outlier detection, is an area of statistics which seeks to identify data points that do not conform to expected behavior. (Pasha & Umesh, 2013). The terms "outlier" and "anomaly" are often used interchangeably, yet important distinctions exist. While both terms describe data which does not follow normal or expected behavior, the cause of this unexpectedness determines which is the most appropriate usage. 'Outlier' is the more general term which simply describes deviant data which could be caused by noise, error, or unexpected behavior. 'Anomaly' more specifically describes a special kind of outlier which arises from a rare, novel, or unexpected intervening event and which may be of key interest (Aggarwal, 2017). 'Outlier' typically describes data which requires cleaning or correcting, while 'anomaly' describes accurate data which follow different patterns than the majority of data and often require further investigation (Fernández et al., 2022). I describe hot moments as 'anomalies,' rather than outliers which they have also been described as, to more precisely reflect that these data are the result of biogeochemical shifts distinct from noise or error.

AD fundamentally consists of two tasks: a method of quantifying how anomalous each point is within a dataset, and the establishment of a decision threshold which divides points beyond the threshold as anomalies and points within the threshold as inliers (Fernández et al., 2022). There are several available methods for performing anomaly detection, each with different methods of quantifying the "anomalousness" of points or how to draw the decision threshold, and each with strengths and weaknesses that should be considered when selecting a method. As the field of AD has advanced, it has become increasingly common for methods of AD to be identified and even developed based on specific research goals and the nature of data at hand (Singh & Upadhyaya, 2012). Because there are infinite combinations of distribution behaviors, especially across multiple variables, as well as unique goals, there is no universally optimal AD method. Rather, proper AD requires the formulation of a problem, assessment of the available data, and the matching of a specific method to the problem and dataset.

There are many factors to consider when selecting an AD method. One is the distribution of data: many of the most commonly used AD methods require the assumption of normally distributed data. Such methods include Z-score, Grubb's Test, and Dixon's Test (Bendre & Kale, 1987). If the distribution of data is non-normal, alternative methods applicable to a wide variety of distribution patterns should be used.

Another consideration is variability of the extremeness of anomalies amongst diverse datasets. The presence of anomalies affects some measures of the distribution of data, including the mean and standard deviation. When the presence of many or extreme anomalies affects metrics used by an AD method to set a decision threshold such that true but less extreme anomalies fall below the decision threshold, it is said that these lesser anomalies were 'masked' by the presence of other outliers (Ben-Gal, 2005; Rousseeuw & Hubert, 2011). Dixon's test, Grubbs's test, and standard deviation are susceptible to this 'masking' effect, and thus caution should be used if the proportion of true anomalies is unknown (Bendre & Kale, 1987). In contrast, if an AD method is minimally affected or unaffected by the presence of multiple anomalies, it is said to be 'robust.' Popular examples of 'robust' methods include IQR and mean absolute deviation (MAD) (Andreou & Karathanassi, 2014; Rousseeuw & Hubert, 2011)

Relatedly, an AD method may also fail when the true proportion of anomalies is unknown or variable if it assumes a specific proportion of anomalies. For example, the use of percentiles as decision thresholds for AD will definitionally result in the classification of a certain percentage of data points as anomalies regardless of the true portion of anomalies, as these methods set a threshold at a specific percentile and classify all data which falls above that percentile as anomalies. If the true proportion of anomalies, also called the 'contamination rate,' is variable, then it will either overclassify or underclassify anomalies at a rate equal to the difference between the actual and assumed contamination rate (Hampel, 1971; Rousseeuw & Hubert, 2011). A useful method of AD must be able to dynamically adjust the proportion of points it classifies as anomalies in response to differences in the data's distribution, or else it cannot be useful in detecting hot moments across multiple datasets with varying underlying temporal flux variability. There are also multiple types of anomalies, the most common being global point anomalies and contextual anomalies (**Figure 1.1**) (Ben-Gal, 2005; Chandola et al., 2009; D & Babu, 2016). Global anomalies are the simplest to detect, and the majority of research on AD has focused on these types of anomalies (Smiti, 2020). At its most basic level the identification of global anomalies only requires comparison of a single univariate data point to the distribution and behavior of the univariate dataset to which it belongs. The detection of contextual anomalies, however, depends upon the consideration of additional contextual and behavioral attributes, requiring the use of multivariate data (Smiti, 2020). At minimum, the detection of contextual anomalies requires a univariate dataset plus some additional quantification of the context of each data point, such as the sequential order or temporal position. For example, a mean monthly temperature of 20 °C may not be considered anomalous for the city of Knoxville, Tennessee. However, if additional context is added to the data point providing the context that a mean annual temperature of 20 °C was observed in the month of February, this data point could then be considered anomalous given its context of occurring during winter.

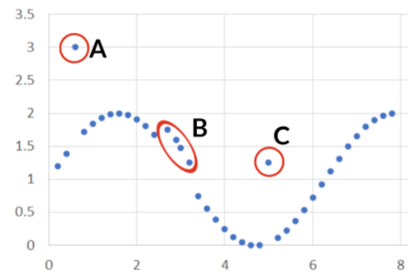

Figure 1.1: Types of outliers. A) global outliers occur where data points deviate significantly from the distribution or behavior of the data set; B) collective outliers are groups of points which when considered together are anomalous, but not individually; C) contextual outliers are anomalous due to their position in relation to the neighbors

Research gaps and implications

Many uncertainties remain surrounding hot moments, their significance, and how best to represent them in models. At the heart of these uncertainties is the lack of consensus in how to systematically identify N_2O hot moments within measurement datasets- an essential preliminary step in any quantitative analysis of hot moments (Bernhardt et al., 2017). A handful of statistical methods have been used for this task previously, though no comprehensive comparative analysis has been performed, despite widely different conclusions about the impact and prevalence of hot moments being drawn from different methods (Molodovskaya et al., 2012). Very few large scale synthesis analyses of hot moments exist, and I have identified none that have attempted to model hot moments across multiple sites and experiments. This is likely due to the uncertainty around the use of statistical methods to identify hot moments, and the prohibitive difficulty and time investment of manually identifying them across large datasets. The accurate, consistent identification of hot moments within datasets would open new doors of investigation. For example, the complex and varied environmental conditions which give rise to these events could be more comprehensively distinguished and described. This may in turn, for example, permit the distinct modeling of N_2O emissions under hot moment and background emissions, in recognition of the differential underlying biogeochemical dynamics. If the occurrence of hot moments could be predicted, this could address known shortcomings of existing models underestimating hot moments, and lead to improved quantitative modeling of N_2O emissions. Such advancements would hold significant implications for both models and predictions of agriculture's climate impact and the implementation of management intervention strategies.

My work will take up this challenge. I will begin with the investigation of statistical methods for the identification of flux measurements consistent with the hot moment concept, comparing their performances, strengths, and weaknesses in classifying fluxes in accordance with qualitative descriptions of hot moments in surrounding literature. Next, I will exemplify the opportunities to build upon this work by leveraging statistical hot moment identification toward modeling and predicting the occurrences of hot moments from environmental information. I will also further the knowledge of environmental drivers of hot moments by investigating the impact of extreme weather events on N_2O emissions. Together, the work described in this dissertation will advance the ability to quantify and predict agricultural N_2O emissions and point toward a path to effective mitigation efforts.

CHAPTER 2: STATISTICAL IDENTIFICATION OF NITROUS OXIDE HOT MOMENTS AND THEIR SIGNIFICANCE ACROSS GLOBAL AGROECOSYSTEMS

A version of this chapter was previously submitted for publication to Journal of Geophysical Research: Biogeochemistry. Ryan Ackett was responsible for conceptualization, formal analysis, investigation, methodology, software, and writing. Debasish Saha. Ilya Gelfand, and Haileab Hilafu provided input on methodology, review & editing.

Abstract

Nitrous oxide (N_2O) emissions from agricultural soils contribute ~4% of total anthropogenic greenhouse gasses (GHG) emissions globally. Events known as 'hot moments' can occur following environmental changes that favor N_2O production, which contribute disproportionately to annual cumulative emissions. Despite their significance, hot moments have not been statistically well defined, particularly on a global scale. We collected 13,787 soil N_2O flux measurements from 42 publications and evaluated 14 methods of statistical anomaly detection for their ability to identify hot moments within datasets. Two methods achieved highest overall performance by Matthews correlation coefficient (MCC): median absolute deviation (MCC: 0.80) and minimum covariance determinant (MCC: 0.80), the latter which also performed evenly across highly dissimilar datasets and identified more difficult-to-detect contextual hot moments than other top overall performers (39%). Interquartile range, which has previously been used and recommended, performed poorly when hot moments were either very rare or very common within a dataset, and identified few local hot moments (14%). Overall, hot moments comprised ~19% of measurements while contributing ~75% of cumulative emissions. The median background N_2O emission reported in all datasets was 2.2 g N ha^{-1} day^{-1}, while the median hot moment emission was 10x higher, ranged from 23 to 25 g N ha^{-1} day^{-1}. These findings advance knowledge of how to accurately define and identify hot moments globally - a crucial task to investigating and mitigating these critical biogeochemical events.

Introduction

Anthropogenic emissions of nitrous oxide (N_2O) have grown rapidly since the preindustrial period and contributed ~4% of the total greenhouse gas (GHG) emissions in 2019, predominately from fertilized croplands (EPA, 2023; Hénault et al., 2012; IPCC, 2022; Mosier et al., 1998; Thompson et al., 2019; Tian et al., 2019). As climate externalities already threaten global yields and food systems (Ray et al., 2019), achieving a sustainable future requires a wide variety of strategies to efficiently manage soil nitrogen in agriculture without sacrificing global food security (Erisman et al., 2008).

One key avenue in pursuit of this goal lies in the distinct pattern in which N_2O is emitted over time from agroecosystems (Wagner-Riddle et al., 2020). These emissions most often maintain relatively stable and low-level rates which are globally estimated to be about 2-3 g N ha^{-1} day^{-1} (Yin et al., 2022). However, changes in environmental conditions can create "short periods of time that show disproportionately high reaction rates relative to longer intervening time periods" (McClain et al., 2003), raising emissions by orders of magnitude (Butterbach-Bahl et al., 2013; Clayton et al., 1997; C. Huang, 2020; H. Huang et al., 2014; Johnson, 2021; McClain et al., 2003; Molodovskaya et al., 2012; Sistani, 2020; Wagner-Riddle et al., 2020). These distinct periods are termed 'hot moments,' and have been shown to have outsized and even preeminent importance on overall emissions (Anthony & Silver, 2021; Molodovskaya et al., 2012; Wagner-Riddle et al., 2017; X. Wang et al., 2023), thus attracting attention for further investigation into their prevalence, significance, drivers, and potential mitigation strategies (Venterea et al., 2012; Wagner-Riddle et al., 2020).

To precisely answer such questions as "how often do hot moments occur, and how much do they contribute to total emissions?" the qualitative definition given above for hot moments must be translated into to a quantitative framework. Considering that hot moments are by definition anomalous events, researchers have attempted to do this using "anomaly detection" (Anthony & Silver, 2021; Corre et al., 1996; Molodovskaya et al., 2012; Stuchiner et al., 2025), which uses statistical methods to classify data as either within expected behavior or anomalous (Pasha & Umesh, 2013). However, there exist a large and growing number of methods of anomaly detection, each with particular capabilities, strengths, weaknesses, and methods of measuring "anomalousness," and their selection has a large impact on which and what proportion of the data are classified as anomalies, or in this case hot moments (Ben-Gal, 2005; Chandola et al., 2009; Domingues et al., 2018; Molodovskaya et al., 2012). Differences in statistical anomaly detection methods alone have resulted in widely varying estimates of hot moment prevalence, ranging from 2-18% within the same dataset (Molodovskaya et al., 2012). This variation raises a critical question: which method best aligns with our understanding of N_2O hot moments within a given context?

This uncertainty has led to a lack of scientific progress stemming from hesitance to apply numerical methods, and some to therefore question the very usefulness of the concept (Bernhardt et al., 2017). Bernhardt et al. (2017) point out that discussions of hot moments have been predominately qualitative, always suggesting the importance of these phenomena yet rarely quantifying it or suggesting a clear path to applying this concept toward solutions. Yet statistical anomaly detection is commonly and effectively applied across a wide range of fields to identify key events, with the caveat that the method selected should be evaluated for its appropriateness within a specific context (Ayadi et al., 2017; Dastjerdy et al., 2023; Robinson et al., 2005; Russo et al., 2021; Singh & Upadhyaya, 2012). What has been holding back advancements in quantitative research around biogeochemical hot moments is not a flaw in the concept, rather a lack of systematic evaluation of potential statistical methods of hot moment identification for their suitability, taking into account the specific nature of the data.

To date, the quantitative methods used and evaluated have prioritized familiarity over suitability, gravitating toward methods like standard deviation and interquartile range (IQR; e.g., 1.5 IQR) which, while simple to compute, have key weaknesses in the context of hot moment identification. For example, anomalies can be considered 'global,' or anomalous within the entire dataset, or 'local,' or anomalous only within the context of neighboring data (see Text S2) (Ben-Gal, 2005; Chandola et al., 2009). All prior analyses have used univariate methods which were only capable of identifying global anomalies, while we argue that because hot moments are contextual in nature, methods with the capacity to identify both global and temporally local anomalousness may have significant advantages in their ability to accurately identify off-season hot moments of smaller magnitudes.

Moreover, the magnitude and frequency of hot moments also varies significantly with climate, management, season, and other factors (Groffman et al., 1988; Groffman et al., 2009). Both high magnitude and frequency of anomalies can distort the data characteristics used by many anomaly detection methods to measure anomalousness (such as the mean, standard deviation, and quartiles) and can lead to 'masking' of smaller anomalies or a statistical 'breakdown point' (see Text S3), resulting in false negatives (Hampel, 1971; Rousseeuw & Hubert, 2011). Methods that use these susceptible characteristics, like IQR and standard deviation, have been shown to have a poor ability to identify small and moderate hot moments within datasets where hot moments are relatively more common or significant, such as those which sample during early Spring (Stuchiner et al., 2025). To date, limited studies have systematically evaluated how the performance of statistical hot moment identification may be affected by variations in hot moment magnitude and frequency, nor have they thoroughly assessed methods that are robust against such variations (Hubert et al., 2018; Leys et al., 2013; Rousseeuw & Hubert, 2011).

This study moves beyond previous research in three key aspects: first, we evaluate novel methods of statistical hot moment identification, including those which are highly robust to distortion by anomalies and which are capable of considering the temporal context of measurements. Second, we make use of a highly diverse and global database, ensuring that results are not overfit to particular data characteristics. Third, we expand our evaluation approach to independently measure the ability of each method to detect local anomalies. Furthermore, we evaluated how variations in hot moment prevalence and measurement frequency impacts hot moment detection performance of each method. By demonstrating which methods are most suitable and broadly applicable for hot moment identification, we hope to provide confidence in the advancement of quantitative research on soil N_2O biogeochemical hot moments to facilitate implementing effective mitigation strategies.

Materials and Methods

Data collection and diversity of N_2O flux distribution

A global database was compiled from a collection of 44 peer reviewed publications, Greenhouse gas Reduction through Agricultural Carbon Enhancement network (GRACEnet) experiments, and Ag Data Commons datasets published between 1997 and 2024. For inclusion, experiments must have measured N_2O flux for at least 90 days and to have reported no fewer than ten measurements. Data preprocessing was performed to extract data from publications and transform it into a universal structure (**Figure 2.1**). When complete tabular data was not openly accessible, N_2O flux and relevant environmental measurements were extracted from the text and from graphical figures using WebPlotDigitizer (Rohatgi, 2022). Because most published

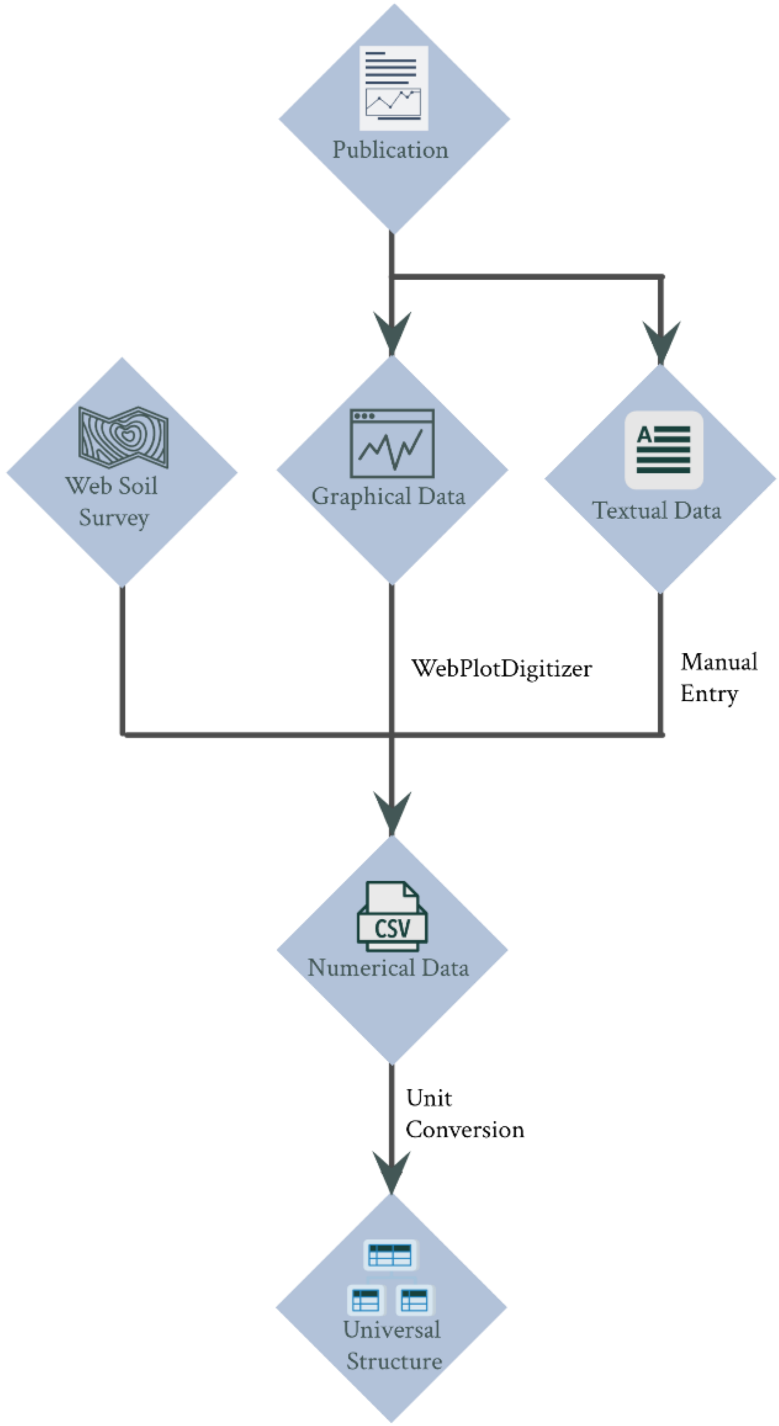

Figure 2.1: Schematic diagram of data collection process from published work and preprocessing steps.

experiments reported N_2O flux as the daily average, we used this temporal resolution as the basis for this analysis. When greater temporal resolution was provided, measurements were scaled to average daily flux values. Additional data from each experiment were gathered when reported, including site location, crop species, soil texture, and fertilization information. When not reported by the authors, the soil texture information was gathered from the Web Soil Survey based on geographical coordinates of the study (Soil Survey Staff, NRCS, 2019).

In total, 34 unique agricultural sites around the globe were represented (**Figure 2.2**). Field sites represented eight out of 12 USDA soil texture classes (**Figure 2.3a**), most commonly loams, silt loams, and clay loams. Nitrogen fertilizer application rate predominately ranged from near 0 to 200 kg N ha^{-1} (with an additional six extreme applications ranging from 300 to 430 kg N ha^{-1}) from diverse forms including organic, inorganic, and environmentally enhanced nitrogen (EEN) fertilizer, which includes slow-release, urease and nitrification inhibitor technologies (**Figure 2.3b**). Finally, the diverse representation of experimental methods, crops, soils, and global locations resulted in corresponding diversity in daily flux measurements, reaching up to ~1500 g N ha^{-1} d^{-1} (**Figure 2.4**). In agreement with prior analyses, N_2O fluxes followed a heavy-tailed distribution (Yates et al., 2006), and had a mean daily average flux of 13.5 g N ha^{-1} d^{-1} and a median of 3.3 g N ha^{-1} d^{-1} .

Supervised and contextualized identification of hot moments

There are three methods for evaluating the performance of anomaly detection methods for a specific task: unsupervised, semi-supervised, and supervised, which differ in how and if they use "ground truth" data labels. Supervised and semi-supervised methods calibrate their statistical classifications against "true" data labels determined by leveraging additional contextual information and domain knowledge of experts to individually classify each datum as

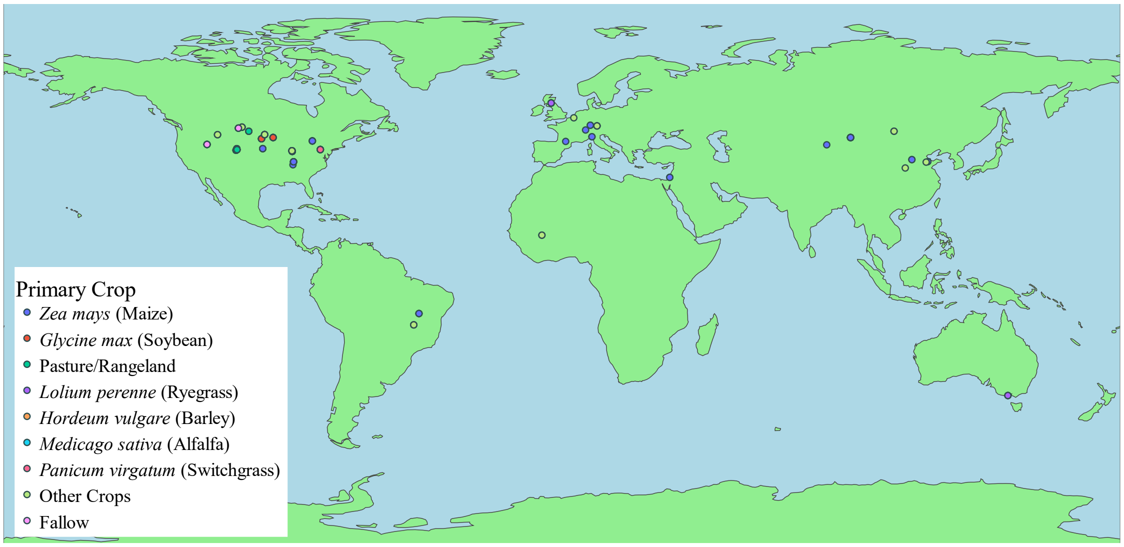

Figure 2.2: Distribution of experimental sites and the primary crops grown at each site across the globe. Many sites performed multiple treatments or experiments using multiple crops. The numbers of time series data for each primary crop includes: 89 *Zea mays*, 18 *Glycine max*, 14 grassland, 9 *Lolium perenne*, 8 *Hordeum vulgare*, 4 *Medicago sativa*, 4 *Panicum virgatum*, 4 fallow, and 20 other various upland crops.

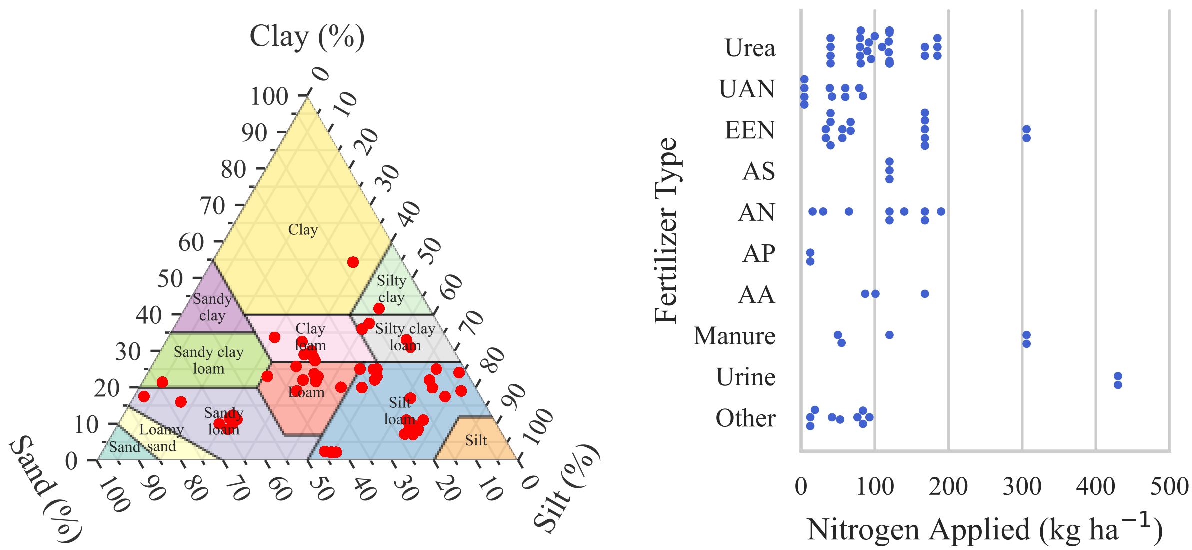

Figure 2.3: (a) Soil texture observed across the experimental sites, with frequent representation of loam, silt loam, clay loam, and silty clay loam soils (left panel). (b) Rate and nitrogen form used in fertilization events which occurred following experiment commencement (right panel). Diversity of fertilizer types is represented, including urea, urea ammonium nitrate (UAN), environmentally enhanced nitrogen (EEN), ammonium sulfate (AS), ammonium nitrate (AN), ammonium phosphate (AP), anhydrous ammonia (AA), livestock urine, manure, and other unreported fertilizer forms.

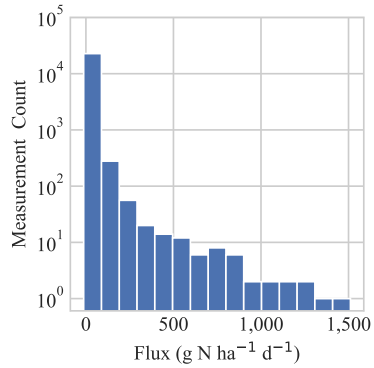

Figure 2.4: Distribution of daily average N_2O flux magnitudes across the entire dataset. Bin width is 100 g N ha^{-1} d^{-1}. Flux values near zero were orders of magnitude more common than higher flux values, and flux values become rarer with increasing magnitude up to 1500 g N ha^{-1} d^{-1}.

characteristic of an inlier or anomalous. The unsupervised method foregoes calibration with data labels and instead assumes that anomalies are always very rare (Chandola et al., 2009; Paulheim & Meusel, 2015). The use of trusted data labels in supervised methods has been shown to improve the accuracy of anomaly detection compared to unsupervised methods when applied to the same environmental datasets. This improvement is often attributed to the complex nature of anomalies varying over time, non-normal data distribution, and context dependent drivers of anomalies in such datasets (Russo et al., 2021). Given that temporal N_2O fluxes and hot moments are a perfect example of this description, we chose to generate data labels to enable the use of a supervised approach for this analysis.

We convened to deliberate upon the labeling of each datapoint as either characteristic of a “hot moment” or “background emission” as defined by McClain et al. (2003). Each time series was considered individually as hot moments are contextual and background emissions levels may vary across regions, crops, or other experimental factors (Yin et al., 2022). Decisions were made in the context of environmental and site information which provided insight into the biogeochemical conditions from which emissions resulted, including air and soil temperature, soil moisture, precipitation, crop species, time of year, and nitrogen fertilizer applications. Hot moments are driven by changes to the environment which affects rates of biogeochemical reactions (McClain et al., 2003), and thus we looked for evidence of such events in our data labeling process. We also wished to distinguish between elevations in flux attributable to random noise and decisive increases in N_2O production rates. Thus, when available (about half of all datasets), the standard error (SE) of each daily average N_2O flux measurement was also considered in decision making.

This information was incorporated into a separate time series figure of each experimental treatment dataset with the average daily flux (g N ha^{-1} d^{-1}) and SE portrayed on one graph and soil temperature, air temperature, soil volumetric water content, and soil water filled pore space were graphed whenever available and temporally scaled to the flux data (**Figure 2.5**). The authors analyzed each data point across 170 constructed graphs, contextualized it within neighboring flux and environmental trends, and labeled it as either a “true” hot moment or background emission (hereafter referred to as data labels). The Labeling process was objectively reviewed three times before finalization to minimize subjectivity.

Anomaly detection methods

We evaluated 14 anomaly detection methods, including the previously proposed 1.5 IQR, 3 IQR, 75^{th} percentile methods, Isolation Forest, and four standard deviations above the mean, along with nine methods that have not yet been explored in biogeochemical hot moment detection (**Table 2.1**). Methods represented a diverse array of categories defined by the underlying strategies used to define “anomalousness,” such as density, distance, probability distribution, and time series analysis. The PyOD (Zhao et al., 2019) python package was used to perform anomaly detection using each of the methods except Arima and Moving Average, which were computed

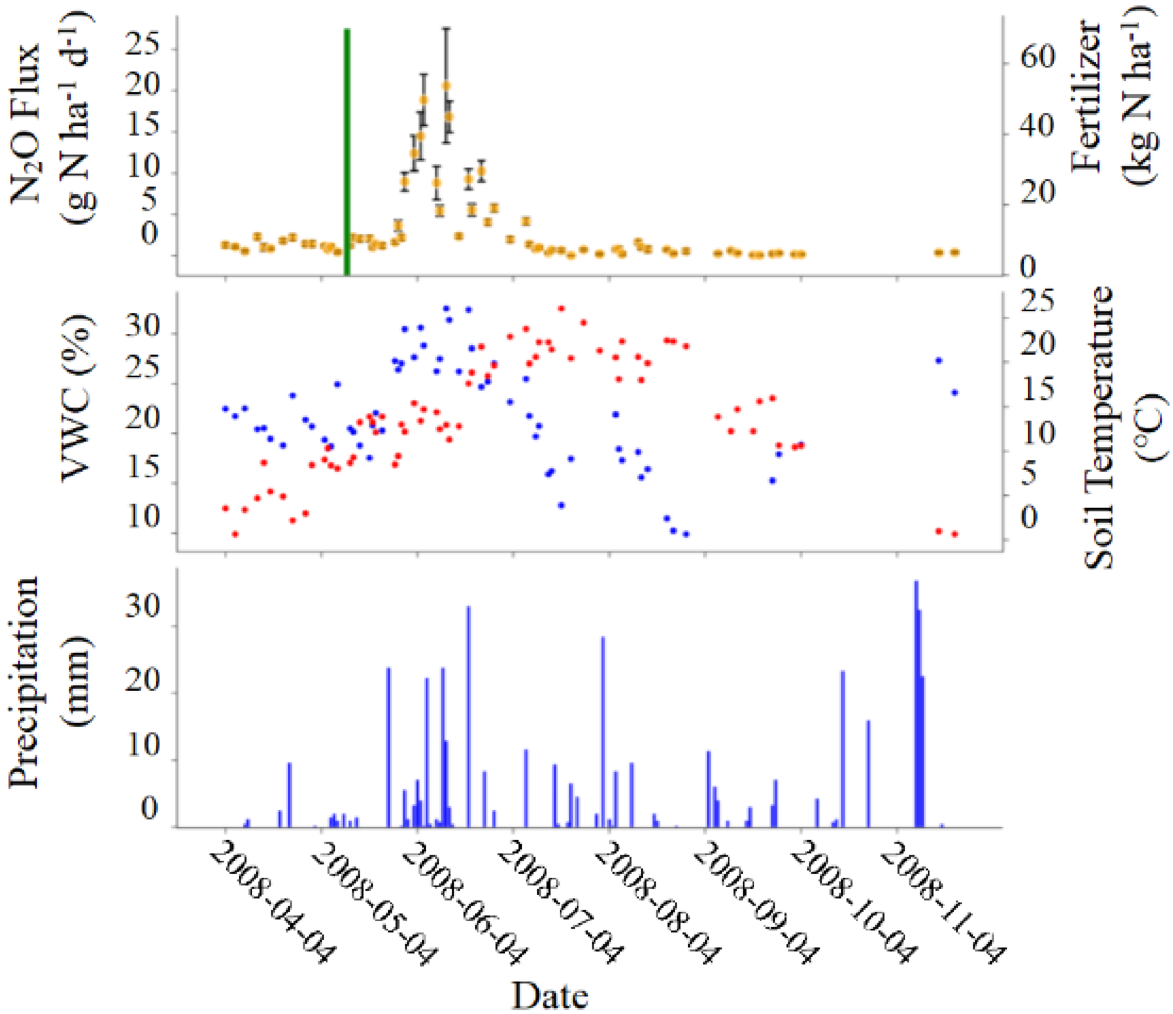

Figure 2.5: An example of data visualization for the hot moment labeling process. In this graph, N_2O emissions (orange dots, top panel) remain at a consistent background level until approximately June 4. After this date, the combination of high and frequent precipitation (bottom panel) raising the soil moisture (middle panel, blue dots) and a recent fertilizer application (green line, top panel) in the early summer led to a significant rise in emissions consistent with a hot moment. Emissions fluctuate for one month until about July 4, corresponding to fluctuations in soil moisture driven primarily by three large precipitation events above 20 mm per day. After July 4, the soil moisture remained comparatively low, and emissions gradually stabilized at a consistent background level.

Table 2.1: Novel anomaly detection methods evaluated for hot moment identification categorized by the method used to quantify the "anomalousness" of points.

Method	Category	Brief Description
Angle Based Outlier Detection (ABOD)	Density	Determines the variance of the angles between vectors from each point to other points, where narrower angles relate to a greater likelihood of being an anomaly.
ARIMA	Time Series	Decomposes a time series to identify patterns, forecasts based on past trends, and calculates anomalousness based on the residual of predicted and actual values.
Copula Based Outlier Detection (COPOD)	Probabilistic	Uses copulas, or a multivariate cumulative distribution function with a uniform marginal distribution across dimensions, to predict tail probabilities and assign anomaly likelihood to each point in a dataset.
Histogram Based Outlier Score (HBOS)	Other (Histogram)	A histogram is constructed for all dimensions of a dataset, where a low frequency of a bin indicates a higher likelihood that observations within that bin are anomalies.
k-Nearest Neighbors (KNN)	Density	Measures the distance to k nearest points, where a higher sum relates to a greater likelihood of being an anomaly.
Local Outlier Factor (LOF)	Density	Calculates the density of each point by averaging the density of each of k neighbors.
Median Absolute Deviation (MAD)	Distance	MAD calculates the median residual within the dataset, and a threshold is set using a Z-score based on this value above which data points are classified as anomalies.
Minimum Covariance Distance (MCD)	Distance	Identifies the data subset with the smallest covariance determinant, then determines the Mahalanobis distance of each point from the subset mean where a higher distance is related to a greater likelihood of being an anomaly.
Moving Average	Time Series	Euclidian distance from the moving average of the previous *n* data points.

using pyOATS (Ye, 2024), and IQR, standard deviation, and 75th percentile, which were computed using NumPy (Harris et al., 2020). For univariate methods, such as IQR and MAD, only a list of daily average N_2O flux values were provided to each algorithm. Multivariate methods, such as KNN and MCD, received two-dimensional datasets including the average daily N_2O flux and the number of days since experiment commencement, which added some chronological information helpful in identifying local anomalies without receiving any additional information related to environmental contexts.

Data handling for training and testing

To prevent overfitting and data leakage from the optimization process, data was split into training and testing subsets. Since hot moments are relative and contextual, the 170 time series datasets were randomly and evenly divided as complete time series into training and testing subsets. Then, anomaly detection was performed on each time series individually, totaling 85 iterations, such that the spatial and temporal context was left intact when classifying hot moments. Model optimization, including hyperparameter tuning and threshold tuning (discussed below), was performed using the training dataset. Final model performance metrics were then evaluated and reported using the testing dataset.

Method tuning

Anomaly detection methods are comprised of two parts, each of which can be tuned to achieve optimal performance: a method of quantifying the degree of "anomalousness" of each data point (which may involve the use of hyperparameters), and a decision threshold below which data are classified as inliers and above which data are classified as anomalies (**Table 2.2**).

We first used a grid search to identify the optimal hyperparameter combination, determined by highest average precision (Equation 1). Average precision is the area under the precision-recall

Table 2.2: Parameters for the implementation of anomaly detection methods optimized for performance across a diverse range of datasets. All parameters used by methods which are not shown here were set to their default values in their respective pyOD (Zhao et al., 2019) and pyOATS (Ye, 2024) implementations.

Method	Package	Hyperparameters	Decision Threshold
Angle Based Outlier Detection (ABOD)	pyOD	method: 'fast' n_neighbors: 75	-0.00003453
ARIMA	pyOATS	p: 1 d: 1 q: 0	4.2181
Copula Based Outlier Detection (COPOD)	pyOD		3.2736
Histogram Based Outlier Score (HBOS)	pyOD	n_bins: 40 alpha: 0.9 tol: 0.5	0.2545
Isolation Forest (IF)	pyOD	n_estimators: 150 max_samples: 10 max_features: 2 bootstrap: False	0.03852
k-Nearest Neighbors (KNN)	pyOD	n_neighbors: 10 method: 'mean' metric: 'manhattan'	8.6769
Local Outlier Factor (LOF)	pyOD	n_neighbors: 17 algorithm: 'kd_tree' metric: 'manhattan' leaf_size: 10	1.0997
Median Absolute Deviation (MAD)	pyOD		2.0247
Minimum Covariance Distance (MCD)	pyOD		16.9729
Moving Average	pyOATS	window: 1	0.7465

curve which graphs the precision (the fraction of correctly identified anomalies among all predicted anomalies) and recall (the fraction of correctly identified anomalies among all true anomalies) at possible decision thresholds (Saito & Rehmsmeier, 2015; Su et al., 2015). This metric is useful in identifying the predictive power of a model or method when no specific decision threshold is yet determined. Optimal hyperparameters were then used to score the anomalousness of all data in each training dataset. Finally, the optimal decision threshold was determined to be that which resulted in the highest Matthews Correlation Coefficient (MCC, Equation 2) on the training dataset scored with optimal hyperparameters. MCC, derived from the confusion matrix (True Positive, TP; True Negative, TN; False Positive, FP; and False Negative, FN), gives a high score when all four confusion matrix outcomes are high, and is more informative and rigorous than other metrics for imbalanced datasets (Boughorbel et al., 2017; Chicco & Jurman, 2020, 2023). MCC is also equivalent to Pearson's Correlation Coefficient using binary values.

$$Average\ Precision = \int_0^1 Precision(t)d[Recall(t)]$$

Equation 1

$$MCC = \frac{TP * TN - FP * FN}{((TP + FP)(TP + FN)(TN + FP)(TN + FN))^{0.5}}$$

Equation 2

Evaluating the performance of hot moment identification methods

The overall performance of each anomaly detection method was evaluated using the MCC. While we pose that MCC is thus the most valuable representation of the overall predictive power of methods, we supplementally determined the average accuracy of each method, calculated by the mean accuracy achieved across the 85 time series in the testing dataset.

We argue that a statistical method of identifying hot moments should perform comparably across datasets with varying flux distribution characteristics to ensure broader applicability with minimum bias. Therefore, we determined how measurement frequency and anomaly prevalence in datasets affect method's classification accuracy, measured by the slope and R^2 of linear regression at a 5% significance level.

Beyond overall performance, we evaluated each method for its detection rate of local anomalies, which we defined as N_2O emissions measurements labeled as hot moments which were lower than other data points within a given dataset classified as background emissions. For example, a winter thaw may cause a conspicuous rise in fluxes compared to the typical seasonally low fluxes. However, They may not exceed the background rate of emissions during summer which can be elevated for a period of several weeks due to favorable environmental conditions and substrate availability, thus making this a 'local' anomaly (Waldo et al., 2019). We argue such a case is still an ecologically significant hot moment driven by distinct biogeochemical mechanisms and should be identified as such. Thus, we additionally evaluated the local anomaly detection rate of each method as the proportion of the total local hot moments identified by each method.

Evaluating the impact of hot moments on total N_2O emissions

The impact of hot moments on total soil N_2O emissions was evaluated by determining the proportion of measurements classified as hot moment among all measurements, as well as the contribution to total measured flux made during hot moments. Since experimental datasets overrepresented the warmer, wetter, and often fertilized growing season and therefore overrepresented hot moments (Zhou et al., 2022), we also calculated these contributions from a subset of eight time series datasets identified with year-round flux measurements available with no gaps between measurements exceeding 20 days.

Results

Performance of methods using optimized thresholds

Among the tested methods, MAD and MCD demonstrated the best performance, with both achieving an MCC of 0.80 and Accuracy of 93.6% and 93.2%, respectively (**Table 2.3**). In agreement with prior analyses, 1.5 IQR performed well in overall performance, ranking 3rd (MCC: 0.77; Accuracy: 93.3%). However, the performances of the methods previously used for statistical hot moment identification—four standard deviation, IQR methods, and 75th Percentile—were highly correlated to the prevalence of hot moments, degrading significantly as hot moments became more common.

We next analyzed the top three overall performing methods—MAD, MCD, and 1.5 IQR—to more thoroughly identify their strengths, weaknesses, and most appropriate applications. When hot moments made up at least 25% or more of measurements, MCD maintained 94% accuracy, MAD slightly fell to 92%, and 1.5 IQR dropped by over 8% to 85% **(Figure 2.6**). Notably, 1.5 IQR also underperformed relative to other methods when few labeled hot moments existed within a dataset (**Figure 2.7**). The diminished accuracy of 1.5 IQR on both extremes of hot moment prevalence were caused by opposing effects: 1.5 IQR resulted in false positives when no labeled hot moments were present, and false negatives when hot moments were common.

An example of classification results using the three methods—1.5 IQR, MCD, and MAD—on one example time series from the dataset is shown in **Figure 2.8**. Approximately one third of N_2O flux measurements from this time series were labeled as hot moments, driven primarily by a

Table 2.3: Optimized method performance evaluated using a variety of metrics using the testing dataset. Matthews Correlation Coefficient (MCC) measures overall model performance across the confusion matrix (Equation 2). R^2 and slope of the regression between method accuracy and the prevalence of hot moments and the measurement frequency are shown. Due to the sharp angular relationship of the accuracy of the 75th Percentile method and the hot moment prevalence, two separate linear regressions were fit and the slopes and coefficients of determination are shown: first one where the hot moment prevalence was less than 25%, and another where it was greater than or equal to 25%.

Method	MCC	Mean accuracy	TP	FP	Local hot moment detection rate	Correlation with hot moment prevalence (slope, R^2)	Correlation with measurement frequency (slope, R^2)
MAD	0.80	93.6%	81.7%	3.3%	29%	-0.16, -0.26***	NS*
MCD	0.80	93.2%	85.2%	4.3%	39%	NS*	NS*
1.5 IQR	0.77	93.3%	70.3%	1.4%	14%	-0.38, -0.58***	NS*
LOF	0.72	91.1%	76.0%	4.7%	50%	-0.19, -0.30***	NS*
IF	0.72	91.1%	80.3%	6.3%	40%	-0.16, -0.24**	NS*
75th Percentile	0.71	89.5%	88.8%	10.0%	53%	0.89, 0.94*** -0.97, -0.96***	NS*
KNN	0.67	89.9%	76.9%	7.7%	59%	-0.24, -0.34***	NS*
ABOD	0.65	89.4%	76.3%	8.4%	54%	-0.26, -0.37***	NS*
HBOS	0.64	88.4%	66.5%	5.3%	41%	-0.35, -0.42***	NS*
COPOD	0.62	87.0%	80.0%	11.8%	41%	NS*	NS*
ARIMA	0.60	86.4%	75.2%	11.0%	56%	-0.22, -0.31***	NS*
3 IQR	0.60	89.1%	41.6%	0.0%	0%	-0.79, -0.86***	NS*
Moving Average	0.47	86.2%	48.1%	6.1%	16%	-0.45, -0.66***	NS*
4 SD	0.24	83.2%	7.0%	0%	0%	-0.99, -0.99***	NS*

Statistical significance at $P < 0.05$ (*), $P < 0.01$ (**), and $P < 0.001$ (***). Not Significant (NS)

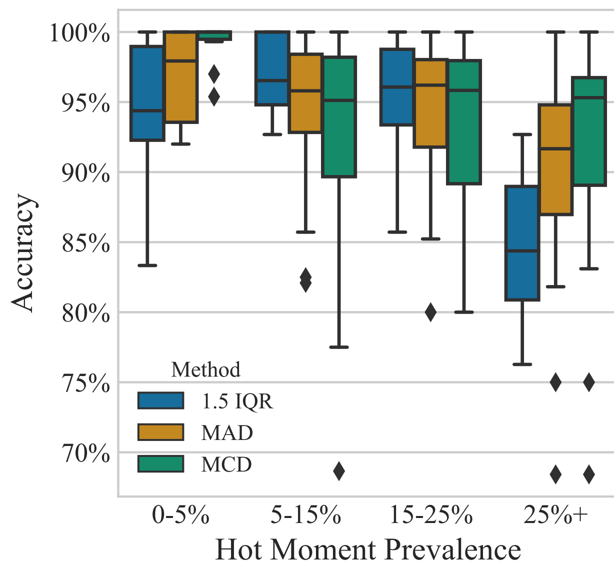

Figure 2.6: Impact of hot moment prevalence on the performance of anomaly detection methods. The accuracy of 1.5 IQR was highest when hot moments comprised 5-25% of the dataset, and underperformed other methods when hot moments were very rare or common. The accuracy of MAD and MCD were more consistent across the full range of hot moment prevalences.

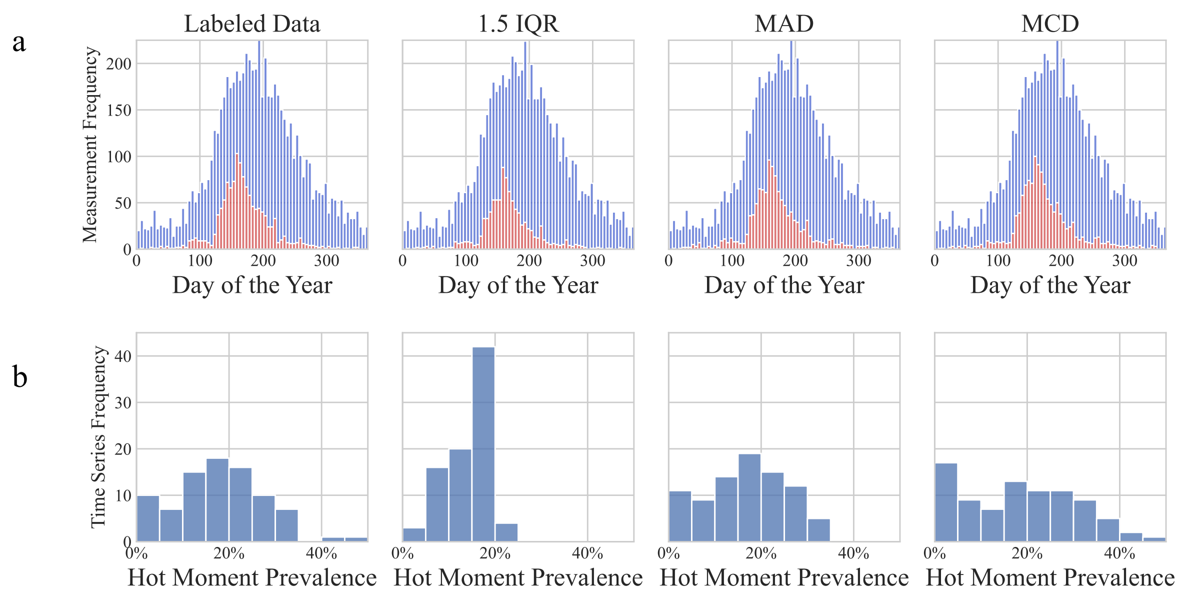

Figure 2.7: Temporal distribution of hot moments (red bars) and background emissions (blue bars) as predicted by the top three performing methods in the testing dataset, compared to the labeled data, using a bin width of five days (a). Histogram of the proportion of hot moments in time-series data as predicted by each method. 1.5 IQR rarely predicted hot moments to comprise more than 20% of a dataset, and more often tended to identify 15-20% of data as anomalous.

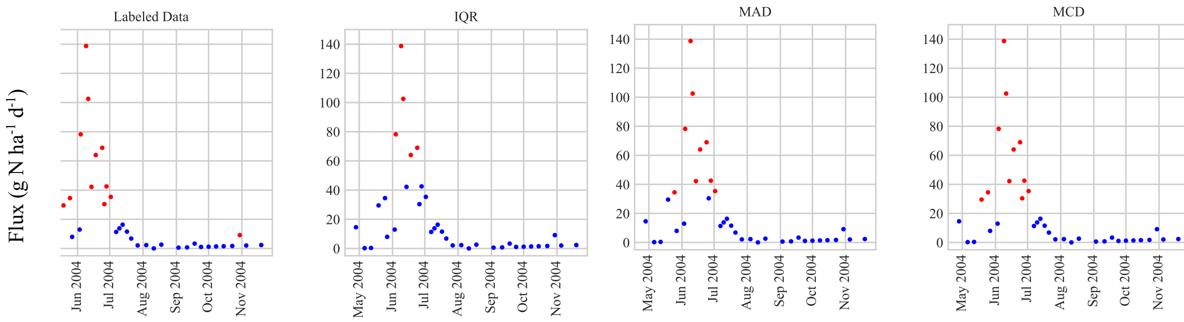

Figure 2.8: Example visual demonstration of anomaly detection method performance in hot moment identification using a sample time-series data. N_2O flux measurements identified as hot moments are highlighted in red, while background emissions are presented in blue. 1.5 IQR identified only extreme anomalies as hot moments above 60 g N ha^{-1} d^{-1}, while MCD and MAD were much more sensitive, identifying smaller hot moments with flux magnitudes of 30 g N ha^{-1} d^{-1}.

large hot moment in early summer during which the fluxes rose above 130 g N ha^{-1} d^{-1} and remained elevated over a month. 1.5 IQR identified the most extreme anomalies above 60 g N ha^{-1} d^{-1} as hot moments but missed emissions between 30 and 50 g N ha^{-1} d^{-1} labeled as hot moments. This mislabeling illustrates how the performance of this method degrades as hot moments become more extreme and common. On the other hand, MCD and MAD resulted in much tighter ranges of background emissions and were more sensitive to smaller hot moments around 30 g N ha^{-1} d^{-1}.

Hot moments and overall N_2O emissions

The mean flux of hot moments estimated by both MCD and MAD classifications was statistically equivalent to that estimated from context-informed data labels (**Table 2.4**). 1.5 IQR estimated higher mean and median fluxes of both hot moments and background emissions compared to context-informed data labels, which can be attributed to its low true positive rate (and therefore high false negative rate) compared to most other methods (**Table 2.3**), which increased the estimates of the background level and typical hot moment flux.

The proportion of measurements classified as hot moments across all 170 time series datasets

Table 2.4: Mean daily soil N_2O flux of background emissions and hot moments emissions, as determined by context-informed labeled data, MAD, MCD, and 1.5 IQR classification methods. The mean values are associated with 95% confidence interval.

	Hot moment emissions (g N ha^{-1} d^{-1})				Background emission (g N ha^{-1} d^{-1})			
	Labeled	MAD	MCD	1.5 IQR	Labeled	MAD	MCD	1.5 IQR
Mean	60.7±8.4	61.5±8.8	58.4±8.2	72.9±0.9	4.28±0.20	4.79±0.27	4.55±0.25	5.28±0.27
Median	24.7	23.0	21.2	29.7	2.20	2.27	2.17	2.52

were also similar for MAD (18.9%), MCD (19.3%), closely matching the context-informed labeled data (17.9%) (**Table 2.4**). In contrast, the 1.5 IQR method predicted substantially lower proportion of hot moments (14.3%). Eight time series from four separate experiments with consistent year-round measurements were identified. In this year-round time series subset, hot moments were found to be slightly less frequent, with proportions identified by the context-informed labeled data (13.8%), MAD (17.0%), MCD (16.8%), and 1.5 IQR (17.0%). As a result, hot moments contribute a lower proportion of the total flux relative to the complete dataset, as indicated by labeled data (60.1%), MAD (63%), MCD (63.2%), and 1.5 IQR (63.3%) (**Table 2.5**). In this temporally resolved data subset, where hot moments made up a smaller proportion of measurements, 1.5 IQR method performed similarly to MAD and MCD.

Discussion

Hot moments of N_2O emissions contribute disproportionately to overall GHG emissions from agriculture, making them critical targets for mitigation. Given the outsized warming potential of N_2O, even small changes in accurately estimating its hot moments can lead to large errors in accounting for soil N_2O emissions. However, lack of consistent and robust quantitative methods of identification across diverse N_2O flux distributions hinders progress in understanding their significance and biogeochemical drivers (Bernhardt et al., 2017). We employed a global dataset

Table 2.5: Contribution of hot moments to cumulative N_2O flux and their relative duration as estimated by context-informed labeled data, MAD, MCD, and 1.5 IQR methods. Values are shown for the complete dataset, which overrepresents studies emphasizing spring and summer months, and for a subset of the data from experiments with available year-round measurement.

	Complete dataset				Data subset with year-round measurements available[1]			
	Labeled	MAD	MCD	1.5 IQR	Labeled	MAD	MCD	1.5 IQR
Time contribution	18.9%	17.9%	19.3%	14.3%	13.8%	17.0%	16.8%	17.0%
Flux contribution	76.7%	73.7%	75.4%	69.6%	60.1%	63.0%	63.2%	63.3%

[1]Eight time series from four separate experiments with consistent, year-round measurements were identified, comprising a total of 690 N_2O flux measurements. Experiments were conducted in Germany (2), Brazil, and the United Kingdom. Crops represented from these experiments included maize (3), rangeland (2), soybean, ryegrass, and potato.

of N_2O flux measurements from diverse agroecosystems to evaluate a wide array of statistical anomaly detection methods which differ in their mathematical principles for data classification. Our analysis highlights the limitations and biases of previously used methods (Molodovskaya et al., 2012; Stuchiner et al., 2025), which are either too conservative or fail to account for the diverse N_2O flux distributions. In this endeavor, we identify robust and novel N_2O hot moment identification methods across this diverse global dataset and outline the appropriate contexts for their use.

Statistical strengths and limitations of hot moment detection methods within the research context

IQR and standard deviation methods have most commonly been used for N_2O hot moment identification (Anthony et al., 2023; Anthony & Silver, 2021; Molodovskaya et al., 2012; Palta et al., 2014; Stuchiner et al., 2025; Zhou et al., 2022). However, the performances of these methods demonstrated strong biased with respect to the proportion of hot moments within the dataset (**Table 2.3**). Standard deviation-based methods are easily distorted by extreme anomalies (Leys et al., 2013), and while IQR is more robust to extreme values, its performance degrades increasingly as anomalies comprise 25% or more of a dataset (Hampel, 1971). The true rate of hot moments within real-world experimental datasets varied from 0% to over 40% (**Figure 7b**), and 1.5 IQR performed poorly compared to other methods on both ends of this range (**Figure 6**). This shortcoming is especially problematic when comparing datasets with vastly different proportions of anomalies, for example multiple treatments of varying fertilization rates, or datasets taken from different seasons as observed by Stuchiner et al. (2025). In such scenarios, 1.5 IQR is likely to overestimate hot moments when they are few and underestimate hot moments when they are common, potentially introducing systematic bias when comparing dissimilar datasets. Additionally, four standard deviations and IQR methods identified very few local hot moments, performing below all other methods at 0% - 14% detection, which follows logically from their methodological inability to consider local context. Poor performance in identifying local anomalies is a significant weakness, as N_2O emissions from North American agriculture often exhibit a primary maxima of higher magnitude in early summer after nitrogen fertilization and a smaller late Winter/early Spring secondary maxima, which can become more important in the northern latitude due to freeze-thaw emissions (Nevison et al., 2023). Therefore, failure to identify relatively smaller in magnitude, but still relevant, hot moments can underestimate risks of N_2O emissions. Due to these limitations, it is important to be cautious when using IQR and standard deviation-based methods, which have been widely used to date, for N_2O hot moment identification.

We identified two statistical methods, MAD and MCD, that were most suitable for hot moments detection across a wide range of datasets with varying N_2O flux distributions. Comparing these two methods, MAD achieved the highest general performance among the methods evaluated

(MCC: 0.80; mean accuracy: 93.6%). Such accuracy was achieved because MAD uses the distance from the median to calculate a modified Z-score for each data point, which makes it more robust to the impact of anomalies than methods based on mean and variance (e.g. Stuchiner et al., 2025; Anthony & Silver, 2021) which are heavily skewed by anomalies (Leys et al., 2013). While the performance of MAD exhibited a modest correlation to hot moment prevalence (R^2: -0.26), only three methods—MCD, IF, and COPOD—evaluated here were more independent of hot moment prevalence. However, MAD's main limitation was its relatively poor ability to identify local anomalies, as it is a strictly univariate method that does not consider local context. However, if small local hot moments (e.g., freeze-thaw or non-growing season emissions) are not a priority, or if extreme variations in hot moment prevalence are not expected, MAD may be a suitable identification method.

On the other hand, MCD matched MAD for overall performance as evaluated by MCC (0.80) but ranked third in mean accuracy (93.2%) (**Table 2.3**). While MCD did not perform as consistently as MAD and 1.5 IQR when hot moment prevalence ranged from 5-25%, it outperformed other methods when hot moments were either very rare or very common - an important attribute given the poor performance of other methods on such datasets (**Figure 2.6**). MCD also identified more local anomalies than the other top three performing methods (39%), and its performance exhibited no significant bias with hot moment prevalence. MCD identifies anomalies by repeatedly subsampling the dataset and identifying the subset with the smallest covariance matrix determinant, or a subset without anomalies, and quantifies anomalousness by the Mahalanobis distance away from this subset. In other words, MCD first isolates a group of background emissions to define their range and covariance, then identifies data points that deviate significantly beyond this range as hot moments. This method is highly robust to the effect of anomalies, and its strong performance, alongside MAD, underscores the importance of accurately identifying hot moments across diverse datasets. In fact, due to its performance being uninfluenced by hot moment prevalence, MCD excels in making comparisons across experiments, geographies, seasons, management techniques, and climates which are widely known to contribute significant variations in N_2O fluxes (Stuchiner et al., 2025).

While MCD and MAD performed well overall, there may be instances when other methods are more suitable to a particular dataset, and we suggest researchers consider the nature of the data or system they are working with and the strengths and weaknesses of the various methods that this study highlighted before settling on a method suited to their purposes. For example, we observed that LOF, KNN, and ARIMA also had notable strengths, with LOF ranked fourth in overall performance (MCC: 0.72; mean accuracy: 91.1%) and identified half of all local anomalies. Whereas KNN and ARIMA were particularly useful at identifying local hot moments (59% and 56%, respectively).

The impact of hot moments

Early analyses, predominantly based on observations from a single site and using IQR and percentile-based methods to identify N_2O hot moments, have reported that hot moments occur throughout 0.2-21.0% of the year in agricultural soils and their contribution to the total emissions widely ranged from 12 to 100% (Anthony et al., 2023; Anthony & Silver, 2021; Molodovskaya et al., 2012; Stuchiner et al., 2025). Here, using 13,787 treatment-average daily N_2O flux measurements from 42 publications and 39 sites across the globe, we found hot moments occurring in approximately ~18-19% of measurements (**Table 2.5**), near the upper end of previous estimates. Similarly, we found the contribution of hot moments to cumulative agroecosystem emissions is near the upper range of previous estimates, at approximately 75%

(**Table 2.5**). However, this estimation may overrepresent hot moments since in general, field experiments heavily overrepresented the warmer growing season where hot moments are expected to be more common. Using a subset of year-round experiments, we found hot moments occurred during about 14-20% of the year and contributed 60-65% of cumulative agroecosystem emissions. Thus, the importance of hot moments on an annual basis was modestly smaller than that estimated from all experimental datasets of varying temporal resolution, but still considerably outsized, signifying the importance of their accurate identification and mitigation.

We found the median background emission rate from agroecosystems estimated by context-informed labeled data, MAD, and MCD to range from 2.2-2.3 g N ha^{-1} day^{-1} **(Table 2.4**), which is in agreement with the 2.2 g N ha^{-1} day^{-1} estimate proposed by Yin et al. (2022), whereas 1.5 IQR resulted in a ~14% higher estimation of 2.5 g N ha^{-1} day^{-1}. While hot moment magnitudes widely vary due to confluence of factors, our global database showed a mean flux of ~60 g N ha^{-1} day^{-1} and a median flux of ~21-25 g N ha^{-1} day^{-1}. This estimate is more than an order of magnitude higher than the estimated global background rates in our study and also in Yin et al. (2022).

The similarity of estimates of hot moment prevalence, contributions, and flux magnitudes by MAD, MCD, and context-informed data labels indicates that the use of these statistical methods for hot moment identification did not lead to notable bias in estimating their ecological significance. In contrast, 1.5 IQR led to substantially lower estimates of the prevalence and contributions of hot moments across the complete dataset, indicating its underestimation of hot moments from spring and summer months (**Figure 2.7**) and in high-prevalence datasets (**Figure 2.6**). This underestimation impacted its ability to assess the environmental significance of hot moments. These results underscore the outsized impact that brief periods have on overall N_2O

emissions from agroecosystems which, by identifying reliable methods for their statistical identification, our analysis provides a step forward toward mitigating.

Potential implications, limitations, and future work

In this analysis, we highlighted the strengths and limitations of 14 statistical methods for N_2O hot moment identification, providing insights relevant to the researchers with different priorities (e.g., maximum mitigation benefits, mechanistic understanding, etc.). While no single anomaly detection method is perfect for all cases, some methods' strengths and limitations can complement each other. For example, MAD and IQR performed well overall but struggled with identifying local hot moments due to their inability to consider local context, while HBOS, KNN, and ARIMA excel in this regard but lacked top tier overall performance. Thus, an ensemble approach combining multiple methods may be capable of achieving the best of both approaches and is worthy of future investigation.

We acknowledge that our supervised approach to assess method performance, which is effective in similar fields, is not devoid of challenges. Defining anomalies as deviations from expected behavior introduces subjectivity, especially with inconsistent data distributions. Despite this, our method leveraged data patterns, context, underlying mechanisms, and environmental information to determine expectations. While this approach doesn't eliminate subjectivity, we argue it offers a more reliable, defensible, and reproducible classification of "true" hot moments than alternative methods. Our estimates were similar to other global-scale estimates (e.g., Yin et al., 2022) which further underscores the robustness and validity of our approach.

Conclusion

This work advances the application of the "hot moment" in critically analyzing the significance of agricultural soil N_2O emissions. A consistent method of identifying hot moments among N_2O

flux emissions measurements is essential to advance quantitative work on these phenomena, including modeling and understanding their ecological significance. While a few methods have previously been proposed for statistically identifying hot moments, their applicability considering specific strengths and limitations has remains largely unexplored, especially in the global context of the complexity and variability of soil N_2O emissions. In this study, we have rigorously evaluated 14 statistical methods of identifying hot moments using a large, heterogeneous, and global dataset. We demonstrate the limitations of commonly used statistical methods, such as 1.5 IQR, for N_2O hot moment identification, resulting in a low detection rate of hot moments and potentially inducing systematic bias when comparing across dissimilar datasets. In contrast, two novel methods proposed in this study- MAD and MCD- consistently and effectively detected N_2O hot moments across a diverse range of data characteristics, an expected behavior given the complexity of this biogeochemical process. We also provide further evidence and specificity to the outsized impact of these pulse events (~19% time of the year) on agriculture's contribution to N_2O emissions (~75% of the total emissions). We hope these findings will contribute to further research toward understanding, predicting, and ultimately mitigating N_2O hot moments from agricultural soils.

CHAPTER 3: MACHINE LEARNING PREDICTS NITROUS OXIDE HOT MOMENTS ACROSS GLOBAL AGROECOSYSTEMS

Abstract

Soil nitrous oxide (N_2O) emissions in agroecosystems are temporally variable. Brief hot moments driven by abrupt changes in local climatic conditions and substrate availability contribute disproportionately to cumulative annual emissions. The ability to accurately predict such temporal dynamics can help to concentrate mitigation efforts and improve hot moments representation in global models. Multiple machine learning models were evaluated for predicting daily hot moments using limited management, environmental, and climate data from 22 agricultural sites worldwide. The XGBoost model trained using data labels of N_2O flux measurements generated through a context-informed hand labeling process produced the best overall performance (Matthews Correlation Coefficient, MCC: 0.69; Accuracy: 90%), with fewer errors made when flux was <10 g N ha^{-1} d^{-1} or >50 g N ha^{-1} d^{-1}. The dataset used for the models training captured diverse conditions, and model behavior aligned with known drivers of nitrification and denitrification, and model behavior aligned with known drivers of nitrification and denitrification. These results demonstrate a practical pathway toward applying machine learning to improve soil N_2O flux predictions.

Introduction

In the past four decades, anthropogenic emissions of the potent greenhouse gas (GHG) nitrous oxide (N_2O) have risen 40% to 7.3 Tg N yr^{-1}, with more than half of these attributed to agriculture (IPCC, 2023; Tian et al., 2019, 2020). N_2O is produced in soil by a combination of complex biogeochemical processes which result in high spatial and temporal variability of emissions, making field-level monitoring methods expensive and arduous (Groffman et al., 2009; Hénault et al., 2012; Venterea et al., 2012). Reliable models of N_2O emissions are thus important on two fronts: first, they are essential for the work of researchers and policymakers in determining N_2O budgets, trajectories, and potential contribution to radiative forcing and climate change (Del Grosso et al., 2008). Second, accurate models have the potential to aid mitigation efforts by estimating the timing and impact of specific events to overall emissions, revealing pathways to lower these emissions (Bastos et al., 2021; Venterea et al., 2012; Wagner-Riddle et al., 2020).

Periods of anomalously high emissions (termed “hot moments”) have been proposed as targets for site-specific mitigation efforts (Hénault et al., 2012; Wagner-Riddle et al., 2020) given their disproportionate contribution to the total emissions (Anthony et al., 2023; Anthony & Silver, 2024; Molodovskaya et al., 2012; Stuchiner et al., 2025). Process-based models predictions of daily fluxes are often weakly correlated with measurements, due in part to systematic underestimation of hot moments (Brilli et al., 2017; Del Grosso et al., 2008; Fuchs et al., 2020; Gaillard et al., 2018; Jarecki et al., 2008; Parton et al., 2001; Zimmermann et al., 2018). Poor representation of the temporal dynamics of emissions and underestimation of peak events undercut the potential of process-based models to guide effective mitigation strategies (Vemuri, 2024).

Machine learning (ML) offers an alternative modeling approach with key advantages over process-based modeling. First, ML offers the potential to learn hidden relationships between variables without guidance by empirical knowledge- advantageous given the complexity of relevant biogeochemical processes- and can thus contribute to conceptual knowledge (Anthony & Silver, 2024; Dhaliwal et al., 2025; Saha et al., 2021a). Second, ML can harness the growing accessibility of data to improve model accuracy, breadth, and generalizability in more labor-efficient ways than process-based models which necessitate site-specific calibration and parameterization (Dhaliwal et al., 2025; Dorich et al., 2020; Fuchs et al., 2020; Kotlar et al., 2022; Saha et al., 2021a). With these strengths, ML models have been shown to outperform process-based models in some studies (Hamrani et al., 2020; Liu et al., 2022; Saha et al., 2021a). Yet much of the promise offered by ML within this domain is yet latent. The ideal model is one that is broadly applicable, highly accessible in terms of input requirements, and accurate. However, we have identified no ML model of daily N_2O flux which satisfies each of these conditions simultaneously. Many ML models substitute the complex parameterization of process-based models with laborious and time-intensive data input requirements, such as determination of high resolution soil mineral nitrogen (N) dynamics– a key N_2O driver – using destructive sampling, which limit their accessibility (Chiaravalloti et al., 2023; Dhaliwal et al., 2025; Glenn et al., 2021; Saha et al., ; Liu et al., 2022; Wang et al., 2024). Furthermore, the correlative nature of ML leads models to struggle when applied outside the data characteristics used to train them (Saha et al.,), yet nearly every N_2O ML model until now has used data from one or two sites (Adler et al., 2024; Anthony & Silver, 2024; Bastos et al., 2021; Chiaravalloti et al., 2023; Dhaliwal et al., 2025; Glenn et al., 2021; Hamrani et al., 2020; Joshi et al., 2024; Kotlar et al., 2022; Liu et al., 2022; Saha et al., 2021a). This not only precludes the generalizability of these models, but also gives optimistic evaluations of model performances by maintaining a constancy of environmental drivers likely to change with geography. Because hot moments are uncommon, ML models must infer the most complex relationships from a small portion of training data, leading them to often systematically underestimating hot moments (Adler et al., 2024; Anthony & Silver, 2024; Chiaravalloti et al., 2023; Dhaliwal et al., 2025; Hamrani et al., 2020; Joshi et al., 2024; Kotlar et al., 2022). Due to perpetuating major shortcomings of process-based models in addition to unique ones like low interpretability, applications of ML in the prediction of soil N_2O emissions have been limited (Wrage-Mönnig et al., 2018).

Our objective in this study was to develop and evaluate generalizable, accessible, and accurate ML models of soil N_2O hot moments. To achieve these goals, we gathered a global database of published N_2O flux measurements alongside relevant driving factors collected from diverse environments and agronomic conditions. From this dataset, we selected a limited number of factors as model inputs intended to balance predictive contributions with accessibility to potential users, including natural resource managers. We argue that predicting the qualitative state of emissions rather than the absolute magnitude can reduce model complexity and input requirements while reliably reproducing the temporal dynamics of emissions, which are particularly relevant to agricultural managers and ultimately to the goal of mitigating N_2O emissions (Bastos et al., 2021; Vemuri, 2024).

Methods

Collection and description of a diverse agroecosystem database

We conducted a literature search using Google Scholar and Connected Papers. Publications were identified using Google Scholar using the search terms "agriculture," "field," and "N_2O emissions," and were selected based on following inclusion criteria : (1) soil N_2O emissions were measured from an agricultural field experiment, (2) daily average N_2O fluxes and associated soil temperature, soil moisture, and precipitation were measured and data made available in the manuscript in tabular or graphical form or as supporting data, (3) N fertilization timing, rate, and form were described, (4) a minimum of ten N_2O flux measurements were taken during the study period, (5) the period between initial and final flux measurements was at least 30 days to ensure a minimum level of data density and temporal coverage. Subsequently, publications meeting these criteria were entered into “Connected Papers” (www.connectedpapers.com) to discover additional publications, to which the same inclusion criteria were applied. Finally, we accessed the Greenhouse gas Reduction through Agricultural Carbon Enhancement network (GRACEnet) database (https://www.ars.usda.gov/anrds/gracenet/gracenet-home/) and included experimental datasets based on our inclusion criteria. GRACEnet is a US project overseen by the United States Department of Agriculture to measure agricultural GHG emissions and the effect of management practices across dozens of field sites (Del Grosso et al., 2013).

All published data was input into a single tabular database with the following columns: ID (unique identifier for each treatment-level timeseries), date, daily average N_2O flux (g N ha^{-1} d^{-1}), daily average surface soil volumetric water content (VWC; %), daily average soil temperature (°C), total precipitation (mm), N rate (kg N ha^{-1}), N form (e.g. urea), latitude (decimal degrees), longitude (decimal degrees), mean annual precipitation (MAP; mm), mean annual temperature (MAT; °C), sand content (%), silt content (%), clay content (%), primary planted crop species, and management style (e.g. conventional, organic, no-till). When data was published in tabular form, all N_2O fluxes, soil temperature, soil moisture, and precipitation measurements were downloaded and input into the database. When tabular data were not made available, data were extracted from figures using WebPlotDigitizer (Rohatgi, 2022). Soil texture, crop species, fertilization, geolocation, and management information were extracted from the publication text and input into the database manually.

Unit conversions were performed as necessary according to the aforementioned units for each factor. Where soil moisture was reported as water-filled pore space (WFPS), measurements were converted to VWC using Equation 1, where BD was the bulk density of soil reported for the given site and PD was the soil particle density of 2.65 g cm^{-3}. VWC was selected over WFPS due to its greater availability within the identified publications in this study.

$$VWC = WFPS * (1 - \mathrm{BD} / \mathrm{PD}) \qquad \text{Equation 1}$$

This resulted in a collection of 6753 replicated daily average N_2O flux measurements from 26 published papers or datasets, 22 unique sites, and 104 treatment timeseries datasets. The United States was most heavily represented due to the size and availability of the GRACEnet database, comprising half of the unique sites, while datasets from an additional 11 locations were included from China, Canada, Europe, Brazil, Israel, and Australia (**Figure 3.1**). The large number of datasets and diversity of geography related to a similar diversity of climactic conditions. Soil VWC ranged from ~5% to >60%, with greatest frequency between 20-30%, while temperature ranged from <0 °C to >30 °C, with greatest frequency between 15-25 °C (**Figure 3.2**).

Four distinct management practices were represented: conventional (using both synthetic fertilizer and tillage), organic (using only organic fertilizer inputs), reduced till (some strategy of conservation tillage and no restrictions on fertilizer inputs), and no-till (no tillage and no restrictions on fertilizer inputs). By far the most frequently planted crop species was Maize, which was planted in combination with each of the four management practices, while 16 other crop types were represented (**Figure 3.3**). The variety of climactic conditions, management practices, soil characteristics, and crop types contributed to significant variability in daily N_2O fluxes, ranging from <0 up to ~1400 g N ha^{-1} d^{-1} with a long and heavy tail flux distribution (**Figure 3.3**), which is characteristic of soil N_2O emissions (Yates et al., 2006).

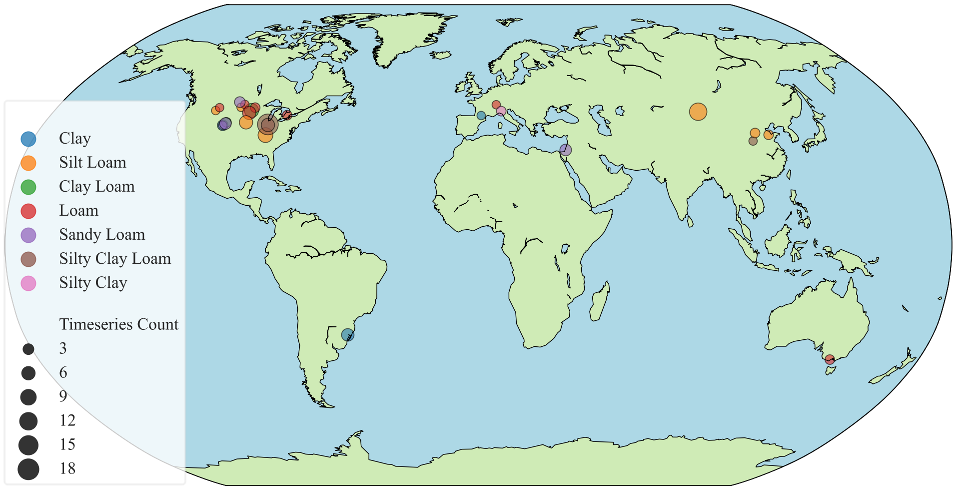

Figure 3.1: Global distribution of study sites and associated soil textural representation within the model dataset. Seven soil textural classes were represented by color, including a variety of loams and clays. The size of circles represents the number of treatment timeseries datasets at each site.

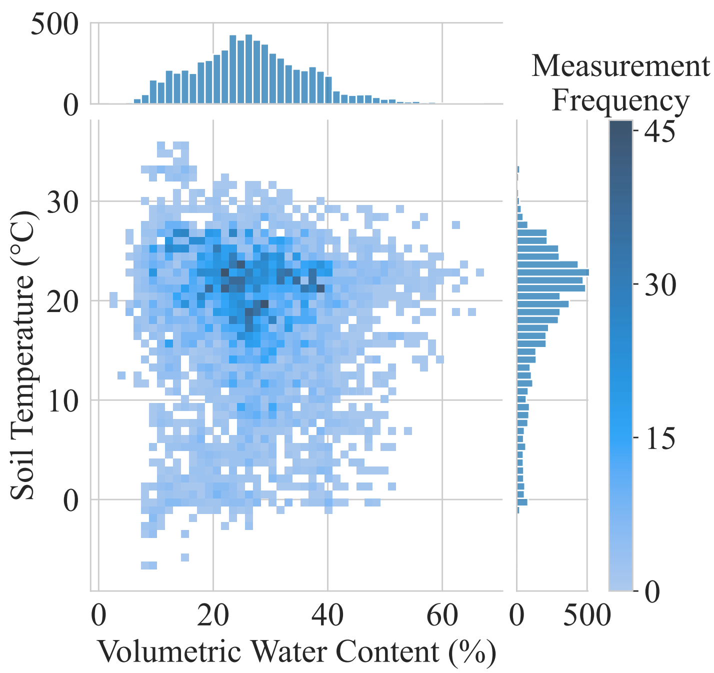

Figure 3.2: The distribution of soil moisture and temperature coincident with N_2O flux measurements. Distributions are shown for each variable independently via histograms, with volumetric water content (VWC) at the top and soil temperature at the right, and their combination shown via heatmap. Color of each tile represents the number of N_2O flux measurements for each combination of VWC and soil temperature.

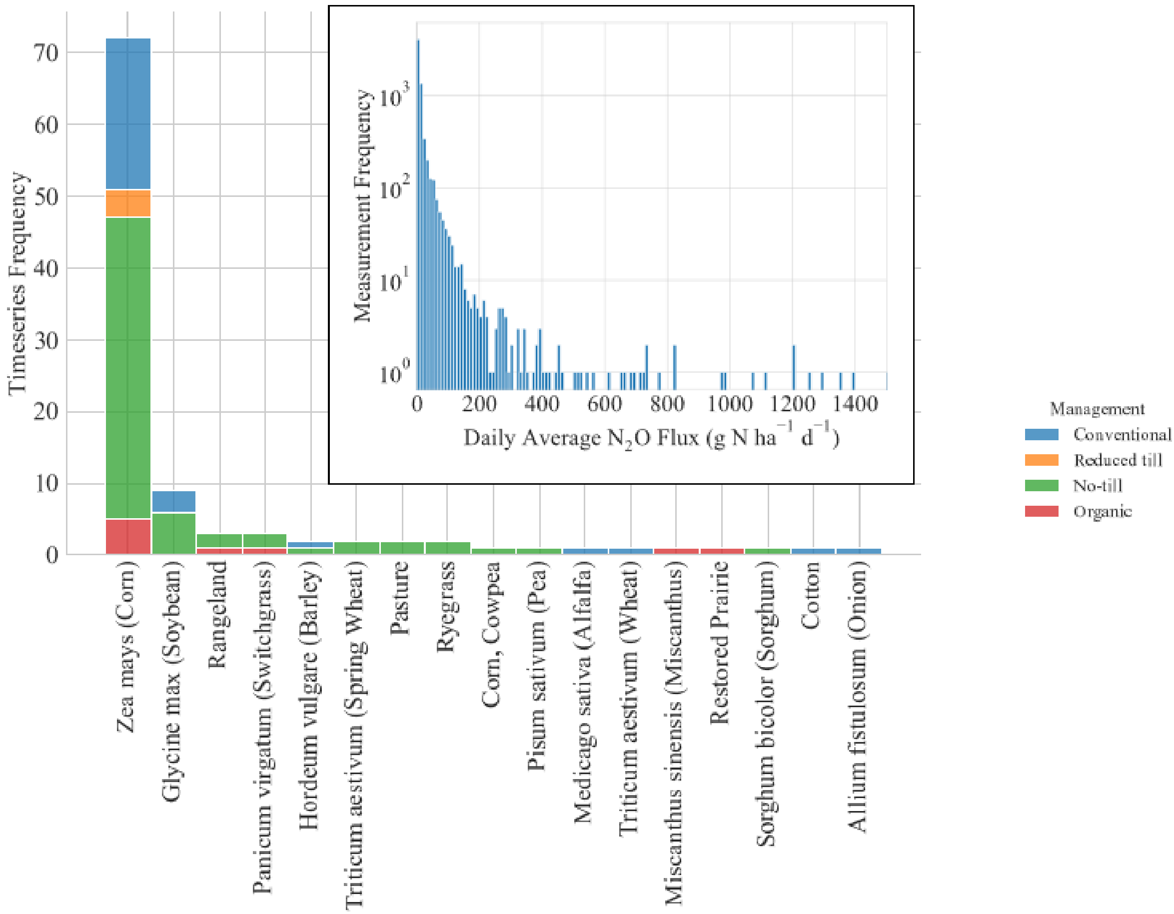

Figure 3.3: Representation of crops and management practices represented in the dataset, as well as the range of magnitudes of daily average N_2O flux measurements.

A complete set of model predictors was determined based on the availability of published data and the accessibility of acquisition from the perspective of a potential model user (**Table 3.1**). These included information about management practices, geographical and climate information about the site, soil physical characteristics, the day of the year, and the soil volumetric water content (VWC) and temperature. Low temporally variable factors were treated as static predictors (e.g. soil texture, mean annual temperature/precipitation), represented as unchanging values in all rows of a given treatment dataset, while high temporally variable predictors (e.g. daily N_2O fluxes, VWC, soil temperature) were considered dynamic and varied from day to day. Environmental factors measured across experiments varied in their measurement frequency and often did not temporarily scale with N_2O flux measurement days. Thus, if VWC were measured the day before or after N_2O flux measurements were taken but not on the same day, these data would contain gaps and be unusable by some ML architectures like neural networks, which prohibit missing values. Therefore, when measurement gaps occurred in these temporally variable predictors (specifically soil temperature and VWC), linear interpolation was used to fill

Table 3.1: Environmental and management drivers of N_2O hot moments and their representation in our ML models.

	Oxygen	Temperature	Soil Nitrogen Availability	Carbon
Continuous Variables	Volumetric Water Content	Soil Temperature	Fertilization (Quantity, Type, and Timing)	Fertilization (Quantity, Type, and Timing)
	Daily Precipitation	Day of Year		
Static Variables	Mean Annual Precipitation	Mean Annual Temperature		Management Style
	Sand/Silt/Clay Content	Latitude/Longitude		Primary Crop Species

gaps up to 14 days between measurements to temporarily scale with N_2O flux measurements. The average gap between VWC measurements was 1.6 days. No datasets which met the inclusion criteria had gaps in precipitation measurement data. N_2O flux measurements were not interpolated.

Most ML algorithms (including all used in this analysis) can only learn relationships between contemporaneous data, and lack "memory" of past events. For example, fertilizer application occurs on a single day, yet it has a lasting impact on soil N availability as this N is gradually lost to multiple loss pathways. Feature engineering was therefore used to represent past conditions as additional variables. These included the number of days since the last fertilization event, the quantity of N applied on the last fertilization event, the number of days since the last precipitation event, the depth of rainfall which occurred during the last precipitation event, and the depth of precipitation, mean soil moisture, and mean soil temperature on each of the preceding seven days.

One Hot Encoding was applied to all categorical variables, such as the primary crop and management style, representing each unique value (e.g. organic, conventional) within a variable as a new column with a value of 1 (true) or 0 (false). Scaling between 0 and 1 was applied to each of the numerical timeseries predictors. After removing rows with any missing values of predictors, the complete dataset comprised a total of 6753 replicated N_2O flux measurements alongside measured or estimated values for all model predictors.

Classification of true hot moments

In contrast to regression models of N_2O fluxes, the training and development of a classification model requires an additional processing step which sorts quantitative flux measurements into qualitative classes, here being background emissions and hot moments. According to the definition given by McClain et al. (2003), hot moments are driven by changes to environmental conditions which affect biogeochemical reaction rates, resulting in anomalously high fluxes in comparison to their context across longer time periods. We applied this framework to the entire dataset through a context-informed process of hand-labeling each flux measurement to train and validate the classification models. Human-labeled data has been shown to improve model performance in environmental systems with high complexity compared to ‘unsupervised’ models which learn patterns from unlabeled data (Russo et al., 2021). Given the contextual nature of hot moments and even the background level (Yin et al., 2022), each treatment-level dataset was considered individually. A time series graph of the average daily flux (g N ha^{-1} d^{-1}) and standard error of each measurement was constructed. Then, to contextualize these fluxes within environmental shifts indicative of hot moments, temporally scaled graphs were generated portraying the soil moisture, soil temperature, precipitation depth, and quantity and timing of N applications. The magnitude, variability, and temporal and environmental context of each flux measurement was considered by the authors and a consensus expert decision was made whether the evidence supported a classification as either background level or hot moment. This process resulted in ~23% of flux measurements classified as hot moments and ~77% classified as background emissions.

In addition, we generated sets of data labels using statistical anomaly detection methods for hot moment identification (Stuchiner et al., 2025). Unlike manual labeling, statistical classification approaches do not require significant time and labor inputs nor the availability of contextual environmental data, and thus enable the rapid and easy generation of data labels for large datasets. However, anomaly detection methods differ in their quantitative approaches, each have strengths and weaknesses, and the selection of methods can have a dramatic impact on which measurements will be identified as hot moments (Molodovskaya et al., 2012). Consequently, the predictive performance and behavior of ML models may be sensitive to the method used to classify fluxes in their training data, especially if some methods better capture the contextuality of anomalous data. We selected 1.5 interquartile range (IQR), median absolute deviation (MAD), and minimum covariance determinant (MCD) for labeling training data flux measurements based on prior studies and our own unpublished analysis (Molodovskaya et al., 2012; Stuchiner et al., 2025). IQR has been recommended for hot moments identification for its performance over other simple methods like percentile thresholds (Molodovskaya et al., 2012; Stuchiner et al., 2025) MAD simply identifies anomalies by their distance from the median. MCD subsamples data minimizing covariance, and identifies anomalies based on their difference from the minimum covariance subset. A comprehensive comparative analysis of these and other methods has been conducted in the previous chapter.

Model tuning

Five classification ML architectures were selected based on their suitability: Random Forest (RF), XGBoost, multilayer perceptron (MLP), k-Nearest Neighbors (KNN), and Support Vector Classification (SVC). RF and XGBoost models are tree-based and have both demonstrated strong predictive power for soil N_2O emissions relative to other ML algorithms in individual experiments (Dhaliwal et al., 2025; Wang et al., 2024). MLP, a neural network, is noteworthy for its strengths in time series classification and relative simplicity (Bachmann et al., 2023; Popov et al., 2024). KNN is purposed to measure multidimensional density and thus classifies data within their local context (Cover & Hart, 1967). Finally, SVC is well adapted to high dimensional data (J. A. Gualtieri & S. Chettri, 2000).

Hyperparameter tuning of each model was performed through a grid search using stratified 10-fold cross-validation. The stratified cross-validation approach ensured that hot moments were represented equally across all folds, maintaining balance in the dataset during model building. Tuned hyperparameters were selected by highest Matthews correlation coefficient of predictions evaluated against the expert-labeled data (MCC; Equation 2). Similar to the F1-score, MCC is a single-value performance summary metric derived from the confusion matrix (True Positive, TP; True Negative, TN; False Positive, FP; and False Negative, FN) notable for its reliability and rigor (Chicco & Jurman, 2020, 2023). MCC is equivalent to Pearson's Correlation Coefficient when all inputs are binary values. A MCC of 0 indicates a model performs equivalently to random guessing, while a MCC of 1 or -1 represents perfect classification or misclassification, respectively.

$$MCC = \frac{TP * TN - FP * FN}{((TP + FP)(TP + FN)(TN + FP)(TN + FN))^{0.5}} \qquad \text{Equation 2}$$

Model evaluation

Model performance was evaluated for all five ML architectures and four methods of hot moment classification, resulting in a total of 20 models. We used a10-fold stratified cross validation, where overall performance was the average MCC of predictions across all folds. Predictions were always compared to context-informed data labels to prevent error propagation and to provide a consistent and high-quality measure of performance across models.

Additionally, classification prediction errors may have varying impacts based upon the magnitude of flux. For example, a false negative when flux is 20 g N ha^{-1} d^{-1} may be considered less consequential than a false negative when flux is 200 g N ha^{-1} d^{-1}. Therefore, we assessed the performance of the best overall model across magnitudes of fluxes by sorting all flux measurements into bins by magnitude and computing a confusion matrix of model predictions on holdout data for each bin.

Binary classification models assign a score or probability between 0 and 1 corresponding to the likelihood that the target belongs to each possible class, and a decision threshold is applied assigning scores above the threshold to one class and scores below the threshold to the other. By default, a probability score of 0.5 was used as the threshold for all models, such that a 50% or greater predicted probability of a hot moment resulted in a prediction of a hot moment, and probabilities less than 50% were predicted to be background emissions. However, applications of this model may encompass a variety of aims, some requiring higher sensitivity to hot moments and others benefitting from more conservative predictions. We investigated how different decision thresholds would affect predictions using a receiver operator characteristic (ROC) curve, which plots the resulting true positive rate and false positive rate for all possible decision thresholds. We also plotted the true N_2O flux magnitude of each measurement against our model's predicted likelihood of a hot moment occurring.

Model interpretation

One deficit of ML is that these models are often considered "black boxes" due to their high complexity which makes interpretation challenging. In addition to limiting the potential for using ML modeling to advance understandings of biogeochemical processes, this also lowers trust in ML models and therefore their usage. We aimed to address this limitation both in the diversity of our input data and through model interpretation techniques illuminating underlying model drivers and relationships.

We first investigated the relative importance and impact of model predictors by plotting Shapley values. Shapley values are an interpretable ML technique derived from game theory which quantify the marginal contribution of multiple factors toward a collective output. Positive and negative Shapley values indicate influence toward predicting hot moments and background emissions, respectively. The magnitude of the Shapley value indicates the magnitude of impact on the prediction. Equal values of a predictor may have varying impacts on the model output depending upon relationships with other predictors. Because of the large number of predictors, and that many were autocorrelated (such as the time-lagged soil moisture and temperature values), we plotted the ten most significant predictors based on having an absolute Shapley value of at least 0.05 and at most 90% redundancy with any other predictor.

We further investigated the impact and interactions of four predictors- days since fertilization, type of fertilizer, soil VWC, and soil temperature- on the best overall performing model. We created heatmaps of predictions binned by contemporaneous values of these four predictors. The result was similar to a two-factor partial dependence plot, visualizing trends of binary predictions in response to interactions between predictors.

Results

Model performances

The performance of models evaluated by MCC varied from 0.47 to 0.69 (**Table 3.2**). Overall, RF and XGBoost models performed similarly and better than other model architectures. Models trained on context-informed data labels achieved the highest prediction performance across model architectures (0.62). The use of MAD or MCD for labeling training data each resulted in an average MCC of 0.58, which was slightly lower (8%) than hand labeling. IQR produced the lowest performing models with an average MCC of 0.53 across architectures- 14% lower than when trained on hand-labeled data. The top performing model overall was therefore the

Table 3.2: Matthews Correlation Coefficient assesses the overall predictive power of 20 hot moment prediction models which varied by ML architecture and the method of classifying N_2O fluxes as hot moments and background emissions in training data. Average MCC of models grouped by architecture and labeling method are also given.

Classification Method	Random Forest	Multilayer Perceptron	XGBoost	KNN	SVC	Average
MAD	0.63	0.54	0.64	0.52	0.57	0.58
MCD	0.62	0.55	0.63	0.51	0.58	0.58
1.5 IQR	0.57	0.47	0.60	0.49	0.53	0.53
Hand-Labeling	0.67	0.56	0.69	0.57	0.62	0.62
Average	0.62	0.53	0.64	0.52	0.58	

XGBoost trained on context informed data labels, with a MCC of 0.69 indicating a strong correlation between predictions and data labels.

Once identified as the best performing model, XGBoost using hand-labeled data was used for further analysis. We analyzed how the rate and type of prediction errors made were related to the magnitude of flux (**Figure 3.4a**). This model made errors most frequently (~35%) when fluxes ranged from 15 to 30 g N ha^{-1} d^{-1}, and declined as flux deviated from this range. Error rates in predictions of hot moment were reduced to ~10% when measured flux was greater than 50 g N ha^{-1} d^{-1} and less than 1% when flux was less than 5 g N ha^{-1} d^{-1}. False positives were rare when flux was above 20 g N ha^{-1} d^{-1}, with nearly all errors made in this range being false negatives (**Figure 3.4a**).

The probability decision threshold may also be adjusted to achieve a different balance of sensitivity and specificity of predictions. For example, a conservative probability threshold of 0.7 resulted in lower model sensitivity (~20% TP rate) but nearly zero FP, while a more liberal threshold of 0.3 correctly identified ~80% of hot moments but made more Type 1 errors (**Figure 3.4b**). Greater model confidence in the occurrence of a hot moment was also associated with a higher magnitude of flux (**Figure 3.4c**).

Key model drivers and interactions

Predictions of hot moments were positively influenced by recent fertilization events, soil wetting events, and higher soil temperature (**Figure 3.5**). Fertilization events (recency and quantity) constituted two of the three most important predictors on average, with more recent and greater quantities of fertilizer having strong positive impacts on the model prediction of hot moments (**Figure 3.5**). The amount of precipitation received on the prior day had a greater effect size than the amount of precipitation received on the day of N_2O measurement, indicating the importance

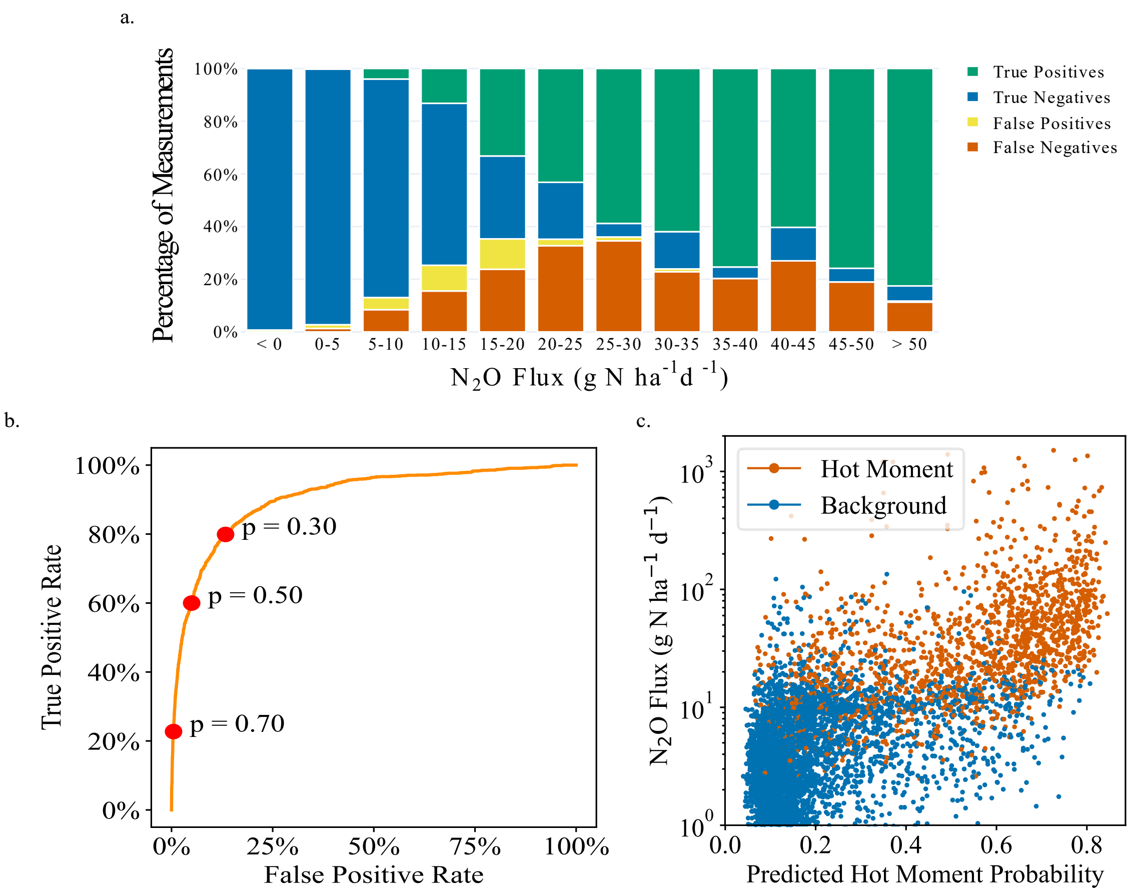

Figure 3.4: Prediction performance of XGBoost model trained using context-informed data labels. a) Prediction results varied with N_2O flux magnitude, with error rate peaking when flux was moderate (which often defines the top of the background level and the lowest hot moments) and decreasing as flux approached more extreme magnitudes, low and high. Probability threshold used was 0.5, and overall model accuracy was 90%. b) The receiver operator characteristic curve plots the true positive rate (TPR) and false positive rate (FPR) across different probability thresholds (p). Using the default probability threshold of 0.5 (50% probability of a hot moment), the model resulted in a TP rate ~60% and a FP rate ~6%. c) The predicted probability of a hot moment was correlated with the magnitude of N_2O flux, with greater model certainty associated with higher fluxes.

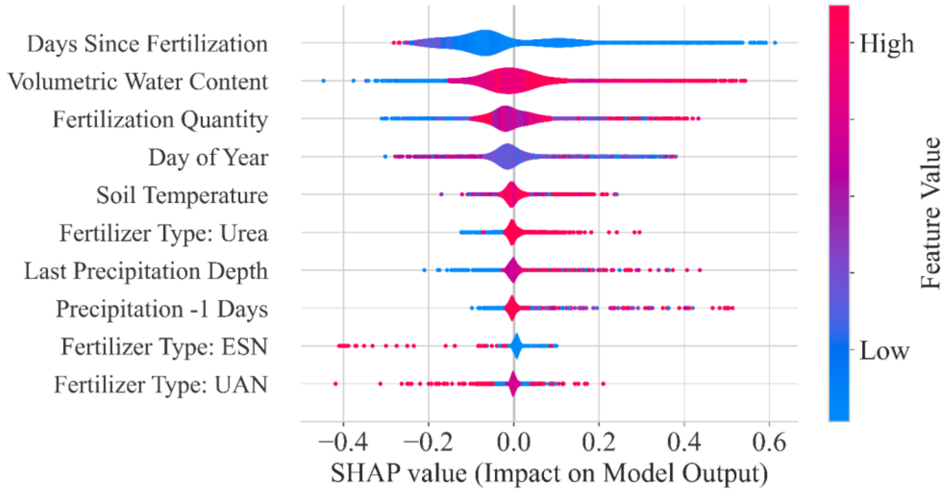

Figure 3.5: Violin plot of Shapley values of model predictors sorted from greatest (top) to least (bottom) average absolute impact. Color represents the value of the predictor, while the X-axis represents the magnitude of impact that predictor had on the output. The widths of violins indicate the frequency of data with a given Shapley value. Most violins are widest near 0 on the X-axis, indicating low impact.

of antecedent conditions. In general, the moderately low values of Day of Year, representative of early Spring, most influenced predictions of hot moment. The use of urea had a positive impact on predictions of hot moments (Tierling & Kuhlmann, 2018), while the use of environmentally smart nitrogen (ESN) had a negative effect, and urea ammonium nitrate's (UAN) impact was ambiguous.

Beyond the individual impact of predictors, the model predicted the greatest probability hot moments when multiple environmental factors were conducive to denitrification. For example, fertilization within the prior 20 days was still unlikely to lead to prediction of hot moments unless VWC was at least 25% (**Figure 3.6**). Similarly, high soil moisture generally could not alone drive hot moment predictions if the temperature was very low, and the highest rates of hot moments were predicted when both moisture and temperature were high.

The form of N fertilizer applied also produced differential results on the timing and rates of hot moments. The application of urea ammonium nitrate, manure, and cover crop residue produced

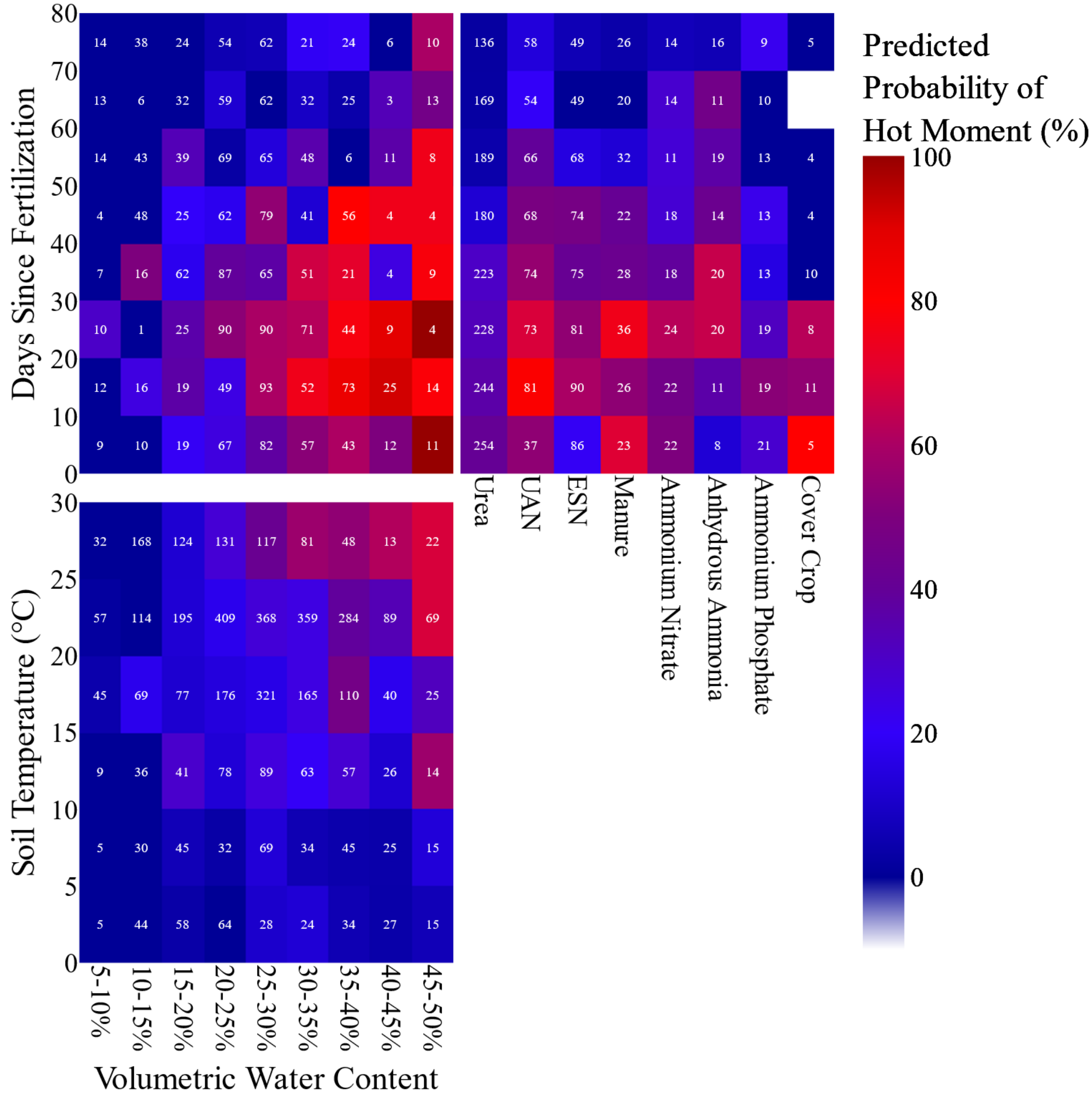

Figure 3.6: Heatmaps indicate the proportions of N_2O flux measurements predicted to be hot moments when segmented into bins based on the synergy of two key predictors: days since fertilization and volumetric water content (VWC), soil temperature and VWC, and days since fertilization and fertilizer form. Color of each tile indicates the proportion of flux measurements within tiles were predicted to be hot moments, where dark red indicates 100% of measurements predicted to be hot moments. The numbers within each tile indicate the total number data points within each tile.

strong and immediate impacts on hot moments, while ESN and anhydrous ammonia (AA) were associated with delayed responses in hot moment predictions (**Figure 3.6**).

Discussion

To improve GHG emission estimates from agriculture and drive mitigation efforts, there is a need to improve the accuracy and accessibility of soil N_2O flux models with high temporal and spatial resolution, particularly during highly dynamic hot moments. Our results demonstrate that ML classification models can accurately predict the occurrences of hot moments, with potential applications of informing mitigation efforts and differentially modeling the biogeochemical processes underlying background emissions and hot moments. Our dataset was notable for its applicability both in terms of its global scope, including N_2O fluxes and environmental measurements from a diverse array of climate, soil, and agronomic practices, as well as its dependence on a limited set of easy to measure input data.

ML classification models accurately predict the occurrences of hot moments

The RF architecture has often been shown to exhibit relatively strong performance in predicting soil N_2O emissions, as was observed in this study (Chiaravalloti et al., 2023; Dhaliwal et al., 2025; Joshi et al., 2024; Kotlar et al., 2022; Philibert et al., 2013; Saha, Basso, et al., 2021b). However, XGBoost achieved slightly higher overall performance across all labeling methods in this study, as in Wang et al. (2024).

Hand-labeled training data resulted in best model performance (average MCC of 0.62), though it comes at the cost of high labor inputs (Russo et al., 2021). Statistical labeling serves as a rapid replacement for hand-labeling, which may be increasingly advantageous as data availability grows. The greater predictive accuracy of models using MAD and MCD labeled fluxes over IQR suggests better accordance with underlying biogeochemical trends, leading to improved learning.

MAD and MCD could therefore be used to label large quantities of training data for new model development in the future, while incurring only about half the penalty to predictive power as IQR when compared to hand labeling.

Predictions made by the best model and training data combination- XGBoost trained on hand-labeled data- were accurate and strongly correlated to true classifications (MCC: 0.69; Accuracy: 90%). Subjectively, model performance further improved when considering that relatively few errors were when N_2O fluxes more obviously belonged to either class. For example, there is little subjectivity in the classification of fluxes of either 0 or 500 g N ha^{-1} d^{-1}, but a flux of 10 g N ha^{-1} d^{-1} may represent a hot moment in one system while reflecting the background level of another (Yin et al., 2022). Errors were most often made when fluxes were within this range adjacent to the lower bound of hot moments and the upper bound of background emissions within the local context (**Figure 3.4a**).

Model behavior replicates biogeochemical processes

N_2O hot moments are driven by a confluence of environmental factors, multiple of which must coincide within favorable ranges for reaction rates to result in a hot moment (McClain et al., 2003). For example, convergence of abundant carbon and N substrate along with anoxia is required to produce a N_2O hot moment from denitrification (Wagner-Riddle et al., 2020). Our model predicted a low frequency of hot moments even after recent fertilization when VWC was $\leq$ 25%, as aerobic conditions stymied anaerobic N_2O producing processes like denitrification (**Figure 3.6**) (Anthony & Silver, 2021; Wagner-Riddle et al., 2020). Our model also correctly predicted greater probability of hot moments with increasing temperature and VWC (Butterbach-Bahl et al., 2013; Smith, 2017; Stanford, Dzienia, et al., 1975). Few hot moments were predicted below 10 °C, in agreement with empirical findings (Firestone, 1982; Krichels & Yang, 2019; W. K. Ma et al., 2007; Wrage-Mönnig et al., 2018).

Finally, the effect of varying types of N fertilizer on hot moment prevalence and timing conforms to expected behavior. Fertilizers such as manure, cover crops, and UAN triggered strong and immediate hot moments, likely because they provide not only N substrate but also at least one additional key driver of denitrification. UAN is typically fertigated, and thus increases soil anoxia upon application. Manure and cover crops supply carbon, a necessary energy source for heterotrophic denitrifiers which produce N_2O, and can also simulate aerobic respiration to consume oxygen, hence induce anoxia (Lazcano et al., 2021; Lussich et al., 2024). Organic fertilizers are also often applied in unprocessed forms like slurries which are high in moisture content, reducing soil oxygen. By providing multiple denitrification substrates and potentially reducing oxygen availability, N addition in organic forms has been demonstrated to induce hot moments which can be greater in magnitude than those induced by synthetic fertilizers (Bouwman, 1994; Clayton et al., 1997; Lazcano et al., 2021; Saha et al., . On the other hand, ESN and AA each produced notably delayed and weaker responses from hot moments. ESN technologies are designed to slow N release and transformations in the soil, directly limiting access by microbes. AA is typically applied in the fall under cooler temperature and has an alkalizing effect on soil in the short term, favoring complete denitrification to N_2 and generally lowering N_2O emissions (Hu et al., 2015; Venterea & Rolston, 2000; Y. Wang et al., 2018). Nitrate fertilizers also produced stronger and quicker responses to emissions than ammonium, which follows that nitrate is immediately usable by denitrifiers while ammonium must first be oxidized by nitrifiers to nitrate (Butterbach-Bahl et al., 2013; Clayton et al., 1997; Tierling & Kuhlmann, 2018). The reflection of these complex biogeochemical processes without explicit representation or even measurements is encouraging, particularly considering that the predictions made to generate such insights were made on unseen holdout data.

Potential applications and future directions

Soil N_2O emissions are driven by complex, interacting, highly dynamic factors, making accurate model predictions at high temporal resolution challenging (Brilli et al., 2017). We addressed this challenge by reducing the quantitative resolution of predictions- converting this task from regression to a classification problem. Our model also simplifies input requirements, requiring only two (soil temperature and VWC) which entail in-field monitoring, and both can commonly be measured simultaneously using a single installed soil sensor. Additional model requirements include access to a nearby weather station measuring precipitation, knowledge of the soil texture and regional climate, and the input of certain management data. While this approach is not devoid of limitations, it holds significant potential for practical applications in mitigating and modeling N_2O emissions.

There is growing interest and investment in grower-centered decision making tools to mitigate agricultural GHG emissions (Climate Action Reserve, 2021; Glauber, 2011). Growers have varying degrees of control over many of the predictors used in our model, such as through fertilization practices, irrigation, management style, and crop selection. A hypothetical management response to mitigate predicted N_2O emissions would likely not differ between a flux of 90 and 100 g N ha^{-1} d^{-1}, but would instead be guided by the qualitative estimation of flux as either ‘typical’ or ‘high,’ as well as the identification of management actions could potentially circumvent or minimize such a hot moment event (Bastos et al., 2021). The ability to adjust the hot moment probability decision threshold also allows these models to be fine-tuned toward specific needs. For example, a grower may weigh that altering management decisions to mitigate hot moments are only worthwhile if the potential mitigation benefits are high and certain. In this case, raising the probability threshold from 0.5 to 0.7, for example, would significantly reduce FP (**Figure 3.4b**) and raise the average flux magnitude of predictions of hot moments (**Figure 3.4c**).

Furthermore, the difficulty of estimating N_2O hot moments flux by both process-based and ML models is related to the fact that hot moments are symptomatic of significant shifts in biogeochemical processes and underlying variable interactions. In other words, hot moments are produced by system dynamics which are fundamentally different from those that prevail during background emissions, and which are inadequately represented by models (Gaillard et al., 2018; Groffman et al., 2009; Necpálová et al., 2015). One path toward improving regression models of N_2O is individually representing these two distinct biogeochemical states as an ensemble model, swapping between submodels for background level and hot moment dynamics as conditions dictate (Vemuri, 2024). This study provides a method to accurately predict when the soil system shifts from one paradigm to the other based on simple inputs, and therefore paves the way for future applications that can enhance process-based and ML learning modeling for accurate predictions.

Conclusion

Our results demonstrate progress toward the application of ML to predict and mitigate daily soil N_2O emissions. By leveraging global datasets, we developed a temporally-resolved model that is more accessible and generalizable than any prior models, demonstrating that the relative magnitude of soil N_2O emissions (hot moment vs background emissions) can be accurately predicted (MCC: 0.69; Accuracy: 90%) from limited data inputs. Furthermore, the diversity of data collected from a variety of soil, climate, and management scenarios across global sites bolstered the model's ability to replicate complex biogeochemical dynamics which reflect empirical knowledge. The prediction of hot moments also holds the potential to differentially model biogeochemical system dynamics during background emissions and hot moments. Our results point toward a practical pathway for growers, modelers, and policymakers to predict and mitigate agricultural N_2O emissions at scale.

CHAPTER 4: THE EFFECT OF EXTENDED SOIL SATURATION ON NITROUS OXIDE EMISSIONS IN MEDITERRANEAN SOILS

Abstract

Extended periods of high soil moisture induced by extreme weather events are likely to become more frequent as global temperatures rise. The effect of such events on N_2O emissions is not well understood and may depend on soil characteristics which vary across time and geographies. We subjected four agricultural soils of varying texture and organic carbon availability to three durations of high soil moisture (90% water-filled pore space): a transient event, three days, and seven days. Soils were also supplied with a small amount of ammonium nitrate fertilizer representative of mid to late season concentrations. In the sand, loamy sand, and clay loam we found that soils flooded for seven days emitted significantly more N_2O that those wetted to the same degree but were immediately allowed to air dry. Ordinary least squares regression analysis determined that dissolved organic carbon was the strongest predictor of cumulative N_2O emissions ($p<0.0001$), but that a longer flooding duration also predicted increased N_2O emissions ($p<0.0001$). The effect of flooding period on cumulative emissions also depended on soil texture. Soils with greater expansive clay content permitted greater gas emissions during the flooding period, likely driven by lowered bulk density and increased macroporosity, thus contributing to increased N_2O emissions. On the other hand, gas emissions in the sand and loamy sand were restricted by poor gas diffusion during the flooding period. Despite evidence of N_2O entrapment, we found cumulative emissions to increase with longer flooding periods in these soils as well, and higher though delayed peak emissions compared to the transient flooding treatments. These findings suggest that increased frequency of extreme weather events has the potential to create a positive feedback loop between climate change and agricultural soil N_2O emissions.

Introduction

One of the most critical concerns in climate research is the potential for tipping points, which are thresholds beyond which positive feedback loops between greenhouse gas (GHG) emissions and changing climatic conditions they give rise to are accelerated. Understanding even lesser positive feedback mechanisms is key to accurate predictions of future warming scenario and the identification of effective adaptation and mitigation strategies. Rising temperatures are changing weather patterns, heating the ocean, and causing the air to hold more water vapor, all of which may convene to create extreme storms and precipitation events with unprecedented frequency (Greenbaum et al., 2010; Rastogi et al., 2020). Biogeochemical cycling can be profoundly influenced by water dynamics, most notably in the occurrence of 'hot moments' during which process rates accelerate (McClain et al., 2003). Many of these biogeochemical processes, such as those involved in soil nitrogen cycling, are themselves important contributors of GHG emissions (Butterbach-Bahl et al., 2013). Nitrous oxide (N_2O) is a potent greenhouse gas produced in soils and which is particularly influenced by moisture conditions (E. M. Baggs, 2011; Barrat et al., 2021). Soil wetting events promote N_2O production by improving the mobility of microbes and substrates and reducing oxygen availability, accelerating the rate of the anaerobic process of denitrification, which is key to producing N_2O in soils.

Although often deserts, the soils of the Mediterranean basin experience seasonal rivers and flash floods which are becoming more frequent with climate change, affecting even the arid regions of the South (Greenbaum et al., 2010; Saber & Habib, 2016). Soil moisture and nitrogen dynamics are complicated by other intertwining factors like texture, which affects the structure and distribution of pore spaces, the water holding capacity, the relationship between water content and hydraulic pressure, the diffusion of gas through the soil system, and other features which play important roles in biogeochemical dynamics (Balaine et al., 2013; Gu et al., 2013; Weier et al., 1993). The Eastern Mediterranean is also home to remarkable soil typological diversity linked to strong climatological gradients which have affected pedogenesis over time, with more coarse loess soils to the dry South and more weathered, finer soils to the wetter North (Cerdà, 1998; Singer, 2007). The response of N_2O emissions to such events across the highly varied soils of the region is not well understood, particularly in combination with the relatively limited availability of carbon and nitrogen which can be expected to predominate in mid to late season and offseason in agricultural soils.

Soil N_2O emissions have been shown to increase with the degree of rewetting, suggesting that more intense precipitation events will contribute to a positive feedback of correspondingly higher N_2O emissions (Barrat et al., 2021; Guo et al., 2014). On the other hand, high soil moisture has been shown to conversely lead to a sharp decline in N_2O emissions as moisture rises above the air entry value (AEV), a hydraulic property controlled by texture and structure which describes the point at which air is first permitted to enter the largest pores when drying from saturation (Balaine et al., 2013; Es-haghi et al., 2022; Rabot et al., 2016). Because N_2O diffusion through water is approximately 10,000 times slower than through air (Heincke & Kaupenjohann, 1999), N_2O can become temporarily entrapped within the soil system under saturated conditions (Harter et al., 2016; Rabot et al., 2014). Eventually, soil moisture again falls and the opportunity for gas diffusion to the atmosphere is restored. What this means for subsequent N_2O emissions, however, depends on many factors which have not been sufficiently explored in the context of agricultural soils. N_2O is not the terminal product of microbial denitrification process, but is emitted from soil due to the “hole in the pipe” of nitrate reduction to dinitrogen (Firestone & Davidson, 1989). N_2O is thus produced and consumed by denitrification, and the amount of N_2O released after a entrapment depends upon the absolute and relative rates of subprocesses which produce and consume N_2O (Stanford, et al., 1975). Lowered gas diffusivity and higher tortuosity of finer textured soils may lead to greater N_2O entrapment at or near saturation, potentially allowing for complete reduction to lowered N_2O:N_2 ratio of emitted gases after long periods of entrapment (Gu et al., 2013). Conversely, if the rate of nitrite reduction to N_2O exceeds the rate of N_2O reduction to N_2, a lengthened period of anoxia would permit greater N_2O generation over time leading to increased emissions (Betlach & Tiedje, 1981).

Additional factors at play include the availability of denitrification substrates, particularly nitrogen and organic carbon. High soil organic matter substrate availability accelerates the overall rate of heterotrophic denitrification and can significantly or completely reduce available nitrate to N_2 (Panday et al., 2022; Senbayram et al., 2012; Stanford, Vander Pol, et al., 1975)- a key principle to improving water quality through woodchip bioreactors (Audet et al., 2021; Rivas et al., 2020). Under carbon limited conditions, however, denitrifying microbes may preferentially reduce more oxidized species of nitrogen, resulting in an accumulation of entrapped N_2O (Betlach & Tiedje, 1981; Firestone & Davidson, 1989). Thus, the overall impact of extended flooding on N_2O emissions is likely to be contextual, depending on site specific factors like texture, soil organic matter, and nitrogen availability. Investigating these competing dynamics during extended periods of high soil moisture on N_2O emissions is critical to understanding and predicting N_2O emissions from agriculture under altered precipitation distribution.

We hypothesize that increased flood duration will result in lower overall N_2O emissions due to increased gas entrapment and complete denitrification, and that this effect will be strongest in fine textured compared to coarse textured soils. It is our aim that the findings of this research will contribute to a better understanding of greenhouse gas emissions in response to extreme events and how emissions are expected to change in a warming climate.

Materials and Methods

Soil collection and characterization

Surface soil (0-15 cm) was collected from sites across four regions of Israel. Soil sampling locations were located along a 160-kilometer distance running North to South coinciding with a major historic mean annual precipitation (MAP) gradient from ~100 mm yr^{-1} to ~600 mm yr^{-1} (Singer, 2007). These included a Rhodoxeralf red sandy soil (locally referred to as Hamra) from the coastal plains (31°51'24.7"N 34°48'16.6"E), a Camborthid (locally loess) soil typical of northern Negev and the Beer Sheeva basin (30°52'18.4"N 34°47'19.7"E), an Aquic Rhodoxeralf (locally Nazaz) of the foothills of the Shefela region (31°35'26.6"N 34°49'54.3"E), and a vertisol (locally Grumusol) from the transition zone from the coastal plains to the foothills East of Netanya (32°19'05.3"N 34°59'54.5"E). Of note, the vertisol and Aquic Rhodoxeralf are both characterized by their common composition including expansive 2:1 phyllosilicate clay. Soils were sampled from agricultural lands previously under wheat production, a major crop in the region. Soil physical and chemical properties are given in **Table 4.1**. The percentages of sand, silt, and clay were determined using the hydrometer method (Gee & Or, 2002). Dissolved organic carbon (DOC) was measured with a Elementar vario TOC cube CN analyzer (Ronkonkoma, NY) using an HCl acid injection to first remove carbonate carbon. Total nitrogen was measured using the dry combustion method with an Elementar vario Max cube CN analyzer (Ronkonkoma, NY).

The air entry value (AEV) of soils is an important hydraulic characteristic which describes the negative pressure at which air begins to reenter pore spaces after saturation. This property has

Table 4.1: Soil physical and chemical properties.

Property	Sand	Loamy Sand	Sandy Clay Loam	Clay Loam
Sand (%)	91.6	83.9	60.6	40.3
Silt (%)	0.0	5.0	17.0	28.0
Clay (%)	8.4	11.1	22.4	31.7
pH	8.3	8.7	8.6	8.9
DOC (mg kg^{-1})	19.1	47.1	107.1	43.1
TN (mg kg^{-1})	0.3	1.6	7.2	4.0
Air Entry Value (% WFPS)	85	83	92	96
Historic MAP (mm)	500	100	400	600
Historic MAT (°C)	18	19	18	18
Taxonomy (Soil Survey Staff, USDA, 1999)	Typic Rhodoxeralf	Camborthid	Aquic Rhodoxeralf	Vertisol

been demonstrated to dictate at what degree of moisture soils will behave as saturated, with restricted gas diffusivity due to entrapment by moisture (Balaine et al., 2013; Rabot et al., 2016). The WFPS of soils at their AEV were estimated by generating soil water retention curves of aliquots using a Hyprop 2 instrument (Meter Group, Washington, USA). Soil was packed to a bulk density of 1.4 g cm^3 in rings and submersed to 5 mm below the ring's top and allowed to fully saturate for 7 days. Then, rings were transferred to the Hyprop 2 and allowed to air dry while continuously weighing and measuring soil tension. Once soil tension reached at least -50 kPa, rings were removed and oven dried to determine dry mass. Gravimetric water content was determined from the dry mass of soil, metal soil ring, and weighing measurements by Hyprop 2. Water retention curves of each soil texture were created relating the matric pressure to moisture content, and the AEV was estimated to be the inflection point where soil moisture sharply declines with respect to increasing soil tension (Fredlund & Xing, 1994). Finally, the gravimetric water content at this inflection point was related to the WFPS using the bulk densities of soils.

Experimental design

Soils were first air dried and sieved at <4 mm to remove rocks and debris, and the remaining moisture content was determined by oven drying subsamples at 105 °C for 48 hours. Soil was uniformly packed into 4.8 cm diameter, 10 cm height plastic cylinders to a bulk density of 1.4 g cm^{-3}, equaling 190 g of soil (dry basis) and 7.5 cm height for flux measurement cores and 126.7 g of soil (dry basis) and 5 cm height for destructive soil chemical analysis. The bottoms of soil cores were sealed with Parafilm to prevent soil loss and needlepoint holes were punctured in the Parafilm to allow water absorption. Soils were exposed to equal wetting and drying magnitudes across all treatments. An initial wetting to 35% WFPS was performed after which soils were allowed to air dry to 30% WFPS. Gas flux measurements were taken during this time to determine the background emission levels of soils under oxic conditions. Then, a simulated flooding event was performed in which soils were raised to 90% WFPS. This level was selected as a practical degree of saturation able to be maintained in soil cores without creating artifacts under laboratory condition, as well as a degree of moisture which has been shown to lead to significantly inhibited gas diffusion in soils across a range of bulk densities (Balaine et al., 2013; Klefoth et al., 2014). To investigate the impact of flooding duration on biogeochemical dynamics, three levels of flooding period were used for which 90% WFPS was maintained: zero days (0F), three days (3F), and seven days (7F). At the end of the flooding period, soils were allowed to air dry inside the incubation chamber. A full factorial experiment design was used giving a total of 48 experimental units (four textures by three flooding periods by four replications). Additional soil cores for each of the 12 treatment combinations were added to permit destructive soil analysis immediately before and after the flooding period for each treatment, with three replications for each time point, adding 72 experimental units (4 textures x 3 flooding periods x 3 replications). In total, 120 soil cores were prepared.

Soil moisture management

Soil cores were placed into plastic weighing boats and pre-incubated at 23 °C for seven days to allow soils to reach stable biogeochemical activity rates after disturbance. An initial wetting was performed to 35% WFPS, after which soil cores were allowed to air dry to 30% WFPS. Soil flux measurements were performed once every three days during this period to establish a baseline flux level of soils. The experiment commenced by weighing each soil core and adding Milli-Q water via a pipette to each weighing boat necessary to bring each core to 35% WFPS, allowing water to absorb via capillary action and diffuse uniformly. Soil cores were stored in the incubation chamber and weighed daily for moisture measurement. When cores of a given treatment reached an average of 30% WFPS, the flooding period was initiated. 20 mg N kg^{-1} soil of ammonium nitrate fertilizer was dissolved in Milli-Q water and added to the weighing boats, and additional Milli-Q water was added via pipette to a mass necessary to bring cores to 90% WFPS. This rate of N addition was intended to replicate the levels of ammonium and nitrate in soils during the middle to late period of the growing season experienced in wheat growing soils of this region (Shrestha et al., 2022). Furthermore, our objective was to capture the textural influence on N_2O emissions under varied saturation duration by avoiding the overpowering influence of large N fertilizer addition that is known to trigger emissions and potentially overshadowing other controlling factors. Cores were sealed on the bottom by two additional layers of Parafilm and tape to prevent leakage at high moisture content. Cores from the 3F and 7F treatments were additionally covered on the top by Parafilm punctured with needlepoint holes to reduce evaporation but still allow gas exchange. The weight of additional materials added to each core was measured and factored into subsequent core weighing. Upon adding water to reach 90% WFPS, the sandy clay loam and clay loam soils swelled due to their expansive clay content from their initial 7.5 cm height to 8 cm (1.31 g cm^{-3}) and 8.6 cm (1.22 g cm^{-3}), respectively. Water was added to weighing boats of these soils upon expansion to bring cores to 90% WFPS given their lowered bulk densities. On each subsequent day of the flooding period, all soil cores were weighed and any lost water mass was added via pipette to the top of the soil core to maintain 90% WFPS. At the end of the flooding period, Parafilm was removed from the top of the soil cores.

N_2O flux measurements

N_2O flux was measured from soil cores during the pre-incubation period and immediately prior to flooding (Day 0) to establish a baseline flux level. Then, gas flux was again sampled on days

1, 3, 4, and 7 days after wetting during the flooding periods and on days 1, 2, 3, 4, 7, and 10 after the end of the flooding period. For gas sampling, soil cores were placed inside sealed and airtight Mason jars (0.5 L) with rubber septa installed in the lids. Three 20 mL headspace gas samples were taken from each Mason jar using a syringe and deposited into 15 mL exetainer vials (Labco Limited, United Kingdom) at four time periods: 0 minutes, 50 minutes, 100 minutes, and 150 minutes. A gas chromatograph (Shimadzu GC-2014, Japan) with an electron capture detector was used to determine N_2O concentrations, while a flame ionization detector was used to determine CO_2 and CH_4 concentrations. Flux was calculated using the headspace volume and change in gas concentrations over time.

N_2O isotopomer analysis for microbial source identification

We determined the biogenic source of N_2O from soil cores by isotopomer analysis at key periods: immediately prior to wetting, approximately 24 hours after the end of the flooding period, and during the middle of the flooding period for 3F and 7F treatments. 120 mL of gas was collected from the headspace of Mason jars 150 minutes after enclosure of cores and stored into evacuated 100 mL crimp-top glass serum bottles (Sigma-Aldrich, St. Louis, MO). Gas samples were also taken from the laboratory air on each day of isotopomer sampling for ambient concentration. Bottles were shipped to the Stable Isotope Facility at the University of California-Davis for analysis using a GasBench-Precon isotope ration mass spectrometer (Mohn et al., 2014). ^{15}N site preference of the N_2O molecule was determined, which is indicative of the biogeochemical processes responsible for N_2O production (Sutka et al., 2006; Toyoda et al., 2005). The site preferences of nitrogen oxidation by nitrifiers and nitrogen reduction by nitrifiers and denitrifiers have been shown to be about 30-35% and -2-2%, respectively (Sutka et al., 2006). Thus, we compared the overall site preference of N_2O sampled from soil cores to an assumed a nitrification site preference of 35% and denitrification site preference of 0% to determine broadly the relative contributions of nitrification and denitrification to fluxes (Kravchenko et al., 2018; Saha et al., 2021b).

Soil chemical property measurements

Soil cores intended for destructive sampling were bagged and frozen. Remaining soil cores at the end of the incubation period were also bagged and frozen. Soils were analyzed for inorganic NH_4^+ and NO_3^- by extracting 10 g of fresh soil with 40 mL of 2 M KCl solution. Extractions were centrifuged and reagents were added to make colorimetric determinations of samples and known concentrations of NH_4^+ and NO_3^- (Doane & Horwáth, 2003; Forster, 1995; Mulvaney, 1996; Verdouw et al., 1978) using a Microplate reader (BioTek Instruments, Winooski, VT). Soils were also analyzed for DOC by extracting 4 g of dry soil with 40 mL of Milli-Q water (Jones & Willett, 2006). Extractions were centrifuged and analyzed on an Elementar vario TOC cube in liquid mode (Hanau, Germany).

Statistical analysis

It was initially theorized that flux would be relatively low or stable during the flooding period due to impeded gas diffusion, and thus flux was not measured every day during this period. Most notably, this presented a difficult decision in that flux was not measured on day 2 after wetting for the 3F and 7F treatments. In actuality, some soil textures experienced large spikes in flux on day 1 of the flooding period, and by day 3 had fallen back near the baseline level, with no measurement on day 2. Interpolating between gaps in N_2O measurements, particularly during hot moments and periods of high variability, has been shown to introduce significant error in cumulative flux estimation. Therefore, no interpolation was used in the estimation of cumulative flux. Rather, cumulative N_2O flux was calculated as the sum of flux measurements from each treatment on days -1, 0, 1, 3, 4, 7, and 10 where day 0 was the day of soil wetting. These dates were selected because flux was measured on each of these days across all treatments, and could be used to provide a fair comparison between treatments. The shortcoming of this method is that by omitting flux measurements on days where significant differences in fluxes across treatments may have existed, it could lead to an underestimation of treatment effects.

The existence of significant differences in cumulative flux between soil textures and flooding periods was investigated by two-way ANOVA. Subsequently, the effect of flooding period on cumulative flux was evaluated independently for each soil texture using post-hoc Tukey's pairwise honest significant difference (HSD) tests. Finally, the significance and marginal relative impact of both characteristics unique to each soil type and the flooding period were determined by ordinary least squares (OLS) linear regression. A full factorial, second-order equation including flooding period, clay content, and DOC content was evaluated. DOC was used as a metric of organic carbon availability due to its immediate accessibility by denitrifiers compared to total organic carbon, which is often dominated by mineral protected carbon and has been shown to be a poor predictor of N_2O emissions (Stuchiner et al., 2024). Clay was used as a proxy for soil texture due to clay's dominant role in many soil physical characteristics related to texture. Other relevant factors to N_2O emissions, including pH and initial total nitrogen content, were excluded due to only minute differences being found between textures.

Results

Temporal N_2O fluxes in response to flooding under different soil textures

N_2O fluxes across all treatments were near 0 ug N kg^{-1} d^{-1} after the initial wetting event to 35% WFPS. After wetting to 90% WFPS, all soils experienced an increase in N_2O emissions, with variations in the timing and magnitude of increase across different textures and flooding period treatments. Across all soil textures, the peak magnitudes of N_2O fluxes after flooding were lowest in the 0F treatments (**Figure 4.1**). The timing of peak flux magnitude also varied across soil textures. In clay loam and sandy clay loam soils, N_2O flux always sharply rose immediately after wetting, regardless of flooding treatment. The clay loam, which experienced the highest peak flux of all textures, also experienced the briefest hot moments, returning to negligible fluxes on the next measurement day after peaking. The sandy clay loam experienced smaller but more sustained hot moments, with emissions above the baseline level for 2-3 days after wetting.

On the other hand, the sand and loamy sand experienced delayed hot moments. Fluxes measured in these soils remained at the background level on the first day after wetting to 90% WFPS. Emissions from the loamy sand first increased on the second measurement day following flooding, which was either two or three days after the wetting event depending on the flooding period treatment. Hot moments were most delayed in sand. Average flux first rose notably four days after flooding in the 3F and 7F treatments but remained near the baseline on this day in the 0F treatment. It is possible that emissions rose earlier than was measured, i.e. five or six days after flooding, but was unmeasured. As a result, a notable increase in flux for the sandy soil was first measured seven days after flooding in the 0F. Notably, hot moments from sand and loamy sand occurred prior to the end of the flooding period in the 3F and 7F treatments, indicating that gas diffusion to the atmosphere was not completely prevented by wetting beyond the AEV.

Changes in soil chemical properties

Prior to the initialization of flooding which carried dissolved fertilizer, nitrate and ammonium content was below 3 mg N kg^{-1}. 24 hours after flooding of the 0F treatment, the nitrate concentration of all soils had increased, with the clay loam and sandy clay loam soils increasing by a greater extent (**Figure 4.2a**). Ammonium concentration of the 0F treatment increased

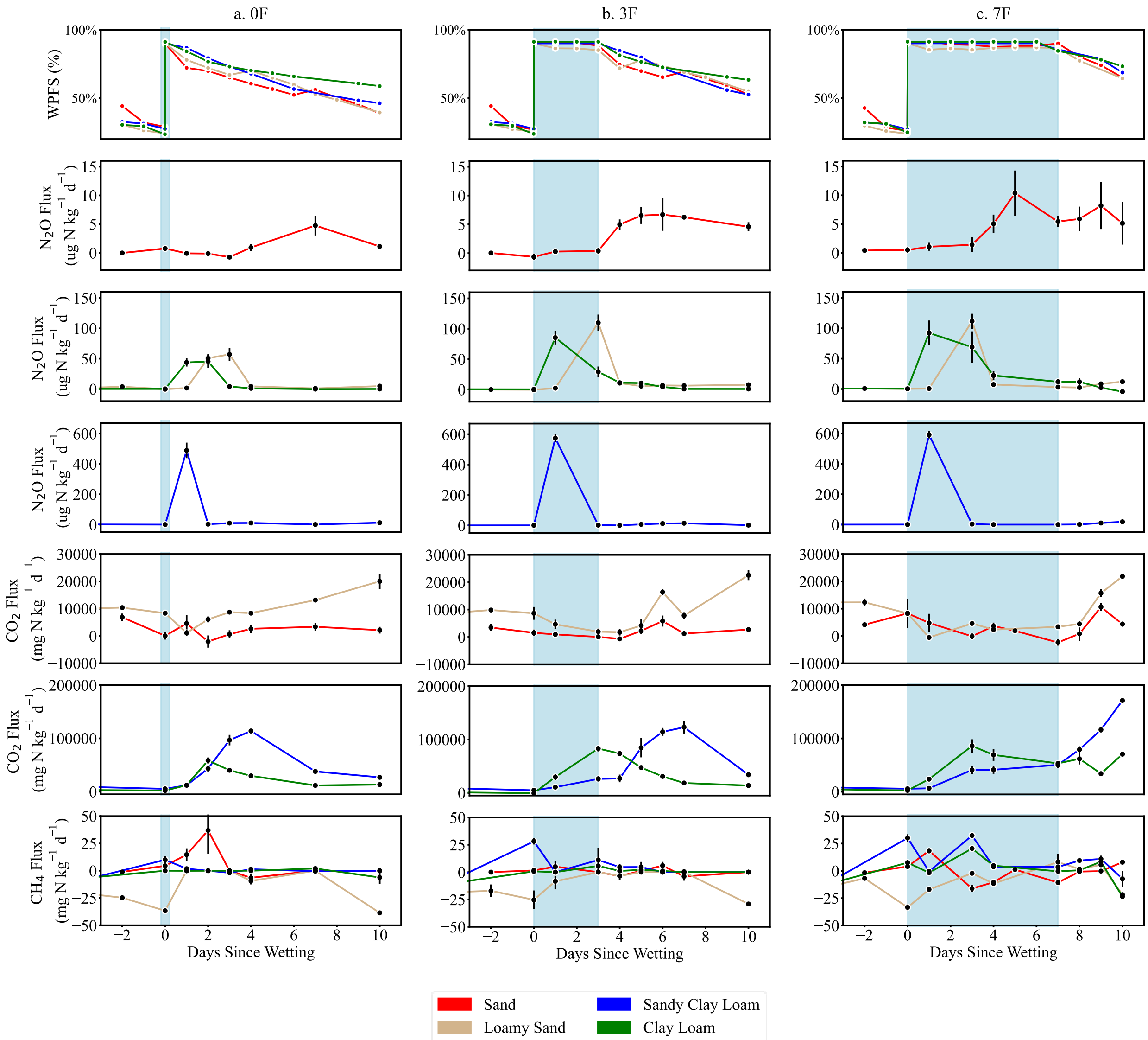

Figure 4.1: Daily soil moisture and N_2O, CO_2, and CH_4 fluxes measured for the a) 0F, b) 3F, and c) 7F flooding duration treatments. Multiple panels of N_2O and CO_2 fluxes are shown due to significantly different ranges of fluxes across soil textures. Light blue area indicates the flooding period during which 90% WFPS was maintained.

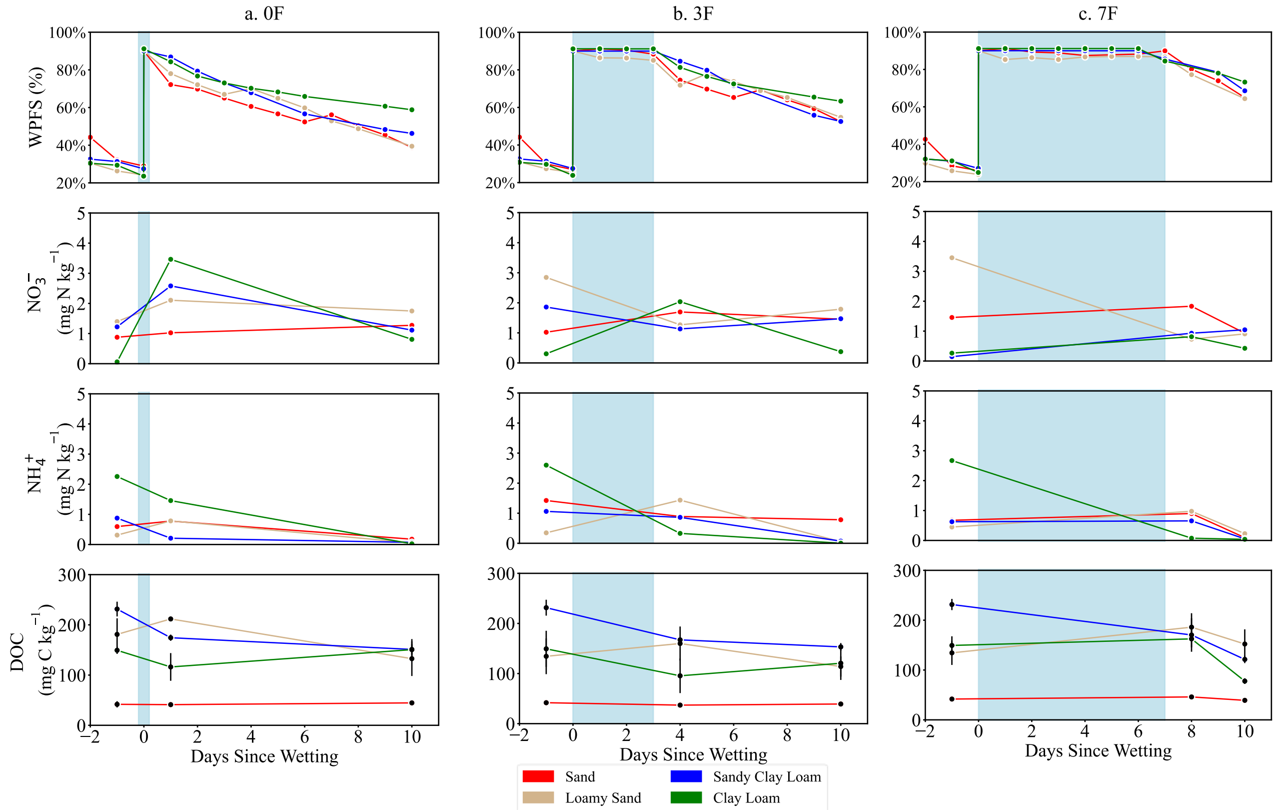

Figure 4.2: Daily soil moisture, inorganic nitrogen content, and dissolved organic matter measured for the a) 0F, b) 3F, and c) 7F flooding duration treatments. Light blue area indicates the flooding period during which 90% WFPS was maintained.

slightly in the sand and loamy sand over this time period, and decreased in the clay loam and sandy clay loam soils (**Figure 4.2a**). Similarly, by 10 days after the initialization of flooding all soils had an ammonium content below 1 mg N $kg^{-1}$and nitrate content below 2 mg N kg^{-1} (**Figure 4.2a**). In contrast to the other soil textures, ammonium concentration of the clay loam fell during the flooding period across all treatments, with greater flooding duration corresponding to greater decreases in ammonium. From the end of the flooding period to the end of the experiment, the ammonium concentration of all textures and treatments decreased. The nitrate concentration of loamy sand, sandy clay loam, and clay loam 24 hours after the end of the flooding treatment was associated with the flooding duration, with longer flooding periods measured to have lower subsequent nitrate concentrations. Finally, the DOC concentration consistently decreased throughout the flooding period in the sandy clay loam, while all other textures maintained a statistically equivalent concentration throughout flooding periods of all durations (**Figure 4.2**)

Isotopomer analysis and biological processes driving hot moments

It was anticipated that hot moments would be most likely to occur upon the commencement of drying following the flooding period, and thus gas sampling for isotopomer analysis was performed 24 hours after the final addition of water to maintain 90% WFPS. Additional isotopomer gas sampling was collected in the middle of the flooding period for the 7F treatments. In reality, however, these days did not always line up with elevated emissions. As a result, analysis of the biological processes underlying hot moments could only be obtained for certain treatments. For sand, this included the 7F treatment during and immediately after the flooding treatment. For loamy sand, this included during the flooding period for the 7F treatment and immediately after the flooding period for the 3F treatment. For sandy clay loam, isotopomer analysis was performed during elevated emissions only for the 0F treatment 24 hours after flooding. Finally, for the clay loam, analysis of biological contributors to hot moments could be determined for the 0F and 3F treatments 24 hours after the end of the flooding period and for the 7F treatment in the middle of the flooding period. All other gas samples analyzed for microbial source contribution before, during, and after the flooding period were found to have N_2O concentrations equal to the ambient atmospheric concentration.

Isotopomer analysis indicated that denitrification was the primary biotic process responsible for soil N_2O production across all soil textures, although variation occurred with soil texture and the timing of gas sampling (**Table 4.2**). Nitrification, and potentially fungal denitrification, were most significant in sand (~35%) during all periods of elevated emissions. Nitrification also played a relatively important role in hot moment emissions of the clay loam and sandy clay loam, though only in the 0F treatments. Denitrification was estimated to have contributed more than 90% of hot moment N_2O emissions for all other flooding treatments and soil textures.

Effect of flooding period and soil properties on cumulative N_2O flux

Cumulative flux varied from 7 to 616 ug N kg^{-1}. Lengthening the duration of flooding events significantly increased cumulative N_2O flux in three of the four soil textures (**Figure 4.3**). Cumulative flux of the 3F treatments were on average 108% higher than the 0F treatments, while cumulative flux of the 7F treatments were on average 28% higher than the 3F treatments across different soil textures. Cumulative flux from the 3F and 7F treatments were never statistically significant for a given soil texture, indicating that the effect of flooding time on emissions experienced diminishing returns over the week period (**Figure 4.3**).

Beyond the effect of flooding duration, several other factors and interactions were significant in driving cumulative N_2O emissions, particularly the major differences found between soil

Table 4.2: Isotopomer analysis of gases sampled during periods of elevated emissions. Site preference (SP) of ^{15}N and relative contributions of bacterial denitrification (f_D) and nitrification/fungal denitrification (f_{N+FD}) and their standard deviations across soil textures are given. Depending on texture and flooding treatment, elevated emissions coincided with isotopomer gas sampling 24 hours after first allowing flooded soils to dry (After Flooding) or at some point during the maintenance of the flooding period (During Flooding).

	Treatment	Period	SP	f_D (%)	f_{N+FD} (%)
Sand	3F	After Flooding	11.3	67.7 ± 0.4	32.2 ± 0.4
Sand	7F	During Flooding	11.9	66.1 ± 6.8	33.9 ± 6.8
Sand	7F	After Flooding	13.0	62.9 ± 16.4	37.1 ± 16.4
Loamy Sand	7F	During Flooding	2.65	91.5 ± 7.4	8.4 ± 7.4
Loamy Sand	3F	After Flooding	0.94	91.6 ± 7.4	8.5 ± 8.6
Sandy Clay Loam	0F	After Flooding	4.66	74.7 ± 3.2	25.3 ± 3.2
Clay Loam	0F	After Flooding	5.0	84.6 ± 11.1	15.4 ± 11.1
Clay Loam	3F	After Flooding	2.0	94.4 ± 1.8	5.6 ± 1.8
Clay Loam	7F	During Flooding	2.3	93.4 ± 1.3	6.6 ± 1.3
All Samples			6.19	83.3 ± 14.6	17.7 ± 14.6

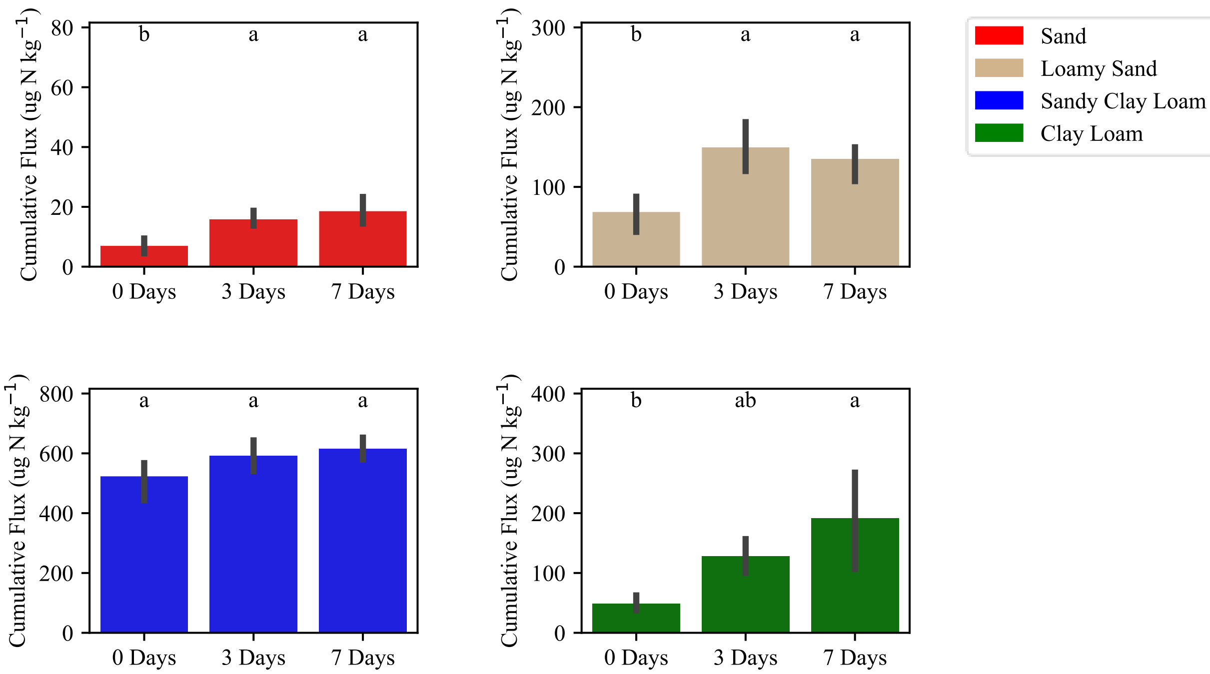

Figure 4.3: Cumulative N_2O emissions of flooding treatments segmented by soil texture. Error bars represent the standard error across replications, while letters above each bar represent significant differences in cumulative fluxes by Tukey's HSD. Significance was determined for each texture individually- equivalent letters does not indicate statistical equivalence from one quadrant graph to another.

textures. Averaged across flooding duration treatments the loamy sand (138.8 ug N kg^{-1}) and clay loam (145.3 ug N kg^{-1}) emitted around an order of magnitude more N_2O than did the sand (36.5 ug N kg^{-1}), and the sandy clay loam (601.0 ug N kg^{-1}) emitted roughly four times more than that (**Figure 4.3**). OLS multiple linear regression identified DOC, flooding duration, and clay content each to play significant roles in predicting cumulative flux (**Table 4.3**). Because factor values were first regularized, the coefficients can be used as a measure of the relative impact each factor had on cumulative N_2O flux. Increasing flooding duration and DOC both positively impacted predicted cumulative flux, though the large coefficient of DOC (185) indicates a much greater impact overall than flooding duration (coefficient = 41). Similarly, the positive coefficient of the second order of DOC indicates that increasing soil carbon led to an exponential increase in cumulative N_2O fluxes. Conversely, the negative coefficient of the second order of flooding days indicates a diminishing effect of the flooding period's increase on cumulative flux, in agreement with results from Tukey's HSD evaluation (**Figure 4.3**).

The importance of texture to N_2O emissions was identified in its interaction with flooding period, which is illustrated in the contour plot in **Figure 4.4**. At low flooding duration, increasing clay content had a negative but small impact on cumulative emissions, indicated by the relatively straight lines of the contour plot. At longer flooding duration, however, increasing clay content predicted higher cumulative N_2O emissions. The impact of clay content on emissions increased with flooding duration, illustrated by the contour lines shifting from straight to L-shaped curves further to the right. The final reduced model, including only effects reaching a 0.95 significance level, explained nearly all variance in cumulative flux across treatments (R^2 = 0.96) (**Figure 4.5**).

Table 4.3: Ordinary least squares multiple linear regression of cumulative N_2O flux.

Factor	Coefficient	t-score	P-value
Intercept	154.3	9.8	<0.0001
DOC	206.8	31.6	<0.0001
Flood Days	41.0	5.0	<0.0001
Clay Content	-17.5	-1.8	0.07
Flood Days x DOC	0.72	-0.7	0.49
DOC x Clay	-35.2	-1.5	0.14
Flood Days x Clay	22.1	2.1	0.04
$(DOC)^2$	40.6	4.6	<0.0001
$(Flood\ Days)^2$	-21.5	-2.0	0.05
$(Clay)^2$	7.0	0.04	0.97

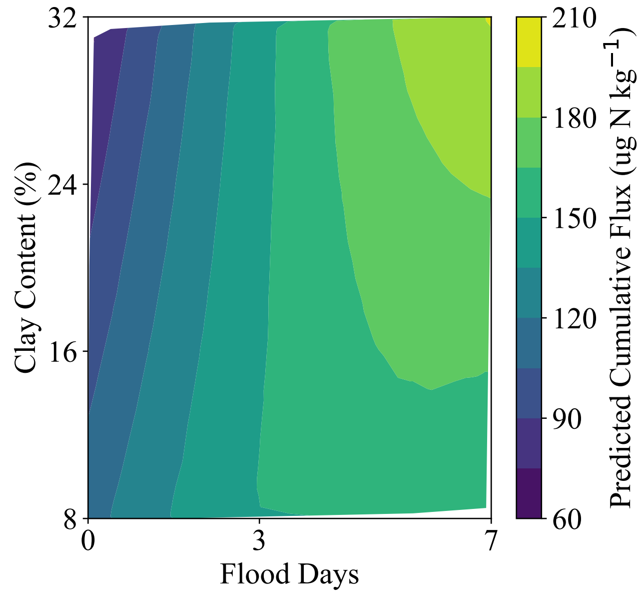

Figure 4.4: Predicted impact of the interaction between flooding duration (x-axis) and clay content (y-axis) on cumulative N_2O emissions (color).

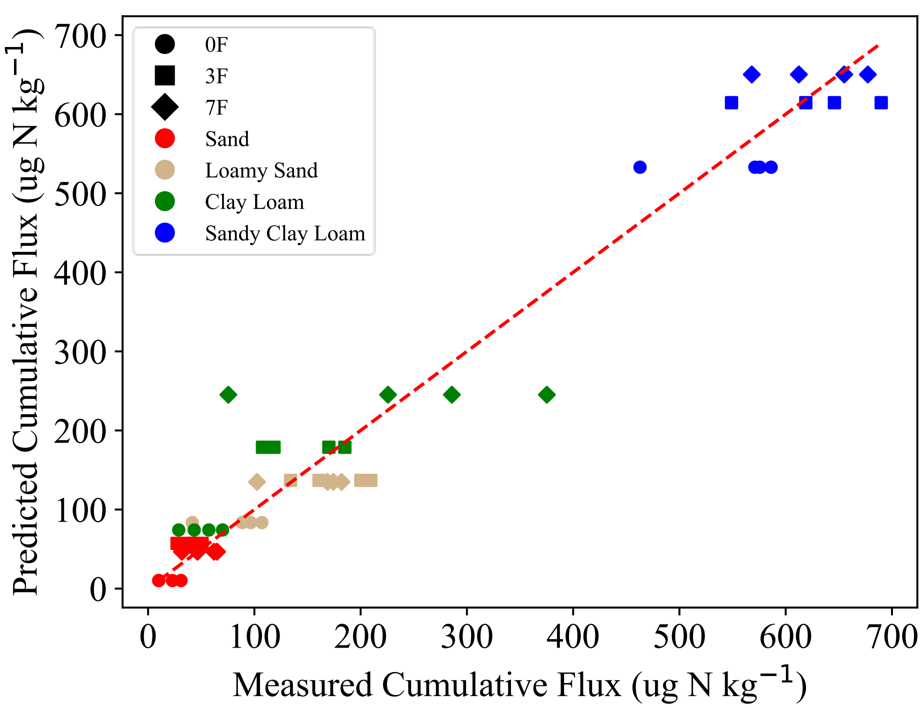

Figure 4.5: Actual and predicted cumulative N_2O emissions by the reduced regression model. Soil texture is indicated by color, while flooding duration is indicated by shape.

Discussion

Increased frequency of extreme weather events has the potential to create prolonged soil saturation events, the impact of which on N_2O emissions is not well understood. Soil moisture dynamics and gas diffusivity are profoundly influenced by soil texture, potentially creating varying outcomes in emissions across different soil types. We subjected four soils ranging from sand to clay loam to three durations of high moisture content: a transient period, three days, and seven days at a maintained 90% WFPS. Soils also varied in DOC content, and a small amount of ammonium nitrate fertilizer representative of late-season inorganic nitrogen content was added. We found that cumulative emissions were primarily driven by DOC availability, though increased flooding duration also contributed to significantly greater cumulative emissions.

Expansion of clay promoted gas diffusivity during flooding period

At very high soil moisture, higher gas diffusivity has typically been observed in coarse textured soils compared to fine textured soils due to the greater proportion of macropores and lower tortuosity, leading to lesser entrapment of gases and higher N_2O:(N_2O + N_2) of emitted gases (Fujikawa & Miyazaki, 2005; Gu et al., 2013; Klefoth et al., 2014). However, we observed the opposite relationship. First, analysis of soil water characteristic curves revealed that the two finer textured soils had AEV at higher moisture contents than did the sand and loamy sand (**Table 4.1**), indicating relatively greater gas diffusivity at 90% WFPS. In agreement, we measured high rates of N_2O and CO_2 emissions throughout the flooding period more commonly in fine textured soils, while gas emissions were depressed or delayed during this period in the coarse textured soils. We theorize these seemingly counterintuitive results can be explained by the expansive and aggregation properties also associated with the higher clay content of the two fine textured soils. Upon wetting, both the sandy clay loam and clay loam soils expanded, lowering their bulk densities from the initial 1.4 g cm^{-3} to 1.31 g cm^{-3} and 1.22 g cm^{-3}, respectively. While soil moisture was managed in response to maintain 90% WFPS, bulk density and the associated structural effects of swelling have profound impacts on gas diffusivity and N_2O emissions. The expansion of clays disrupts aggregates and may release a sudden flush of mineralized carbon and nitrogen into the soil solution, leading to a subsequent burst of microbial activity (Barrat et al., 2021; X. Guo et al., 2014; Navarro-García et al., 2012). This may lead to such rapid gas production that emissions become significant despite the effect of moisture slowing diffusion (Barrat et al., 2021).

Additionally, swelling tends to both increase overall porosity and macroporosity, increasing gas diffusivity and reducing the potential for gas entrapment (T. Ma et al., 2020). Lower bulk density has been associated with increased N_2O emissions at high moisture content due to higher gas diffusivity and lower residence time of N_2O (Harrison-Kirk et al., 2015; Klefoth et al., 2014; Rabot et al., 2016). Correspondingly, the higher expansive clay content of the clay loam compared to the sandy clay loam resulted in a greater degree of expansion, which was matched by higher CO_2 and N_2O emissions during the flooding period for the clay loam (**Figure 4.1**). Though not completely inhibited, CO_2 emissions from the sandy clay loam remained comparatively flatter during the flooding period than those of the clay loam, and subsequently rose sharply upon drying. These findings suggest that the greater degree of expansion of the clay loam led to consequently greater gas diffusion during the flooding period than other soil textures.

Texture impacted the timing of hot moments and underlying biological drivers

N_2O and CO_2 emissions from sandy soils were depressed immediately after wetting to 90% WFPS, and nearly always reached their peak days after the wetting event. These results were in line with our expectations, as these soils were wetted to moisture levels beyond their AEV, which has been shown to lead to gas entrapment (Balaine et al., 2013; Harter et al., 2016; Weier et al., 1993). In the 3F and 7F treatments, hot moments of N_2O emissions from the sand and loamy sand commenced three days after wetting, while soils were still being held at 90% WFPS. This suggests that gases were not permanently entrapped, but their diffusion and escape to the atmosphere was slowed. Consistent with high degree of anoxia during this period, isotopomer analysis indicated that denitrification was overwhelmingly responsible for N_2O production in the loamy sand during and immediately after the flooding period (~92%). On the other hand, nitrification played a much larger role in hot moment emissions in the sand (~33%), which would seem to contradict this explanation. However, the high contribution of nitrification to emissions from sand can be explained not by an increased rate of nitrification driven by aerobia, but rather the relatively low rate of denitrification. N_2O emissions from sand were substantially lower than those from other soil textures, with peak hot moment emissions an order of magnitude less than the loamy sand. The occurrence of hot moments depends upon both anoxia and substrate availability (McClain et al., 2003). We hypothesize that the low carbon content of the sand inhibited the rate of heterotrophic denitrification, leading to the relatively, but not necessarily absolutely, higher importance of nitrification.

In contrast to the coarse textured soils, both loamy soils produced peak hot moments within 24 hours of wetting. We observed that water absorbance in the loamy soils via capillary action and moisture diffusion was much slower than the sandy soils, related to their much higher clay content and consequently lower hydraulic conductivity (Sarki et al., 2014), and had likely not reached a uniform water potential by the time of the first subsequent gas sampling. This, combined with the swelling properties of the finer textured soils increasing porosity in response to wetting, likely allowed for a prolonged period of both oxic and anoxic microsites. Thus, N_2O

produced via nitrification within aerobic microsites and denitrification within anaerobic microsites simultaneously was permitted to move through remaining air-filled pore spaces and exit the soil easily during this early period, producing immediate hot moments. Corroborating this hypothesis, isotopomer analysis demonstrated that nitrification played a disproportionately large role in driving N_2O emissions from the sandy clay loam (25.3%) and clay loam (15.4%) soils 24 hours after wetting to 90% WFPS (**Table 4.2**). Soil ammonium content also fell in both the clay loam and sandy clay loam soils during this 24-hour period despite the addition of ammonium nitrate fertilizer (**Figure 4.2**), indicating considerable remaining areas of air-filled pores permitting aerobic nitrification.

Soon after N_2O emissions from the clay loam and sandy clay loam soils peaked upon wetting, they dropped precipitously across all flooding treatments. Two possible mechanistic explanations for these sharp declines include (1) an expenditure of available substrate for denitrification, and (2) an increase in gas entrapment upon finally reaching saturation, promoting complete denitrification and a shift to N_2 as the major product emitted. Evidence indicates gas entrapment may have played a role in reducing N_2O emissions in the sandy clay loam. This soil experienced only slight expansion upon wetting, limiting the impact of lowered bulk density to gas diffusion. Correspondingly, the sandy clay loam exhibited relatively low emissions of all gases measured during the flooding period beyond the first 24 hours, which is consistent with impeded gas diffusion and entrapment (**Figure 4.6**). However, our hypothesis that expansion of soils upon wetting led to an increase in gas diffusivity would suggest that gas entrapment is unlikely to have led to the decline in N_2O emissions in the clay loam. The clay loam expanded greatly due to its high clay content, thus it should follow that gas diffusion and emissions were promoted to the greatest extent. Corroborating this explanation, significant emissions of N_2O, CO_2, and, to a lesser extent, CH_4 indeed persisted throughout the flooding periods in the clay loam. Rather, a likely mechanism for the decline in N_2O emissions in the clay loam, and playing a contributing role in the sandy clay loam, was the expenditure of available nitrogen and carbon substrates (Guo et al., 2014). Soils were supplied with a small amount of inorganic nitrogen, intended to replicate late-season quantities. As a result, available substrate was likely expended after only a short period due to the rapid microbial activity.

Dissolved organic carbon availability primarily drove cumulative emissions

The most impactful effect on cumulative N_2O emissions identified by OLS regression was the availability of dissolved organic carbon upon commencement of the experiment. This pool of carbon represents the most readily available pool to denitrifiers, in contrast to the total organic carbon which is often dominated by more physically protected mineral-associated organic matter (Stuchiner et al., 2024). As such, over the course of a brief incubation experiment with limited time allowing for depolymerization, mineralization, and respiration, it is logical that this most immediately accessible portion of organic carbon was most strongly related to the denitrification rate and total N_2O emissions. We also observed an exponential increase in N_2O emissions with increasing DOC content (**Table 4.3**), which has also been reported in prior work (Harrison-Kirk et al., 2013). However, it should be considered that DOC availability was tightly associated with soil texture, considering that soil cores were prepared from bulk samples from each texture.

Flooding duration increased cumulative emissions to a limited extent

Four soils encompassing a broad range of textures were wetted to 90% WFPS and held at this high moisture level for varying periods of time. We hypothesized that entrapment of gas by high soil moisture would lead to more complete denitrification and a reduction in emissions in hot moments delayed by low gas diffusion, with a more pronounced effect in finer textured soils

(Harter et al., 2016). In contrast to our expectations, increased flooding duration led to equal or greater magnitudes of hot moments and cumulative emissions in all soils, whether or not there was evidence that high soil moisture led to temporary gas entrapment. In three out of four soil textures, cumulative flux was significantly greater after seven days of flooding compared to emissions from the transient flooding event (**Figure 4.3**). In the fourth soil, the sandy clay loam, emissions were 14% higher in the 3F and 7F treatments than the 0F treatment, though the impact of flooding duration may have been diluted by the strong influence of high DOC availability driving much higher emissions than observed in other soils (**Figure 4.3**). However, evidence from temporal flux measurements, Tukey's HSD, and regression analysis all indicated that the effect of flooding duration on increased emissions greatly diminished between the 3F and 7F treatments, which were never significantly different in cumulative emissions for a given soil. OLS regression analysis also indicated that the impact of flooding duration on increasing cumulative emissions also depended on clay content (**Table 4.3**). Our model predicted that as the flooding period was extended, clay content had an increasingly positive impact on cumulative emissions (**Figure 4.4**). This again follows from our hypothesis that texture and clay content played a key role in dictating cumulative N_2O emissions through its expansive properties. Considering that the clays found in our soils were expansive, greater clay content led to greater expansion and a magnified impact on bulk density, porosity, and gas diffusivity at high soil moisture, and therefore greater N_2O emissions while flooded. Therefore, longer flooding period magnified the impact of texture on cumulative N_2O emissions.

Conclusion

Our findings suggest that an increased frequency of extreme precipitation events leading to extended saturation conditions may result in a positive feedback loop of increased soil N_2O

emissions in response. Across a wide range of soil textures, we found greater hot moment magnitudes and cumulative emissions from soils which were held at 90% WFPS for at least three days compared to those which were permitted to immediately dry by evaporation after wetting. However, our findings also contextualize the impact of this mechanism. The difference in cumulative emissions between soil textures was much greater than those observed between different flooding durations within the same texture. We explain these differences as resulting from variations in the availability of organic matter and the effect of expansive clay material on soil physical characteristics, water dynamics, and gas diffusivity. We also showed that substantial hot moments can occur even with relatively low mineral nitrogen and organic matter content, reaffirming that hot moments driven by soil water dynamics may contribute substantially to agricultural N_2O emissions even late in the growing season or offseason.

CHAPTER 5: CONCLUSION

This study has delved into the important concept of hot moments in the context of soil N_2O emissions. I have shown that these transient events are responsible for the majority of all agricultural N_2O emissions, and have focused my research on methods to identify, predict, and better understand these phenomena. This began with the evaluation of quantitative methods for the identification of hot moments within N_2O flux measurement datasets. This was the first ever investigation which tested the performance of statistical methods across many experimental datasets encompassing a broad range of environmental, geographical, management, and statistical characteristics. I showed that the methods most often used to identify hot moments in prior research are significantly flawed, and that other methods, namely median absolute deviation and minimum covariance determinant, are broadly more suitable to identifying hot moments within temporal N_2O flux datasets from global agricultural soils. By conducting this comprehensive evaluation of methods at a global scale, I directly addressed the uncertainty within the scientific community born from the large variability of these data which has been an impediment to progress in the field of hot moments. The methods I identified as robust and successful in identifying hot moments, as well as the discussion I provide in their specific strengths and weaknesses, will allow future researchers to apply the hot moment concept to novel quantitative work investigating the role and drivers of these events.

Building on this work, I leveraged methods of identifying hot moments to classify experimental datasets to train machine learning models to predict their occurrences from simple environmental data. For the first time, I approached the prediction of soil N_2O emissions from the perspective of a classification problem. By simplifying the prediction task in terms of quantitative specificity, I showed that the relative rate of emissions can be accurately predicted (90%) across a broad range of conditions at high temporal resolution. I found that random forest and gradient boosting models performed well, and that expert-led hand classification produced the highest quality training data but that statistical methods I recommended in the previous chapter also produce accurate models. These findings are valuable on multiple fronts. First, this work has the potential to inform farm management and intervention strategies to avert or mitigate predicted future hot moments. Certain practices, such as the type and timing of fertilizer and the use of irrigation, were shown to significantly impact the likelihood of hot moments. By incorporating this information into predictive models and modeling future scenarios, land managers may be able to implement strategies to reduce agriculture's climate impact. Additionally, this work has the potential to improve quantitative modeling of N_2O emissions. Hot moments are driven by distinct biogeochemical conditions with are not accurately represented in process-based models due to their relative infrequence. Yet, with the ability to predict when such shifts conducive to hot moments are likely to occur, models may in the future adjust their mathematical representations of biogeochemical dynamics accordingly.

Finally, the relationship between N_2O hot moments and climate change led me to investigate how a specific environmental scenario likely to grow increasingly common, that of flooding, may impact emissions. Accurate models rely upon large numbers of individual studies researching the impacts of many factors, often one at a time, which come together to form a body of evidence that can be quantified and generalized. Contributing to this important task, I subjected four different soil textures to different durations of flooding events and measured the response of soil N_2O emissions and inorganic nitrogen dynamics. This experiment put to the test conflicting theories of either increased N_2O production under extended anoxia or increased N_2O consumption under extended entrapment within the soil system in a real-world scenario under relatively low soil nitrogen and carbon levels. I found that longer periods of flooding contribute to greater magnitudes of hot moments and overall cumulative emissions, at least up to a point. In some soils, high soil moisture temporarily impeded gas diffusion and delayed the occurrence of hot moments, but even these delayed hot moments were greater in magnitude than in soils which experienced only brief flooding. I also found that while the impact of flooding duration was significant, it was much less impactful that the availability of dissolved organic carbon in increasing emissions. The evidence presented in this study suggests that there is a potential for a positive feedback loop between climate change and N_2O emissions, as greater warming emissions contribute to more extreme precipitation events and in turn further increasing warming emissions. This knowledge is important to incorporate in modeling emissions at both the local and global scale to prepare for and work to mitigate global climate change.

There can be no silver bullets or magic solutions to a problem as grand in scale and severity as global climate change. Rather, rising appropriately to the challenge will require a great collective effort of thousands, millions of solutions enacted in every industry, region, and workplace. Each tiny moving of the needle is achieved through the significant effort of individual groups seizing opportunities endemic to their own context, and together they will change the world. Within my own context as an agriculturalist, passionate about cultivating the Earth and feeding people, I have identified hot moments of N_2O emissions as just such an opportunity for change. It is my hope that the work enclosed in this dissertation will contribute to efforts to better understand, quantify, predict, and ultimately mitigate N_2O hot moments from our farms, ensuring that we achieve the ability to feed the world without cooking the planet.

REFERENCES

Achakulwisut, P., Erickson, P., Guivarch, C., Schaeffer, R., Brutschin, E., & Pye, S. (2023). Global fossil fuel reduction pathways under different climate mitigation strategies and ambitions. *Nature Communications*, *14*(1), 5425. https://doi.org/10.1038/s41467-023-41105-z

Adler, P. R., Nguyen, H., Rau, B. M., & Dell, C. J. (2024). Modeling N2O emissions with remotely sensed variables using machine learning. *Environmental Research Communications*, *6*(9), 091004. https://doi.org/10.1088/2515-7620/ad707c

Aggarwal, C. C. (2017). *An introduction to outlier analysis*. Springer.

Andreou, C., & Karathanassi, V. (2014). Estimation of the Number of Endmembers Using Robust Outlier Detection Method. *IEEE Journal of Selected Topics in Applied Earth Observations and Remote Sensing*, *7*(1), 247–256. IEEE Journal of Selected Topics in Applied Earth Observations and Remote Sensing. https://doi.org/10.1109/JSTARS.2013.2260135

Anthony, T. L., & Silver, W. L. (2021). Hot moments drive extreme nitrous oxide and methane emissions from agricultural peatlands. *Global Change Biology*, *27*(20), 5141–5153. https://doi.org/10.1111/gcb.15802

Anthony, T. L., & Silver, W. L. (2024). Hot spots and hot moments of greenhouse gas emissions in agricultural peatlands. *Biogeochemistry*, *167*(4), 461–477. https://doi.org/10.1007/s10533-023-01095-y

Anthony, T. L., Szutu, D. J., Verfaillie, J. G., Baldocchi, D. D., & Silver, W. L. (2023). Carbon-sink potential of continuous alfalfa agriculture lowered by short-term nitrous oxide emission events. *Nature Communications*, *14*(1), Article 1. https://doi.org/10.1038/s41467-023-37391-2

Audet, J., Jéglot, A., Elsgaard, L., Maagaard, A. L., Sørensen, S. R., Zak, D., & Hoffmann, C. C. (2021). Nitrogen removal and nitrous oxide emissions from woodchip bioreactors treating agricultural drainage waters. *Ecological Engineering*, *169*, 106328. https://doi.org/10.1016/j.ecoleng.2021.106328

Ayadi, A., Ghorbel, O., Obeid, A. M., & Abid, M. (2017). Outlier detection approaches for wireless sensor networks: A survey. *Computer Networks*, *129*, 319–333. https://doi.org/10.1016/j.comnet.2017.10.007

Bachmann, G., Anagnostidis, S., & Hofmann, T. (2023). Scaling MLPs: A Tale of Inductive Bias. *Advances in Neural Information Processing Systems*, *36*, 60821–60840.

Baggs, E. M. (2011). Soil microbial sources of nitrous oxide: Recent advances in knowledge, emerging challenges and future direction. *Current Opinion in Environmental Sustainability*, *3*(5), 321–327. https://doi.org/10.1016/j.cosust.2011.08.011

Baggs, E., & Philippot, L. (2010). Microbial Terrestrial Pathways to Nitrous Oxide. In *Nitrous Oxide and Climate Change*. Routledge.

Balaine, N., Clough, T. J., Beare, M. H., Thomas, S. M., Meenken, E. D., & Ross, J. G. (2013). Changes in Relative Gas Diffusivity Explain Soil Nitrous Oxide Flux Dynamics. *Soil Science Society of America Journal*, *77*(5), 1496–1505. https://doi.org/10.2136/sssaj2013.04.0141

Barrat, H. A., Charteris, A. F., Le Cocq, K., Abadie, M., Clark, I. M., Chadwick, D. R., & Cardenas, L. (2022). N2O hot moments were not driven by changes in nitrogen and carbon substrates or changes in N cycling functional genes. *European Journal of Soil Science*, *73*(1), e13190. https://doi.org/10.1111/ejss.13190

Barrat, H. A., Evans, J., Chadwick, D. R., Clark, I. M., Le Cocq, K., & M. Cardenas, L. (2021). The impact of drought and rewetting on N2O emissions from soil in temperate and Mediterranean climates. *European Journal of Soil Science*, *72*(6), 2504–2516. https://doi.org/10.1111/ejss.13015

Bastos, L. M., Rice, C. W., Tomlinson, P. J., & Mengel, D. (2021). Untangling soil-weather drivers of daily N2O emissions and fertilizer management mitigation strategies in no-till corn. *Soil Science Society of America Journal*, *85*(5), 1437–1447. https://doi.org/10.1002/saj2.20292

Bendre, S. M., & Kale, B. K. (1987). Masking effect on tests for outliers in normal samples. *Biometrika*, *74*(4), 891–896. https://doi.org/10.1093/biomet/74.4.891

Ben-Gal, I. (2005). Outlier Detection. In O. Maimon & L. Rokach (Eds.), *Data Mining and Knowledge Discovery Handbook* (pp. 131–146). Springer US. https://doi.org/10.1007/0-387-25465-X_7

Benoit, M., Garnier, J., & Billen, G. (2015). Temperature dependence of nitrous oxide production of a luvisolic soil in batch experiments. *Process Biochemistry*, *50*(1), 79–85. https://doi.org/10.1016/j.procbio.2014.10.013

Bernhardt, E. S., Blaszczak, J. R., Ficken, C. D., Fork, M. L., Kaiser, K. E., & Seybold, E. C. (2017). Control Points in Ecosystems: Moving Beyond the Hot Spot Hot Moment Concept. *Ecosystems*, *20*(4), 665–682. https://doi.org/10.1007/s10021-016-0103-y

Betlach, M. R., & Tiedje, J. M. (1981). Kinetic Explanation for Accumulation of Nitrite, Nitric Oxide, and Nitrous Oxide During Bacterial Denitrification. *Applied and Environmental Microbiology*, *42*(6), 1074–1084. https://doi.org/10.1128/aem.42.6.1074-1084.1981

Boughorbel, S., Jarray, F., & El-Anbari, M. (2017). Optimal classifier for imbalanced data using Matthews Correlation Coefficient metric. *PLOS ONE*, *12*(6), e0177678. https://doi.org/10.1371/journal.pone.0177678

Bouwman, A. F. (1994). *Method to estimate direct nitrous oxide emissions from agricultural soils* (773004004). Nat. Inst. Public Health and Environ. Protection (RIVM).

Bowles, D. C., Butler, C. D., & Morisetti, N. (2015). Climate change, conflict and health. *Journal of the Royal Society of Medicine*, *108*(10), 390–395. https://doi.org/10.1177/0141076815603234

Bremner, J. M., Blackmer, A. M., & Waring, S. A. (1980). Formation of nitrous oxide and dinitrogen by chemical decomposition of hydroxylamine in soils. *Soil Biology and Biochemistry*, *12*(3), 263–269. https://doi.org/10.1016/0038-0717(80)90072-3

Brilli, L., Bechini, L., Bindi, M., Carozzi, M., Cavalli, D., Conant, R., Dorich, C. D., Doro, L., Ehrhardt, F., Farina, R., Ferrise, R., Fitton, N., Francaviglia, R., Grace, P., Iocola, I., Klumpp, K., Léonard, J., Martin, R., Massad, R. S., … Bellocchi, G. (2017). Review and analysis of strengths and weaknesses of agro-ecosystem models for simulating C and N fluxes. *Science of The Total Environment*, *598*, 445–470. https://doi.org/10.1016/j.scitotenv.2017.03.208

Butterbach-Bahl, K., Baggs, E. M., Dannenmann, M., Kiese, R., & Zechmeister-Boltenstern, S. (2013). Nitrous oxide emissions from soils: How well do we understand the processes and their controls? *Philosophical Transactions of the Royal Society B: Biological Sciences*, *368*(1621), 20130122. https://doi.org/10.1098/rstb.2013.0122

Caranto, J. D., & Lancaster, K. M. (2017). Nitric oxide is an obligate bacterial nitrification intermediate produced by hydroxylamine oxidoreductase. *Proceedings of the National Academy of Sciences*, *114*(31), 8217–8222. https://doi.org/10.1073/pnas.1704504114

Cassidy, E. S., West, P. C., Gerber, J. S., & Foley, J. A. (2013). Redefining agricultural yields: From tonnes to people nourished per hectare. *Environmental Research Letters*, *8*(3), 034015. https://doi.org/10.1088/1748-9326/8/3/034015

Cerdà, A. (1998). Effect of climate on surface flow along a climatological gradient in Israel: A field rainfall simulation approach. *Journal of Arid Environments*, *38*(2), 145–159. https://doi.org/10.1006/jare.1997.0342

Chandola, V., Banerjee, A., & Kumar, V. (2009). Anomaly detection: A survey. *ACM Computing Surveys*, *41*(3), 15:1-15:58. https://doi.org/10.1145/1541880.1541882

Chaplin-Kramer, R., Chappell, M. J., & Bennett, E. M. (2023). Un-yielding: Evidence for the agriculture transformation we need. *Annals of the New York Academy of Sciences*, *1520*(1), 89–104. https://doi.org/10.1111/nyas.14950

Chiaravalloti, I., Theunissen, N., Zhang, S., Wang, J., Sun, F., Ahmed, A. A., Pihlap, E., Reinhard, C. T., & Planavsky, N. J. (2023). Mitigation of soil nitrous oxide emissions during maize production with basalt amendments. *Frontiers in Climate*, *5*. https://doi.org/10.3389/fclim.2023.1203043

Chicco, D., & Jurman, G. (2020). The advantages of the Matthews correlation coefficient (MCC) over F1 score and accuracy in binary classification evaluation. *BMC Genomics*, *21*(1), 6. https://doi.org/10.1186/s12864-019-6413-7

Chicco, D., & Jurman, G. (2023). The Matthews correlation coefficient (MCC) should replace the ROC AUC as the standard metric for assessing binary classification. *BioData Mining*, *16*(1), 4. https://doi.org/10.1186/s13040-023-00322-4

Clark, M. A., Domingo, N. G. G., Colgan, K., Thakrar, S. K., Tilman, D., Lynch, J., Azevedo, I. L., & Hill, J. D. (2020). Global food system emissions could preclude achieving the 1.5° and 2°C climate change targets. *Science*, *370*(6517), 705–708. https://doi.org/10.1126/science.aba7357

Clayton, H., McTaggart, I. P., Parker, J., Swan, L., & Smith, K. A. (1997). Nitrous oxide emissions from fertilised grassland: A 2-year study of the effects of N fertiliser form and environmental conditions. *Biology and Fertility of Soils*, *25*(3), 252–260. https://doi.org/10.1007/s003740050311

Climate Action Reserve. (2021). *U.S. Nitrogen Management Protocol*. U.S. Nitrogen Management Protocol. https://www.climateactionreserve.org/how/protocols/ncs/nitrogen-management/

Corre, M. D., van Kessel, C., & Pennock, D. J. (1996). Landscape and Seasonal Patterns of Nitrous Oxide Emissions in a Semiarid Region. *Soil Science Society of America Journal*, *60*(6), 1806–1815. https://doi.org/10.2136/sssaj1996.03615995006000060028x

Cover, T., & Hart, P. (1967). Nearest neighbor pattern classification. *IEEE Transactions on Information Theory*, *13*(1), 21–27. https://doi.org/10.1109/TIT.1967.1053964

Crippa, M., Solazzo, E., Guizzardi, D., Monforti-Ferrario, F., Tubiello, F. N., & Leip, A. (2021). Food systems are responsible for a third of global anthropogenic GHG emissions. *Nature Food*, *2*(3), Article 3. https://doi.org/10.1038/s43016-021-00225-9

D, D. & Babu, S. S. (2016). Methods to detect different types of outliers. *2016 International Conference on Data Mining and Advanced Computing (SAPIENCE)*, 23–28. https://doi.org/10.1109/SAPIENCE.2016.7684114

Dastjerdy, B., Saeidi, A., & Heidarzadeh, S. (2023). Review of Applicable Outlier Detection Methods to Treat Geomechanical Data. *Geotechnics*, *3*(2), Article 2. https://doi.org/10.3390/geotechnics3020022

Davies, K., & Riddell, T. (2017). The Warming War: How Climate Change Is Creating Threats to International Peace and Security. *Georgetown Environmental Law Review*, *30*, 47.

Del Grosso, S. J., White, J. W., Wilson, G., Vandenberg, B., Karlen, D. L., Follett, R. F., Johnson, J. M. F., Franzluebbers, A. J., Archer, D. W., Gollany, H. T., Liebig, M. A., Ascough, J., Reyes-Fox, M., Pellack, L., Starr, J., Barbour, N., Polumsky, R. W., Gutwein, M., & James, D. (2013). Introducing the GRACEnet/REAP Data Contribution, Discovery, and Retrieval System. *Journal of Environmental Quality*, *42*(4), 1274–1280. https://doi.org/10.2134/jeq2013.03.0097

Del Grosso, S. J., Wirth, T., Ogle, S. M., & Parton, W. J. (2008). Estimating Agricultural Nitrous Oxide Emissions. *Eos, Transactions American Geophysical Union*, *89*(51), 529–529. https://doi.org/10.1029/2008EO510001

Deng, L., Zhu, G., Tang, Z., & Shangguan, Z. (2016). Global patterns of the effects of land-use changes on soil carbon stocks. *Global Ecology and Conservation*, *5*, 127–138. https://doi.org/10.1016/j.gecco.2015.12.004

Dhaliwal, J. K., Panday, D., Robertson, G. P., & Saha, D. (2025). Machine learning reveals dynamic controls of soil nitrous oxide emissions from diverse long-term cropping systems. *Journal of Environmental Quality*, *54*(1), 132–146. https://doi.org/10.1002/jeq2.20637

Doane, T. A., & and Horwáth, W. R. (2003). Spectrophotometric Determination of Nitrate with a Single Reagent. *Analytical Letters*, *36*(12), 2713–2722. https://doi.org/10.1081/AL-120024647

Domingues, R., Filippone, M., Michiardi, P., & Zouaoui, J. (2018). A comparative evaluation of outlier detection algorithms: Experiments and analyses. *Pattern Recognition*, *74*, 406–421. https://doi.org/10.1016/j.patcog.2017.09.037

Dorich, C. D., Conant, R. T., Albanito, F., Butterbach-Bahl, K., Grace, P., Scheer, C., Snow, V. O., Vogeler, I., & van der Weerden, T. J. (2020). Improving N2O emission estimates with the global N2O database. *Current Opinion in Environmental Sustainability*, *47*, 13–20. https://doi.org/10.1016/j.cosust.2020.04.006

EPA. (2023). *Inventory of U.S. Greenhouse Gas Emissions and Sinks: 1990-2021*. U.S. Environmental Protection Agency, EPA 430-R-23-002. https://www.epa.gov/ghgemissions/inventory-us-greenhouse-gas-emissions-and-sinks-1990-2021.

Erisman, J. W., Sutton, M. A., Galloway, J., Klimont, Z., & Winiwarter, W. (2008). How a century of ammonia synthesis changed the world. *Nature Geoscience*, *1*(10), Article 10. https://doi.org/10.1038/ngeo325

Es-haghi, M. S., Rezania, M., & Bagheri, M. (2022). Machine learning-based estimation of soil's true air-entry value from GSD curves. *Gondwana Research*. https://doi.org/10.1016/j.gr.2022.06.012

Eshel, G., Shepon, A., Makov, T., & Milo, R. (2014). Land, irrigation water, greenhouse gas, and reactive nitrogen burdens of meat, eggs, and dairy production in the United States. *Proceedings of the National Academy of Sciences*, *111*(33), 11996–12001. https://doi.org/10.1073/pnas.1402183111

Fernández, Á., Bella, J., & Dorronsoro, J. R. (2022). Supervised outlier detection for classification and regression. *Neurocomputing*, *486*, 77–92. https://doi.org/10.1016/j.neucom.2022.02.047

Firestone, M. K. (1982). Biological denitrification. *Nitrogen in Agricultural Soils*, *22*, 289–326.

Firestone, M. K., & Davidson, E. A. (1989). Microbiological basis of NO and N2O production and consumption in soil. *Exchange of Trace Gases between Terrestrial Ecosystems and the Atmosphere*, *47*, 7–21.

Forster, J. C. (1995). 3—Soil sampling, handling, storage and analysis. In K. Alef & P. Nannipieri (Eds.), *Methods in Applied Soil Microbiology and Biochemistry* (pp. 49–121). Academic Press. https://doi.org/10.1016/B978-012513840-6/50018-5

Fredlund, D. G., & Xing, A. (1994). Equations for the soil-water characteristic curve. *Canadian Geotechnical Journal*, *31*(4), 521–532. https://doi.org/10.1139/t94-061

Fuchs, K., Merbold, L., Buchmann, N., Bretscher, D., Brilli, L., Fitton, N., Topp, C. F. E., Klumpp, K., Lieffering, M., Martin, R., Newton, P. C. D., Rees, R. M., Rolinski, S., Smith, P., & Snow, V. (2020). Multimodel Evaluation of Nitrous Oxide Emissions From an Intensively Managed Grassland. *Journal of Geophysical Research: Biogeosciences*, *125*(1), e2019JG005261. https://doi.org/10.1029/2019JG005261

Fujikawa, T., & Miyazaki, T. (2005). Effects of Bulk Density and Soil Type on the Gas Diffusion Coefficient in Repacked and Undisturbed Soils. *Soil Science*, *170*(11), 892. https://doi.org/10.1097/01.ss.0000196771.53574.79

Gaillard, R. K., Jones, C. D., Ingraham, P., Collier, S., Izaurralde, R. C., Jokela, W., Osterholz, W., Salas, W., Vadas, P., & Ruark, M. D. (2018). Underestimation of N2O emissions in a comparison of the DayCent, DNDC, and EPIC models. *Ecological Applications*, *28*(3), 694–708. https://doi.org/10.1002/eap.1674

Garnett, T. (2011). Where are the best opportunities for reducing greenhouse gas emissions in the food system (including the food chain)? *Food Policy*, *36*, S23–S32. https://doi.org/10.1016/j.foodpol.2010.10.010

Gee, G. W., & Or, D. (2002). 2.4 Particle-Size Analysis. In *Methods of Soil Analysis* (pp. 255–293). John Wiley & Sons, Ltd. https://doi.org/10.2136/sssabookser5.4.c12

Glauber, J. (2011, February 18). *Development of Technical Guidelines and Scientific Methods for Quantifying GHG Emissions and Carbon Sequestration for Agricultural and Forestry Activities*. Federal Register. https://www.federalregister.gov/documents/2011/02/18/2011-3731/development-of-technical-guidelines-and-scientific-methods-for-quantifying-ghg-emissions-and-carbon

Glenn, A. J., Moulin, A. P., Roy, A. K., & Wilson, H. F. (2021). Soil nitrous oxide emissions from no-till canola production under variable rate nitrogen fertilizer management. *Geoderma*, *385*, 114857. https://doi.org/10.1016/j.geoderma.2020.114857

Greenbaum, N., Schwartz, U., & Bergman, N. (2010). Extreme floods and short-term hydroclimatological fluctuations in the hyper-arid Dead Sea region, Israel. *Global and Planetary Change*, *70*(1), 125–137. https://doi.org/10.1016/j.gloplacha.2009.11.013

Groffman, P., Butterbach-Bahl, K., Fulweiler, R. W., Gold, A. J., Morse, J. L., Stander, E. K., Tague, C., Tonitto, C., & Vidon, P. (2009). Challenges to incorporating spatially and temporally explicit phenomena (hotspots and hot moments) in denitrification models. *Biogeochemistry*, *93*(1), 49–77. https://doi.org/10.1007/s10533-008-9277-5

Groffman, P., Tiedje, J., Robertson, G., & Christensen, S. (1988). Denitrification at different temporal and geographical scales: Proximal and distal controls. *Advances in Nitrogen Cycling in Agricultural Ecosystems*, 174–192.

Grunditz, C., & Dalhammar, G. (2001). Development of nitrification inhibition assays using pure cultures of *nitrosomonas* and *nitrobacter*. *Water Research*, *35*(2), 433–440. https://doi.org/10.1016/S0043-1354(00)00312-2

Gu, J., Nicoullaud, B., Rochette, P., Grossel, A., Hénault, C., Cellier, P., & Richard, G. (2013). A regional experiment suggests that soil texture is a major control of N2O emissions from tile-drained winter wheat fields during the fertilization period. *Soil Biology and Biochemistry*, *60*, 134–141. https://doi.org/10.1016/j.soilbio.2013.01.029

Guo, L. B., & Gifford, R. M. (2002). Soil carbon stocks and land use change: A meta analysis. *Global Change Biology*, *8*(4), 345–360. https://doi.org/10.1046/j.1354-1013.2002.00486.x

Guo, X., Drury, C. F., Yang, X., Reynolds, W. D., & Fan, R. (2014). The Extent of Soil Drying and Rewetting Affects Nitrous Oxide Emissions, Denitrification, and Nitrogen Mineralization. *Soil Science Society of America Journal*, *78*(1), 194–204. https://doi.org/10.2136/sssaj2013.06.0219

Hampel, F. R. (1971). A General Qualitative Definition of Robustness. *The Annals of Mathematical Statistics*, *42*(6), 1887–1896. https://doi.org/10.1214/aoms/1177693054

Hamrani, A., Akbarzadeh, A., & Madramootoo, C. A. (2020). Machine learning for predicting greenhouse gas emissions from agricultural soils. *Science of The Total Environment*, *741*, 140338. https://doi.org/10.1016/j.scitotenv.2020.140338

Harris, C. R., Millman, K. J., Walt, S. J. van der, Gommers, R., Virtanen, P., Cournapeau, D., Wieser, E., Taylor, J., Berg, S., Smith, N. J., Kern, R., Picus, M., Hoyer, S., Kerkwijk, M. H. van, Brett, M., Haldane, A., Río, J. F. del, Wiebe, M., Peterson, P., … Oliphant, T. E. (2020). Array programming with NumPy. *Nature*, *585*(7825), 357–362. https://doi.org/10.1038/s41586-020-2649-2

Harrison-Kirk, T., Beare, M. H., Meenken, E. D., & Condron, L. M. (2013). Soil organic matter and texture affect responses to dry/wet cycles: Effects on carbon dioxide and nitrous oxide emissions. *Soil Biology and Biochemistry*, *57*, 43–55. https://doi.org/10.1016/j.soilbio.2012.10.008

Harrison-Kirk, T., Thomas, S. M., Clough, T. J., Beare, M. H., van der Weerden, T. J., & Meenken, E. D. (2015). Compaction influences N2O and N2 emissions from 15N-labeled synthetic urine in wet soils during successive saturation/drainage cycles. *Soil Biology and Biochemistry*, *88*, 178–188. https://doi.org/10.1016/j.soilbio.2015.05.022

Harter, J., Guzman-Bustamante, I., Kuehfuss, S., Ruser, R., Well, R., Spott, O., Kappler, A., & Behrens, S. (2016). Gas entrapment and microbial N2O reduction reduce N2O emissions from a biochar-amended sandy clay loam soil. *Scientific Reports*, *6*(1), Article 1. https://doi.org/10.1038/srep39574

Heil, J., Liu, S., Vereecken, H., & Brüggemann, N. (2015). Abiotic nitrous oxide production from hydroxylamine in soils and their dependence on soil properties. *Soil Biology and Biochemistry*, *84*, 107–115. https://doi.org/10.1016/j.soilbio.2015.02.022

Heincke, M., & Kaupenjohann, M. (1999). Effects of soil solution on the dynamics of N2O emissions: A review. *Nutrient Cycling in Agroecosystems*, *55*(2), 133–157. https://doi.org/10.1023/A:1009842011599

Hénault, C., Grossel, A., Mary, B., Roussel, M., & Léonard, J. (2012). Nitrous Oxide Emission by Agricultural Soils: A Review of Spatial and Temporal Variability for Mitigation. *Pedosphere*, *22*(4), 426–433. https://doi.org/10.1016/S1002-0160(12)60029-0

Hu, H.-W., Chen, D., & He, J.-Z. (2015). Microbial regulation of terrestrial nitrous oxide formation: Understanding the biological pathways for prediction of emission rates. *FEMS Microbiology Reviews*, *39*(5), 729–749. https://doi.org/10.1093/femsre/fuv021

Huang, C. (2020). *WQFS Study for Greenhouse gas Reduction through Agricultural Carbon Enhancement network in West Lafayette, Indiana* (10579353-ec7d-4274-af95-c2e1e4857fcd) [Dataset]. Ag Data Commons. https://data.nal.usda.gov/dataset/wqfs-study-greenhouse-gas-reduction-through-agricultural-carbon-enhancement-network-west-lafayette-indiana

Huang, H., Wang, J., Hui, D., Miller, D. R., Bhattarai, S., Dennis, S., Smart, D., Sammis, T., & Reddy, K. C. (2014). Nitrous oxide emissions from a commercial cornfield (*Zea mays*) measured using the eddy covariance technique. *Atmospheric Chemistry and Physics*, *14*(23), 12839–12854. https://doi.org/10.5194/acp-14-12839-2014

Hubert, M., Debruyne, M., & Rousseeuw, P. J. (2018). Minimum covariance determinant and extensions. *WIREs Computational Statistics*, *10*(3), e1421. https://doi.org/10.1002/wics.1421

Intergovernmental Panel On Climate Change (IPCC) (Ed.). (2023). Agriculture, Forestry and Other Land Uses (AFOLU). In *Climate Change 2022—Mitigation of Climate Change*

(1st ed., pp. 747–860). Cambridge University Press. https://doi.org/10.1017/9781009157926.009

Intergovernmental Panel on Climate Change (IPCC) (Ed.). (2023). Global Carbon and Other Biogeochemical Cycles and Feedbacks. In *Climate Change 2021: The Physical Science Basis: Working Group I Contribution to the Sixth Assessment Report of the Intergovernmental Panel on Climate Change* (pp. 673–816). Cambridge University Press; Cambridge Core. https://doi.org/10.1017/9781009157896.007

Intergovernmental Panel On Climate Change (IPCC) (Ed.). (2023). Mitigation Pathways Compatible with Long-term Goals. In *Climate Change 2022—Mitigation of Climate Change* (1st ed., pp. 295–408). Cambridge University Press. https://doi.org/10.1017/9781009157926.005

Intergovernmental Panel On Climate Change (IPCC). (2022). *Climate Change and Land: IPCC Special Report on Climate Change, Desertification, Land Degradation, Sustainable Land Management, Food Security, and Greenhouse Gas Fluxes in Terrestrial Ecosystems* (1st ed.). Cambridge University Press. https://doi.org/10.1017/9781009157988

J. A. Gualtieri & S. Chettri. (2000). Support vector machines for classification of hyperspectral data. *IGARSS 2000. IEEE 2000 International Geoscience and Remote Sensing Symposium. Taking the Pulse of the Planet: The Role of Remote Sensing in Managing the Environment. Proceedings (Cat. No.00CH37120)*, *2*, 813–815 vol.2. https://doi.org/10.1109/IGARSS.2000.861712

Jarecki, M. K., Parkin, T. B., Chan, A. S. K., Hatfield, J. L., & Jones, R. (2008). Comparison of DAYCENT-Simulated and Measured Nitrous Oxide Emissions from a Corn Field.

Journal of Environmental Quality, *37*(5), 1685–1690. https://doi.org/10.2134/jeq2007.0614

Johnson, J. (2021). *Carbon Crops Study for Greenhouse gas Reduction through Agricultural Carbon Enhancement network and Resilient Economic Agricultural Practices in Morris, Minnesota* (21d6ff3b-de69-44ff-a2b6-980a9c972a35) [Dataset]. Ag Data Commons. https://data.nal.usda.gov/dataset/carbon-crops-study-greenhouse-gas-reduction-through-agricultural-carbon-enhancement-network-and-resilient-economic-agricultural-practices-morris-minnesota

Jones, D. L., & Willett, V. B. (2006). Experimental evaluation of methods to quantify dissolved organic nitrogen (DON) and dissolved organic carbon (DOC) in soil. *Soil Biology and Biochemistry*, *38*(5), 991–999. https://doi.org/10.1016/j.soilbio.2005.08.012

Joshi, D. R., Clay, D. E., Clay, S. A., Moriles-Miller, J., Daigh, A. L. M., Reicks, G., & Westhoff, S. (2024). Quantification and machine learning based N2O–N and CO2–C emissions predictions from a decomposing rye cover crop. *Agronomy Journal*, *116*(3), 795–809. https://doi.org/10.1002/agj2.21185

Klefoth, R. R., Clough, T. J., Oenema, O., & Van Groenigen, J.-W. (2014). Soil Bulk Density and Moisture Content Influence Relative Gas Diffusivity and the Reduction of Nitrogen-15 Nitrous Oxide. *Vadose Zone Journal*, *13*(11), vzj2014.07.0089. https://doi.org/10.2136/vzj2014.07.0089

Kotlar, A. M., Singh, J., & Kumar, S. (2022). Prediction of greenhouse gas emissions from agricultural fields with and without cover crops. *Soil Science Society of America Journal*, *86*(5), 1227–1240.

Kravchenko, A. N., Guber, A. K., Quigley, M. Y., Koestel, J., Gandhi, H., & Ostrom, N. E. (2018). X-ray computed tomography to predict soil N2O production via bacterial denitrification and N2O emission in contrasting bioenergy cropping systems. *GCB Bioenergy*, *10*(11), 894–909. https://doi.org/10.1111/gcbb.12552

Krichels, A. H., & Yang, W. H. (2019). Dynamic Controls on Field-Scale Soil Nitrous Oxide Hot Spots and Hot Moments Across a Microtopographic Gradient. *Journal of Geophysical Research: Biogeosciences*, *124*(11), 3618–3634. https://doi.org/10.1029/2019JG005224

Lamb, W. F., Grubb ,Michael, Diluiso ,Francesca, & and Minx, J. C. (2022). Countries with sustained greenhouse gas emissions reductions: An analysis of trends and progress by sector. *Climate Policy*, *22*(1), 1–17. https://doi.org/10.1080/14693062.2021.1990831

Lazcano, C., Zhu-Barker, X., & Decock, C. (2021). Effects of Organic Fertilizers on the Soil Microorganisms Responsible for N2O Emissions: A Review. *Microorganisms*, *9*(5), Article 5. https://doi.org/10.3390/microorganisms9050983

Leys, C., Ley, C., Klein, O., Bernard, P., & Licata, L. (2013). Detecting outliers: Do not use standard deviation around the mean, use absolute deviation around the median. *Journal of Experimental Social Psychology*, *49*(4), 764–766. https://doi.org/10.1016/j.jesp.2013.03.013

Li, J., & Culver, T. B. (2022). Review of process-based nitrogen model for agricultural fields with implications for nitrogen simulations in stormwater BMPs. *Environmental Modelling & Software*, *151*, 105363. https://doi.org/10.1016/j.envsoft.2022.105363

Liu, L., Xu, S., Tang, J., Guan, K., Griffis, T. J., Erickson, M. D., Frie, A. L., Jia, X., Kim, T., Miller, L. T., Peng, B., Wu, S., Yang, Y., Zhou, W., Kumar, V., & Jin, Z. (2022). KGML-ag: A modeling framework of knowledge-guided machine learning to simulate agroecosystems: a case study of estimating N_2O emission using data from mesocosm experiments. *Geoscientific Model Development*, *15*(7), 2839–2858. https://doi.org/10.5194/gmd-15-2839-2022

Luo, J., Peng, Y., Jia, Z., Wu, Y., Gao, Y., Jalaid, N., Zhang, X., Ge, H., Qing, B., Chen, H., Zhan, Y., Li, P., & Liu, L. (2025). Moisture–Microbial Interaction Amplifies N2O Emission Hot Moments Under Deepened Snow in Grasslands. *Global Change Biology*, *31*(5), e70254. https://doi.org/10.1111/gcb.70254

Lussich, F., Dhaliwal, J. K., Faiia, A. M., Jagadamma, S., Schaeffer, S. M., & Saha, D. (2024). Cover crop residue decomposition triggered soil oxygen depletion and promoted nitrous oxide emissions. *Scientific Reports*, *14*(1), 8437. https://doi.org/10.1038/s41598-024-58942-7

Ma, T., Wei, C., Yao, C., & Yi, P. (2020). Microstructural evolution of expansive clay during drying–wetting cycle. *Acta Geotechnica*, *15*(8), 2355–2366. https://doi.org/10.1007/s11440-020-00938-4

Ma, W. K., Schautz, A., Fishback, L.-A. E., Bedard-Haughn, A., Farrell, R. E., & Siciliano, S. D. (2007). Assessing the potential of ammonia oxidizing bacteria to produce nitrous oxide in soils of a high arctic lowland ecosystem on Devon Island, Canada. *Soil Biology and Biochemistry*, *39*(8), 2001–2013. https://doi.org/10.1016/j.soilbio.2007.03.001

Mason, C. W., Stoof, C. R., Richards, B. K., Rossiter, D. G., & Steenhuis, T. S. (2016). Spring-Thaw Nitrous Oxide Emissions from Reed Canarygrass on Wetness-Prone Marginal Soil in New York State. *Soil Science Society of America Journal*, *80*(2), 428–437. https://doi.org/10.2136/sssaj2015.05.0182

McClain, M. E., Boyer, E. W., Dent, C. L., Gergel, S. E., Grimm, N. B., Groffman, P. M., Hart, S. C., Harvey, J. W., Johnston, C. A., Mayorga, E., McDowell, W. H., & Pinay, G. (2003). Biogeochemical Hot Spots and Hot Moments at the Interface of Terrestrial and Aquatic Ecosystems. *Ecosystems*, *6*(4), 301–312. https://doi.org/10.1007/s10021-003-0161-9

Mohn, J., Wolf, B., Toyoda, S., Lin, C.-T., Liang, M.-C., Brüggemann, N., Wissel, H., Steiker, A. E., Dyckmans, J., Szwec, L., Ostrom, N. E., Casciotti, K. L., Forbes, M., Giesemann, A., Well, R., Doucett, R. R., Yarnes, C. T., Ridley, A. R., Kaiser, J., & Yoshida, N. (2014). Interlaboratory assessment of nitrous oxide isotopomer analysis by isotope ratio mass spectrometry and laser spectroscopy: Current status and perspectives. *Rapid Communications in Mass Spectrometry*, *28*(18), 1995–2007. https://doi.org/10.1002/rcm.6982

Molodovskaya, M., Singurindy, O., Richards, B. K., Warland, J., Johnson, M. S., & Steenhuis, T. S. (2012). Temporal Variability of Nitrous Oxide from Fertilized Croplands: Hot Moment Analysis. *Soil Science Society of America Journal*, *76*(5), 1728–1740. https://doi.org/10.2136/sssaj2012.0039

Mosier, A. R., Duxbury, J. M., Freney, J. R., Heinemeyer, O., & Minami, K. (1998). Assessing and Mitigating N2O Emissions from Agricultural Soils. *Climatic Change*, *40*(1), 7–38. https://doi.org/10.1023/A:1005386614431

Mulvaney, R. L. (1996). Nitrogen—Inorganic Forms. In *Methods of Soil Analysis* (pp. 1123–1184). John Wiley & Sons, Ltd. https://doi.org/10.2136/sssabookser5.3.c38

Navarro-García, F., Casermeiro, M. Á., & Schimel, J. P. (2012). When structure means conservation: Effect of aggregate structure in controlling microbial responses to rewetting events. *Soil Biology and Biochemistry*, *44*(1), 1–8. https://doi.org/10.1016/j.soilbio.2011.09.019

Necpálová, M., Anex, R. P., Fienen, M. N., Del Grosso, S. J., Castellano, M. J., Sawyer, J. E., Iqbal, J., Pantoja, J. L., & Barker, D. W. (2015). Understanding the DayCent model: Calibration, sensitivity, and identifiability through inverse modeling. *Environmental Modelling & Software*, *66*, 110–130. https://doi.org/10.1016/j.envsoft.2014.12.011

Nevison, C., Lan, X., & Ogle, S. M. (2023). Remote Sensing Soil Freeze-Thaw Status and North American N2O Emissions From a Regional Inversion. *Global Biogeochemical Cycles*, *37*(7), e2023GB007759. https://doi.org/10.1029/2023GB007759

Norton, J., & Ouyang, Y. (2019). Controls and Adaptive Management of Nitrification in Agricultural Soils. *Frontiers in Microbiology*, *10*. https://doi.org/10.3389/fmicb.2019.01931

Palta, M. M., Ehrenfeld, J. G., & Groffman, P. M. (2014). “Hotspots” and “Hot Moments” of Denitrification in Urban Brownfield Wetlands. *Ecosystems*, *17*(7), 1121–1137. https://doi.org/10.1007/s10021-014-9778-0

Panday, D., Saha, D., Lee, J., Jagadamma, S., Adotey, N., & Mengistu, A. (2022). Cover crop residue influence on soil N2O and CO2 emissions under wetting-drying intensities: An incubation study. *European Journal of Soil Science*, *73*(5), e13309. https://doi.org/10.1111/ejss.13309

Parton, W. J., Holland, E. A., Del Grosso, S. J., Hartman, M. D., Martin, R. E., Mosier, A. R., Ojima, D. S., & Schimel, D. S. (2001). Generalized model for NO x and N2O emissions from soils. *Journal of Geophysical Research: Atmospheres*, *106*(D15), 17403–17419. https://doi.org/10.1029/2001JD900101

Parton, W. J., Mosier, A. R., Ojima, D. S., Valentine, D. W., Schimel, D. S., Weier, K., & Kulmala, A. E. (1996). Generalized model for N2 and N2O production from nitrification and denitrification. *Global Biogeochemical Cycles*, *10*(3), 401–412. https://doi.org/10.1029/96GB01455

Pasha, M. Z., & Umesh, N. (2013). A comparative study on outlier detection techniques. *International Journal of Computer Applications*, *66*(24).

Paulheim, H., & Meusel, R. (2015). A decomposition of the outlier detection problem into a set of supervised learning problems. *Machine Learning*, *100*(2), 509–531. https://doi.org/10.1007/s10994-015-5507-y

Philibert, A., Loyce, C., & Makowski, D. (2013). Prediction of N2O emission from local information with Random Forest. *Environmental Pollution*, *177*, 156–163. https://doi.org/10.1016/j.envpol.2013.02.019

Popov, P., Mahmood, U., Fu, Z., Yang, C., Calhoun, V., & Plis, S. (2024). A simple but tough-to-beat baseline for fMRI time-series classification. *NeuroImage*, *303*, 120909. https://doi.org/10.1016/j.neuroimage.2024.120909

Powlson, D. S., Poulton, P. R., Glendining, M. J., Macdonald, A. J., & Goulding, K. W. T. (2022). Is it possible to attain the same soil organic matter content in arable agricultural soils as under natural vegetation? *Outlook on Agriculture*, *51*(1), 91–104. https://doi.org/10.1177/00307270221082113

Project Drawdown. (2021). *Climate Solutions at Work* (p. 43). Drawdown Labs. https://drawdown.org/publications/climate-solutions-at-work

Rabot, E., Hénault, C., & Cousin, I. (2014). Temporal Variability of Nitrous Oxide Emissionsby Soils as Affected by Hydric History. *Soil Science Society of America Journal*, *78*(2), 434–444. https://doi.org/10.2136/sssaj2013.07.0311

Rabot, E., Hénault, C., & Cousin, I. (2016). Effect of the soil water dynamics on nitrous oxide emissions. *Geoderma*, *280*, 38–46. https://doi.org/10.1016/j.geoderma.2016.06.012

Rachetti, F. L., Dhaliwal, J. K., & Saha, D. (2023). *Cover Crop Residue Decomposition Exacerbated Soil Oxygen Depletion to Promote N 2 o Emissions*. ASA, CSSA, SSSA International Annual Meeting.

Rastogi, D., Touma, D., Evans, K. J., & Ashfaq, M. (2020). Shift Toward Intense and Widespread Precipitation Events Over the United States by Mid-21st Century. *Geophysical Research Letters*, *47*(19), e2020GL089899. https://doi.org/10.1029/2020GL089899

Ray, D. K., West, P. C., Clark, M., Gerber, J. S., Prishchepov, A. V., & Chatterjee, S. (2019). Climate change has likely already affected global food production. *PLOS ONE*, *14*(5), e0217148. https://doi.org/10.1371/journal.pone.0217148

Rezaei, E. E., Webber, H., Asseng, S., Boote, K., Durand, J. L., Ewert, F., Martre, P., & MacCarthy, D. S. (2023). Climate change impacts on crop yields. *Nature Reviews Earth & Environment*, *4*(12), 831–846. https://doi.org/10.1038/s43017-023-00491-0

Risk, N., Snider, D., & Wagner-Riddle, C. (2013). Mechanisms leading to enhanced soil nitrous oxide fluxes induced by freeze–thaw cycles. *Canadian Journal of Soil Science*, *93*(4), 401–414. https://doi.org/10.4141/cjss2012-071

Rivas, A., Barkle, G., Stenger, R., Moorhead, B., & Clague, J. (2020). Nitrate removal and secondary effects of a woodchip bioreactor for the treatment of subsurface drainage with dynamic flows under pastoral agriculture. *Ecological Engineering*, *148*, 105786. https://doi.org/10.1016/j.ecoleng.2020.105786

Robinson, R. B., Cox, C. D., & Odom, K. (2005). Identifying Outliers in Correlated Water Quality Data. *Journal of Environmental Engineering*, *131*(4), 651–657. https://doi.org/10.1061/(ASCE)0733-9372(2005)131:4(651)

Rohatgi, A. (2022). *Webplotdigitizer: Version 4.6*. https://automeris.io/WebPlotDigitizer

Rosenzweig, C., Mbow, C., Barioni, L. G., Benton, T. G., Herrero, M., Krishnapillai, M., Liwenga, E. T., Pradhan, P., Rivera-Ferre, M. G., Sapkota, T., Tubiello, F. N., Xu, Y., Mencos Contreras, E., & Portugal-Pereira, J. (2020). Climate change responses benefit from a global food system approach. *Nature Food*, *1*(2), Article 2. https://doi.org/10.1038/s43016-020-0031-z

Rousseeuw, P. J., & Hubert, M. (2011). Robust statistics for outlier detection. *WIREs Data Mining and Knowledge Discovery*, *1*(1), 73–79. https://doi.org/10.1002/widm.2

Russo, S., Besmer, M. D., Blumensaat, F., Bouffard, D., Disch, A., Hammes, F., Hess, A., Lürig, M., Matthews, B., Minaudo, C., Morgenroth, E., Tran-Khac, V., & Villez, K. (2021). The value of human data annotation for machine learning based anomaly detection in environmental systems. *Water Research*, *206*, 117695. https://doi.org/10.1016/j.watres.2021.117695

Saber, M., & Habib, E. (2016). Flash Floods Modelling for Wadi System: Challenges and Trends. In A. M. Melesse & W. Abtew (Eds.), *Landscape Dynamics, Soils and Hydrological Processes in Varied Climates* (pp. 317–339). Springer International Publishing. https://doi.org/10.1007/978-3-319-18787-7_16

Saha, D., Basso, B., & Robertson, G. P. (2021a). Machine learning improves predictions of agricultural nitrous oxide (N2O) emissions from intensively managed cropping systems. *Environmental Research Letters*, *16*(2), 024004. https://doi.org/10.1088/1748-9326/abd2f3

Saha, D., Kaye, J. P., Bhowmik, A., Bruns, M. A., Wallace, J. M., & Kemanian, A. R. (2021b). Organic fertility inputs synergistically increase denitrification-derived nitrous oxide emissions in agroecosystems. *Ecological Applications*, *31*(7), e02403. https://doi.org/10.1002/eap.2403

Saha, D., Kemanian, A. R., Montes, F., Gall, H., Adler, P. R., & Rau, B. M. (2018). Lorenz Curve and Gini Coefficient Reveal Hot Spots and Hot Moments for Nitrous Oxide Emissions. *Journal of Geophysical Research: Biogeosciences*, *123*(1), 193–206. https://doi.org/10.1002/2017JG004041

Saito, T., & Rehmsmeier, M. (2015). The Precision-Recall Plot Is More Informative than the ROC Plot When Evaluating Binary Classifiers on Imbalanced Datasets. *PLoS ONE*, *10*(3), e0118432. https://doi.org/10.1371/journal.pone.0118432

Sanderman, J., Hengl, T., & Fiske, G. J. (2017). Soil carbon debt of 12,000 years of human land use. *Proceedings of the National Academy of Sciences*, *114*(36), 9575–9580. https://doi.org/10.1073/pnas.1706103114

Sarki, A., Mirjat, M. S., Mahessar, A. A., Kori, S. M., & Qureshi, A. L. (2014). Determination of saturated hydraulic conductivity of different soil texture materials. *Journal of Agriculture and Veterinary Science*, *7*(12), 56–62.

Scheer, C., Del Grosso, S. J., Parton, W. J., Rowlings, D. W., & Grace, P. R. (2014). Modeling nitrous oxide emissions from irrigated agriculture: Testing DayCent with high-frequency measurements. *Ecological Applications*, *24*(3), 528–538. https://doi.org/10.1890/13-0570.1

Schreiber, F., Wunderlin, P., Udert, K. M., & Wells, G. F. (2012). Nitric oxide and nitrous oxide turnover in natural and engineered microbial communities: Biological pathways, chemical reactions, and novel technologies. *Frontiers in Microbiology*, *3*. https://doi.org/10.3389/fmicb.2012.00372

Senbayram, M., Chen, R., Budai, A., Bakken, L., & Dittert, K. (2012). N2O emission and the N2O/(N2O + N2) product ratio of denitrification as controlled by available carbon substrates and nitrate concentrations. *Agriculture, Ecosystems & Environment*, *147*, 4–12. https://doi.org/10.1016/j.agee.2011.06.022

Shindell, D., Sadavarte, P., Aben, I., Bredariol, T. de O., Dreyfus, G., Höglund-Isaksson, L., Poulter, B., Saunois, M., Schmidt, G. A., Szopa, S., Rentz, K., Parsons, L., Qu, Z., Faluvegi, G., & Maasakkers, J. D. (2024). The methane imperative. *Frontiers in Science*, *2*. https://doi.org/10.3389/fsci.2024.1349770

Shrestha, R. C., Ghazaryan, L., Poodiack, B., Zorin, B., Gross, A., Gillor, O., Khozin-Goldberg, I., & Gelfand, I. (2022). The effects of microalgae-based fertilization of wheat on yield, soil microbiome and nitrogen oxides emissions. *Science of The Total Environment*, *806*, 151320. https://doi.org/10.1016/j.scitotenv.2021.151320

ŠImek, M., & Cooper, J. E. (2002). The influence of soil pH on denitrification: Progress towards the understanding of this interaction over the last 50 years. *European Journal of Soil Science*, *53*(3), 345–354. https://doi.org/10.1046/j.1365-2389.2002.00461.x

Singer, A. (2007). *The Soils of Israel*. Springer.

Singh, K., & Upadhyaya, D. S. (2012). *Outlier Detection: Applications And Techniques*. *9*(1).

Sistani, K. (2020). *Greenhouse Gas Study for Greenhouse gas Reduction through Agricultural Carbon Enhancement network in Bowling Green, Kentucky* [Dataset]. Ag Data Commons. https://doi.org/10.15482/USDA.ADC/1503968

Smith, K. A. (2017). Changing views of nitrous oxide emissions from agricultural soil: Key controlling processes and assessment at different spatial scales. *European Journal of Soil Science*, *68*(2), 137–155. https://doi.org/10.1111/ejss.12409

Smiti, A. (2020). A critical overview of outlier detection methods. *Computer Science Review*, *38*, 100306. https://doi.org/10.1016/j.cosrev.2020.100306

Soil Survey Staff, Natural Resources Conservation Service, United States Department of Agriculture. (2019, July 31). *Web Soil Survey*. Web Soil Survey. https://websoilsurvey.nrcs.usda.gov/app/

Soil Survey Staff, USDA. (1999). *Soil Taxonomy: A Basic System of Soil Classification for Making and Interpreting Soil Surveys* (Second Edition). https://www.nrcs.usda.gov/Internet/FSE_DOCUMENTS/nrcs142p2_051232.pdf

Song, X., Liu, M., Ju, X., Gao, B., Su, F., Chen, X., & Rees, R. M. (2018). Nitrous Oxide Emissions Increase Exponentially When Optimum Nitrogen Fertilizer Rates Are Exceeded in the North China Plain. *Environmental Science & Technology*, *52*(21), 12504–12513. https://doi.org/10.1021/acs.est.8b03931

Stanford, G., Dzienia, S., & Vander Pol, R. A. (1975). Effect of Temperature on Denitrification Rate in Soils. *Soil Science Society of America Journal*, *39*(5), 867–870. https://doi.org/10.2136/sssaj1975.03615995003900050024x

Stanford, G., Vander Pol, R. A., & Dzienia, S. (1975). Denitrification Rates in Relation to Total and Extractable Soil Carbon. *Soil Science Society of America Journal*, *39*(2), 284–289. https://doi.org/10.2136/sssaj1975.03615995003900020019x

Stuchiner, E. R., Jernigan, W. A., Zhang, Z., Eddy, W. C., DeLucia, E. H., & Yang, W. H. (2024). Particulate organic matter predicts spatial variation in denitrification potential at the field scale. *Geoderma*, *448*, 116943. https://doi.org/10.1016/j.geoderma.2024.116943

Stuchiner, E. R., Xu, J., Eddy, W. C., DeLucia, E. H., & Yang, W. H. (2025). Hot or Not? An Evaluation of Methods for Identifying Hot Moments of Nitrous Oxide Emissions From Soils. *Journal of Geophysical Research: Biogeosciences*, *130*(1), e2024JG008138. https://doi.org/10.1029/2024JG008138

Su, W., Yuan, Y., & Zhu, M. (2015). A Relationship between the Average Precision and the Area Under the ROC Curve. *Proceedings of the 2015 International Conference on The Theory of Information Retrieval*, 349–352. https://doi.org/10.1145/2808194.2809481

Sutka, R. L., Ostrom, N. E., Ostrom, P. H., Breznak, J. A., Gandhi, H., Pitt, A. J., & Li, F. (2006). Distinguishing Nitrous Oxide Production from Nitrification and Denitrification on the Basis of Isotopomer Abundances. *Applied and Environmental Microbiology*, *72*(1), 638–644. https://doi.org/10.1128/AEM.72.1.638-644.2006

Thompson, R. L., Lassaletta, L., Patra, P. K., Wilson, C., Wells, K. C., Gressent, A., Koffi, E. N., Chipperfield, M. P., Winiwarter, W., Davidson, E. A., Tian, H., & Canadell, J. G. (2019). Acceleration of global N2O emissions seen from two decades of atmospheric inversion. *Nature Climate Change*, *9*(12), Article 12. https://doi.org/10.1038/s41558-019-0613-7

Tian, H., Xu, R., Canadell, J. G., Thompson, R. L., Winiwarter, W., Suntharalingam, P., Davidson, E. A., Ciais, P., Jackson, R. B., Janssens-Maenhout, G., Prather, M. J., Regnier, P., Pan, N., Pan, S., Peters, G. P., Shi, H., Tubiello, F. N., Zaehle, S., Zhou, F., … Yao, Y. (2020). A comprehensive quantification of global nitrous oxide sources and sinks. *Nature*, *586*(7828), 248–256. https://doi.org/10.1038/s41586-020-2780-0

Tian, H., Yang, J., Xu, R., Lu, C., Canadell, J. G., Davidson, E. A., Jackson, R. B., Arneth, A., Chang, J., Ciais, P., Gerber, S., Ito, A., Joos, F., Lienert, S., Messina, P., Olin, S., Pan, S., Peng, C., Saikawa, E., … Zhang, B. (2019). Global soil nitrous oxide emissions since the preindustrial era estimated by an ensemble of terrestrial biosphere models: Magnitude, attribution, and uncertainty. *Global Change Biology*, *25*(2), 640–659. https://doi.org/10.1111/gcb.14514

Tierling, J., & Kuhlmann, H. (2018). Emissions of nitrous oxide (N2O) affected by pH-related nitrite accumulation during nitrification of N fertilizers. *Geoderma*, *310*, 12–21. https://doi.org/10.1016/j.geoderma.2017.08.040

Toyoda, S., Mutobe, H., Yamagishi, H., Yoshida, N., & Tanji, Y. (2005). Fractionation of N2O isotopomers during production by denitrifier. *Soil Biology and Biochemistry*, *37*(8), 1535–1545. https://doi.org/10.1016/j.soilbio.2005.01.009

Vemuri, N. (2024). Developing a hybrid data-driven and informed model for prediction and mitigation of agricultural nitrous oxide flux hotspots. *Frontiers in Environmental Science*, *12*. https://doi.org/10.3389/fenvs.2024.1353049

Venterea, R. T., Halvorson, A. D., Kitchen, N., Liebig, M. A., Cavigelli, M. A., Grosso, S. J. D., Motavalli, P. P., Nelson, K. A., Spokas, K. A., Singh, B. P., Stewart, C. E., Ranaivoson, A., Strock, J., & Collins, H. (2012). Challenges and opportunities for mitigating nitrous oxide emissions from fertilized cropping systems. *Frontiers in Ecology and the Environment*, *10*(10), 562–570. https://doi.org/10.1890/120062

Venterea, R. T., & Rolston, D. E. (2000). Nitric and nitrous oxide emissions following fertilizer application to agricultural soil: Biotic and abiotic mechanisms and kinetics. *Journal of Geophysical Research: Atmospheres*, *105*(D12), 15117–15129. https://doi.org/10.1029/2000JD900025

Verdouw, H., Van Echteld, C. J. A., & Dekkers, E. M. J. (1978). Ammonia determination based on indophenol formation with sodium salicylate. *Water Research*, *12*(6), 399–402. https://doi.org/10.1016/0043-1354(78)90107-0

Verheul, J. (2011). Methane as a Greenhouse Gas: Why the EPA Should Regulate Emissions from Animal Feeding Operations and Concentrated Animal Feeding Operations Under the Clean Air Act. *Natural Resources Journal*, *51*(1), 163–187.

Wagner-Riddle, C., Baggs, E. M., Clough, T. J., Fuchs, K., & Petersen, S. O. (2020). Mitigation of nitrous oxide emissions in the context of nitrogen loss reduction from agroecosystems: Managing hot spots and hot moments. *Current Opinion in Environmental Sustainability*, *47*, 46–53. https://doi.org/10.1016/j.cosust.2020.08.002

Wagner-Riddle, C., Congreves, K. A., Abalos, D., Berg, A. A., Brown, S. E., Ambadan, J. T., Gao, X., & Tenuta, M. (2017). Globally important nitrous oxide emissions from croplands induced by freeze–thaw cycles. *Nature Geoscience*, *10*(4), 279–283. https://doi.org/10.1038/ngeo2907

Waldo, S., Russell, E. S., Kostyanovsky, K., Pressley, S. N., O'Keeffe, P. T., Huggins, D. R., Stöckle, C. O., Pan, W. L., & Lamb, B. K. (2019). N2O Emissions From Two Agroecosystems: High Spatial Variability and Long Pulses Observed Using Static Chambers and the Flux-Gradient Technique. *Journal of Geophysical Research: Biogeosciences*, *124*(7), 1887–1904. https://doi.org/10.1029/2019JG005032

Wallenstein, M. D., Myrold, D. D., Firestone, M., & Voytek, M. (2006). Environmental Controls on Denitrifying Communities and Denitrification Rates: Insights from Molecular Methods. *Ecological Applications*, *16*(6), 2143–2152. https://doi.org/10.1890/1051-0761(2006)016[2143:ECODCA]2.0.CO;2

Wang, C., Amon, B., Schulz, K., & Mehdi, B. (2021). Factors That Influence Nitrous Oxide Emissions from Agricultural Soils as Well as Their Representation in Simulation Models: A Review. *Agronomy*, *11*(4), Article 4. https://doi.org/10.3390/agronomy11040770

Wang, Q., Zhou, F., Shang, Z., Ciais, P., Winiwarter, W., Jackson, R. B., Tubiello, F. N., Janssens-Maenhout, G., Tian, H., Cui, X., Canadell, J. G., Piao, S., & Tao, S. (2020). Data-driven estimates of global nitrous oxide emissions from croplands. *National Science Review*, *7*(2), 441–452. https://doi.org/10.1093/nsr/nwz087

Wang, S., Li, J., Yuan, X., Senadheera, S. S., Chang, S. X., Wang, X., & Ok, Y. S. (2024). Machine Learning Predicts Biochar Aging Effects on Nitrous Oxide Emissions from Agricultural Soils. *ACS Agricultural Science & Technology*, *4*(9), 888–898. https://doi.org/10.1021/acsagscitech.4c00114

Wang, X., Wang, S., Yang, Y., Tian, H., Jetten, M. S. M., Song, C., & Zhu, G. (2023). Hot moment of N2O emissions in seasonally frozen peatlands. *The ISME Journal*, *17*(6), 792–802. https://doi.org/10.1038/s41396-023-01389-x

Wang, Y., Guo, J., Vogt, R. D., Mulder, J., Wang, J., & Zhang, X. (2018). Soil pH as the chief modifier for regional nitrous oxide emissions: New evidence and implications for global estimates and mitigation. *Global Change Biology*, *24*(2), e617–e626. https://doi.org/10.1111/gcb.13966

Weier, K. L., Doran, J. W., Power, J. F., & Walters, D. T. (1993). Denitrification and the Dinitrogen/Nitrous Oxide Ratio as Affected by Soil Water, Available Carbon, and Nitrate. *Soil Science Society of America Journal*, *57*(1), 66–72. https://doi.org/10.2136/sssaj1993.03615995005700010013x

Woodward, A., & Porter, J. R. (2016). Food, hunger, health, and climate change. *The Lancet*, *387*(10031), 1886–1887. https://doi.org/10.1016/S0140-6736(16)00349-4

Wrage-Mönnig, N., Horn, M. A., Well, R., Müller, C., Velthof, G., & Oenema, O. (2018). The role of nitrifier denitrification in the production of nitrous oxide revisited. *Soil Biology and Biochemistry*, *123*, A3–A16. https://doi.org/10.1016/j.soilbio.2018.03.020

Yan, X., Ti, C., Vitousek, P., Chen, D., Leip, A., Cai, Z., & Zhu, Z. (2014). Fertilizer nitrogen recovery efficiencies in crop production systems of China with and without consideration of the residual effect of nitrogen. *Environmental Research Letters*, *9*(9), 095002. https://doi.org/10.1088/1748-9326/9/9/095002

Yates, T. T., Si, B. C., Farrell, R. E., & Pennock, D. J. (2006). Probability Distribution and Spatial Dependence of Nitrous Oxide Emission. *Soil Science Society of America Journal*, *70*(3), 753–762. https://doi.org/10.2136/sssaj2005.0214

Ye, B. (2024). *pyOATS* (Version 0.1.3) [Python]. https://github.com/georgian-io/pyoats

Yin, Y., Wang, Z., Tian, X., Wang, Y., Cong, J., & Cui, Z. (2022). Evaluation of variation in background nitrous oxide emissions: A new global synthesis integrating the impacts of climate, soil, and management conditions. *Global Change Biology*, *28*(2), 480–492. https://doi.org/10.1111/gcb.15860

Zhao, Y., Nasrullah, Z., & Li, Z. (2019). PyOD: A Python Toolbox for Scalable Outlier Detection. *Journal of Machine Learning Research*, *20*(96), 1–7.

Zhou, Z., Liao, K., Zhu, Q., Lai, X., Yang, J., & Huang, J. (2022). Determining the hot spots and hot moments of soil N2O emissions and mineral N leaching in a mixed landscape under subtropical monsoon climatic conditions. *Geoderma*, *420*, 115896. https://doi.org/10.1016/j.geoderma.2022.115896

Zhu-Barker, X., Cavazos, A. R., Ostrom, N. E., Horwath, W. R., & Glass, J. B. (2015). The importance of abiotic reactions for nitrous oxide production. *Biogeochemistry*, *126*(3), 251–267. https://doi.org/10.1007/s10533-015-0166-4

Zimmermann, J., Carolan, R., Forrestal, P., Harty, M., Lanigan, G., Richards, K. G., Roche, L., Whitfield, M. G., & Jones, M. B. (2018). Assessing the performance of three frequently used biogeochemical models when simulating N2O emissions from a range of soil types and fertiliser treatments. *Geoderma*, *331*, 53–69. https://doi.org/10.1016/j.geoderma.2018.06.004

Zumft, W. G. (1997). Cell biology and molecular basis of denitrification. *Microbiology and Molecular Biology Reviews*, *61*(4), 533–616. https://doi.org/10.1128/mmbr.61.4.533-616.1997

VITA

Ryan Ackett was born in St. Petersburg, Florida to two teachers, Wayne and Jennifer. Ryan had a passion for learning from a young age, and loved nothing more than thinking about big problems. It was in college at the University of Florida that he discovered the problem that would capture his mind: the challenge of building a sustainable and just global food system. Upon graduation with a degree in agricultural engineering, he followed that pursuit into the fields of a South Florida citrus farm, where he would spend three years learning about the real work of farming. It was through this experience that he became aware of the critical relationship between farmers and researchers, which led him to return to academia to study sustainable irrigation and water resource management at North Carolina State University. Through his research he became more and more fascinated with biogeochemistry, which he saw as the nexus linking the soil, biology, climate, and farm management and upon which so many critical agricultural outcomes depend. Of particular interest to Ryan was the interdependence between soil microbiota and our global climate and the implications that this relationship had for the collective fight against the climate crisis. After his graduation from the University of Tennessee, Ryan will continue to think about big problems and how to come together to solve them in pursuit of an equitable food system for all.